EPA/600/R-95/068
July 1995

# CALCIUM CARBONATE DISSOLUTION RATE IN LIMESTONE CONTACTORS

by

Raymond D. Letterman
Syracuse University
Syracuse, New York 13244

Cooperative Agreement No. CR814926

Jeffrey Q. Adams
Project Officer
Drinking Water Research Division
Risk Reduction Engineering Laboratory
United States Environmental Protection Agency
Cincinnati, OH 45268

RISK REDUCTION ENGINEERING LABORATORY
OFFICE OF RESEARCH AND DEVELOPMENT
U.S. ENVIRONMENTAL PROTECTION AGENCY
CINCINNATI, OHIO 45268

DISCLAIMER

The information in this document has been funded wholly or in part by the United States Environmental Protection Agency under Cooperative Agreement Number CR814926 to Syracuse University. It has been subject to the Agency's peer and administrative review and it has been approved for publication as an EPA document. Mention of trade names or commercial products does not constitute endorsement or recommendation for use.

# FOREWORD

Today's rapidly developing and changing technologies and industrial products and practices frequently carry with them the increased generation of materials that, if improperly dealt with, can threaten both public health and the environment. The U.S. Environmental Protection Agency is charged by Congress with protecting the Nation's land, air and water systems. Under a mandate of national environmental laws, the agency strives to formulate and implement actions leading to a compatible balance between human activities and the ability of natural systems to support and nurture life. These laws direct the EPA to perform research to define our environmental problems, measure the impacts, and search for solutions.

The Risk Reduction Engineering Laboratory is responsible for planning, implementation, and management of research, development, and demonstration programs to provide an authoritative, defensible engineering basis in support of the policies, programs, and regulations of the EPA with respect to drinking water, wastewater, pesticides, toxic substances, solid and hazardous wastes, and Superfund-related activities. This publication is one of the products of that research and provides a vital communication link between the researcher and the user community.

Limestone contactors have been shown to be an effective and economical water treatment device for reducing the tendency of water to dissolve corrosion by-products, such as lead, copper, and zinc, from surfaces in piping systems. Models used to design limestone contactors must predict the effect of a number of

factors on the rate of carbonate mineral dissolution from the stone. This report describes the results of a study to determine the effect of limestone composition and water temperature on the carbonate mineral dissolution rate.

E. Timothy Oppelt, Director
Risk Reduction Engineering
Laboratory

ABSTRACT

The rate of carbonate mineral dissolution from limestone was studied using a rotating disk apparatus and samples of limestone of varied composition. The purpose of this study was to determine the effect of limestone composition on the kinetics of carbonate mineral dissolution. The results are needed to improve the relationships used to design limestone contactors for long term operation.

The stone samples with the highest calcite content and lowest dolomite content had the highest initial rates of dissolution. The magnitude of the overall dissolution rate constant for fresh stone decreased by approximately 60% as the calcite content of the stone decreased from 0.92 to 0.09 g $CaCO_3$/g stone.

The overall dissolution rate constant decreased as the amount of calcium dissolved from the surface of the stone increased. Analysis of several stone surfaces indicated that a residue layer of aluminum, silicon and iron formed as calcium dissolved.

For a given amount of calcium dissolved per unit area of stone surface, the magnitude of the decrease in the dissolution rate constant increased as the initial amount of iron and aluminum in the stone increased. The results suggest that the effect of sample aging on the rate of dissolution is at a minimum if the weighted sum of the Fe and Al content of the stone is less than about 10 mg/g. The weighted sum is equal to the aluminum content in mg Al/g plus 0.30 times the iron content in mg Fe/g.

This report was submitted in fulfillment of CR814926 by Syracuse University under the sponsorship of the U.S. Environmental Protection Agency. This report covers a period from July 1988 to June 1993 and work was completed as of June 30, 1993.

TABLE OF CONTENTS

FIGURES

FIGURES (continued)

FIGURES (continued)

TABLES

TABLES (continued)

ABBREVIATIONS, SYMBOLS AND UNITS

| Notation | | Units |
|---|---|---|
| A | Area of limestone disk | $cm^2$ |
| a | Area of $CaCO_3$ per unit volume of fluid | $cm^{-1}$ |
| C | Bulk calcium concentration | moles/L |
| $Ca_d$ | Calcium dissolved per unit area of disk | $mg/cm^2$ |
| $Ca_r$ | Calcium dissolved during an experiment | mg |
| $Ca_s$ | Calcium dissolved during storage | mg |
| $C_{bo}$ | Calcium concentration in the influent of a contactor | moles/L |
| $C_{bL}$ | Calcium concentration in the effluent of a contactor | moles/L |
| $C_o$ | Initial calcium concentration | moles/L |
| $C_s$ | Calcium concentration at the surface | moles/L |
| D | Diffusivity of calcium ion | $cm^2/s$ |
| d | Diameter of limestone particle | cm |
| $H_{eq}$ | Equilibrium hydrogen ion concentration | moles/L |
| $k_c$ | First order surface reaction rate constant | cm/s |
| $k_f$ | Residue layer mass transfer coefficient | cm/s |
| $k_L$ | Mass transfer rate constant | cm/s |
| $k_o$ | Overall dissolution rate constant | cm/s |
| L | Overall depth of contactor | cm |
| M | Cumulative mass of calcium dissolved per unit area of limestone | $mg/cm^2$ |
| MRe | Modified Reynold's number | dimensionless |
| $N_D$ | Axial dispersion number | dimensionless |
| r | $CaCO_3$ dissolution rate | $moles/(cm^2 s)$ |
| $S_C$ | Schmidt number | dimensionless |

| | | |
|---|---|---|
| $U_s$ | Superficial velocity of fluid | cm/s |
| V | Volume of solution | $cm_3$ |
| Z | Depth | dimensionless |

**Greek letters**

| | | |
|---|---|---|
| $\gamma$ | Activity coefficient | dimensionless |
| $\delta$ | Thickness of residue layer | cm |
| $\delta_N$ | Diffusion boundary layer thickness | cm |
| $\epsilon$ | Porosity of limestone particles | dimensionless |
| $\epsilon_r$ | Porosity of the residue layer | dimensionless |
| $\Theta$ | Mean fluid residence time | sec |
| $\nu$ | Kinematic viscosity | $cm^2/s$ |
| $\rho_s$ | density of residue solids | $mg/cm^3$ |
| $\tau_r$ | Pore length tortuosity | dimensionless |
| $\psi$ | Sphericity of limestone particles | dimensionless |
| $\omega$ | Angular velocity | radians/s |

ACKNOWLEDGEMENTS

The author acknowledges the support and guidance of Jeffrey Q. Adams the USEPA Drinking Water Research Division project officer. The assistance of David A. Hopkins, geologist for the J.E. Baker Company, York, PA, and Professor Donald I. Siegel, Department of Earth Sciences, Syracuse University, is sincerely appreciated.

# CHAPTER I
# INTRODUCTION

## 1.1 BACKGROUND

A limestone contactor is a treatment device in which water flows through and dissolves carbonate minerals (typically calcium carbonate) from a packed bed of crushed limestone. Dissolution of calcium carbonate (under a closed-to-atmospheric-carbon dioxide condition) increases the pH, alkalinity and dissolved inorganic carbon concentration of the water and depletes the amount of calcium carbonate in the bed. Limestone contactors are simple, low-cost devices, which usually require minimal maintenance and are, therefore, especially suitable for small water supplies. In an earlier study sponsored by the United States Environmental Protection Agency (USEPA), it was shown that limestone contactors can effectively reduce the dissolution of corrosion by-products, such as lead, copper and zinc, from surfaces in piping systems (Letterman et al., 1987).

The results of the USEPA sponsored study (Letterman et al., 1987) were used to derive and test a mathematical model for designing limestone contactors. The model relates the depth of limestone required in a contactor to the desired effluent water chemistry, influent water chemistry, limestone particle size and shape, limestone bed porosity, and water temperature and superficial velocity. The model assumes that the kinetics of calcium carbonate dissolution is determined by a heterogeneous reaction, the rate of which is determined by a calcium ion mass transfer resistance and a surface reaction acting in series (Letterman et al., 1991).

In a study that followed the USEPA sponsored investigation, Haddad (1986) monitored the long-term operation of a contactor containing a somewhat impure, high-calcium limestone. Haddad's

steady-state model predicted the initial performance of the column when the limestone was fresh, however, as the unit was operated for a period of several months the effluent pH, alkalinity and calcium ion concentration decreased below the initial values.

Haddad (1986) used a scanning electron microscope with an attachment for x-ray energy spectroscopy to analyze the surfaces of particles of limestone from the contactor employed in the long-term study. He found that the dissolution of calcium carbonate significantly increased the amounts of aluminum, silicon and iron at the limestone surface. He concluded that as calcium carbonate dissolved from the stone the rate of dissolution decreased because relatively insoluble impurities such as silica, alumino-silicates and aluminum and iron oxides/hydroxides remained on the surface and formed a "residue layer". As the residue layer increased in thickness, it tended to decrease the rate of transport of calcium ion from the calcium carbonate surface to the bulk solution and this caused the performance of the contactor to decrease with time.

Field experiments have shown (Letterman et al., 1987) that the temperature of the water flowing through a limestone contactor can affect its performance. For a given set of design and operating conditions, contactor performance decreased with decreasing temperature.

In rotating disk experiments conducted by Sjöberg and Rickard (1983) and Lund (1975), the rate of calcite dissolution decreased with decreasing temperature. The extent to which a given temperature change affected the rate of dissolution varied with the rate limiting step in the dissolution process. At low pH (2 to 4) where the dissolution rate was mass transfer controlled, the effect of temperature was less than at high pH where the rate was apparently controlled by a combination of transport and surface reaction resistances. Relationships are available for correcting mass transfer coefficients for temperature, however, the effect of temperature on the surface reaction rate constant

for calcite dissolving from limestone is not known. This limits the usefulness of Haddad's contactor design model.

## 1.2 PROJECT PURPOSE

The purpose of this study was to: 1) determine the effect of limestone composition, especially the dolomite and impurity content of the stone, on the kinetics of carbonate mineral dissolution, and 2) determine the effect of temperature on the rate of dissolution of calcite from limestone. The results are needed to improve relationships used in computer programs for designing limestone contactors.

## 1.3 PROJECT DESCRIPTION

The dissolution rate experiments were conducted with a 2-liter, temperature-controlled batch reactor and rotating disk apparatus. Samples of solution were withdrawn from the reactor as carbonate minerals dissolved from the disk surface. The calcium and magnesium concentrations in the samples were used to determine dissolution rate constants as a function of the composition of the stone sample, the amount of carbonate mineral dissolved from the sample, and the temperature of the solution. Between dissolution rate experiments, the stone samples were "aged" by controlled dissolution in dilute acid solutions. The limestone ranged in composition from a white, calcitic Vermont marble with a significant amount of insoluble silica to sedimentary limestones that consisted of approximately 100 percent calcite ($CaCO_3$) to essentially pure dolomite ($CaMg(CO_3)_2$). The aluminum and iron content of the sedimentary stones was a variable.

The rotating disk apparatus was used in these experiments instead of limestone contactors because it is difficult to economically study the effect of the amount of mineral dissolved on dissolution kinetics using a continuous-flow, packed-bed device. Given the objectives of this study, contactor operation would have required a significant number of contactors, large

quantities of water and long operational periods to obtain meaningful results.

# CHAPTER 2
# CONCLUSIONS

1. The heterogeneous reaction model of Rickard and Sjöberg (1983) explained the dissolution rate data for all samples except the two with the highest dolomite ($CaMg(CO_3)_2$) content. The heterogeneous reaction model assumes that the rate of carbonate mineral dissolution is controlled by a cation mass transfer resistance and a surface reaction acting in series. For calcite ($CaCO_3$) and the experimental conditions of this study, the surface reaction rate was relatively large and the rate of dissolution was essentially mass transfer controlled.

2. According to the literature and the results of this study, a calcium ion diffusivity of $0.8 \times 10^{-5}$ $cm^2/s$ (at 25°C) can be used to predict the mass transfer resistance in the heterogenous reaction rate model. This value is now being used in the contactor design program DESCON.

3. The stone samples with the highest calcite content and lowest dolomite content had the highest initial rates of dissolution. The magnitude of the overall dissolution rate constant for fresh stone decreased by approximately 60% as the calcite content of the stone decreased from 0.92 to 0.09 g $CaCO_3$/g stone.

4. When the high dolomite content samples were fresh, it appeared that the calcium carbonate component of the dolomite dissolved faster than the magnesium carbonate component. This phenomenon has been reported by Plummer and

Busenberg (1982). The rate of dissolution of magnesium was negligible in all samples except the high dolomite content samples (93 and 100 mass percent dolomite).

5. The rate of dissolution of stones with high amounts of dolomite may be enhanced by the presence of small amounts of calcite. For example, the stone that was essentially pure dolomite had a value of the initial overall dissolution rate constant that was 66% less than the value for another dolomitic stone with approximately 9% calcite.

6. The overall dissolution rate constant decreased as the amount of calcium dissolved from the surface of the stone increased. Analysis of several stone surfaces by scanning electron microscopy and x-ray energy spectroscopy indicated that the density of calcium atoms on the surface of the stone decreased and the density of aluminum, silicon and iron increased as calcium dissolved.

7. For a given amount of calcium dissolved per unit area of stone surface, the magnitude of the decrease in the overall dissolution rate constant increased as the amount of iron and aluminum in the stone increased. For a stone with less than 8 mg Fe/g and 2 mg Al/g, the decrease for 2 mg Ca dissolved/$cm^2$ was about 10% while the decrease was over 70% for a stone with 160 mg Fe/g and 50 mg Al/g. The approximate iron content of the thirteen stone samples used in the study ranged from 15 to 377 mg Fe/100g and the approximate aluminum content from 1 to 134 mg Al/100g.

8. The results suggest that the effect of sample aging on the rate of dissolution is a minimum if the weighted sum of the Fe and Al content of the stone is less than about 10 mg/g. The weighted sum is equal to the aluminum content in mg Al/g plus 0.30 times the iron content in mg Fe/g. To minimize the

negative effect of mineral dissolution and residue-layer build-up on the performance of a limestone contactor during long-term operation, the iron and aluminum content should be less than this weighted sum.

9. The presence of silica as the principal impurity in the white marble sample (35 mass percent silica) did not appear to cause a reduction in the dissolution rate of the calcite surface. It simply reduced the effective surface area of the calcite in proportion to the mass of silica in the sample. The contactor design program DESCON reduces the carbonate mineral surface area according to the amount (mass percent) of silica in the stone.

10. The effect of temperature on the rate of dissolution of calcite was studied in the range of 5° to 25°C using one of the purer calcitic stone (94.5% $CaCO_3$). The dissolution rate decreased with decreasing temperature. The overall dissolution rate constant at 5°C was $0.38 \times 10^{-3}$ cm/s and $2.80 \times 10^{-3}$ cm/s at 25°C.

11. The heterogeneous reaction model was used with the overall dissolution rate constant versus temperature data to determine the apparent activation energy ($E_a$) for the surface reaction rate constant. The value determined, $E_a$ = 101 kJ/mol, is significantly greater than values in the literature (30 to 60 kJ/mol). The exact reason for this discrepancy is not known but could be attributed to compositional and crystallographic differences between the stones used in the studies compared.

12. The effective solubility product for calcium carbonate in limestone is an important parameter in the design program DESCON. Values of this parameter were determined using a number of the stone samples and a set of open-to-

atmospheric-$CO_2$, batch-reactor dissolution experiments. The results ranged from $K_{sp}$ = 1.5 x $10^{-9}$ to 6.3 x $10^{-9}$ (I=0, T=25°C) or $pK_{sp}$ = 8.20 to 8.81. In the solubility product experiments the final concentrations of magnesium were always significantly less than the final concentrations of calcium, even for the stones with the highest dolomite content. It is not known exactly why this occurred but it may be associated with the small amount of calcium dissolved per unit area of stone at equilibrium (≈ 0.5 mg Ca/$cm^2$). The incongruent dissolution of calcium from the dolomite surfaces may have been a factor. The magnitude of $K_{sp}$ for calcite did not seem to be affected by the amount of dolomite in the stone.

# CHAPTER 3
# RECOMMENDATIONS

1. It is not known to what extent, if any, biological films on the stone packing affect the performance of a limestone contactor. Limited data from laboratory and field investigations do not support a conclusion that biological films are a significant factor. Future study should examine the effect of biological film formation on the kinetics of mineral dissolution. Recent work sponsored by the American Water Works Association Research Foundation on bio-films in water treatment systems could provide a starting point.

2. It is well known that compounds such as orthophosphate adsorb on calcium carbonate surfaces and reduce the rate of mineral dissolution. Future study should determine if this phenomenon is an important consideration in limestone contactor design and operation.

3. While effective methods, such as the computer program DESCON, are available for limestone contactor design, the chemical and physical quantities needed as input to the program are sometimes difficult for potential users such as the officials of small communities and some state regulatory officials to determine. Also, some potential users do not have a personal computer. A future investigation might use the more detailed and exact design tools (such as DESCON) and practical ranges of input parameters (raw water chemistry, stone characteristics, etc.) to develop simple, conservative methods for contactor design.

4. Orthophosphate has been shown to be an effective additive for corrosion control in water distribution and home plumbing systems. Packed-bed contactors filled with slightly soluble phosphate-containing minerals should be investigated as devices for orthophosphate addition at small water supply systems.

5. Contactor treatment has the potential to be combined in one unit with other treatment processes such as slow sand filtration or packed-beds of metal oxides that adsorb natural organics. This is an interesting avenue for future research.

6. It is generally assumed that limestone contactor treatment is very cheap, however, accurate cost analyses have not been prepared. Future research should consider this.

# CHAPTER 4
# LITERATURE REVIEW

## 4.0 MINERAL AND LIMESTONE DISSOLUTION KINETICS

### 4.0.1 Introduction

Limestone dissolution kinetics is important in understanding problems such as geochemical weathering (Plummer and Wigley, 1976; Berner and Morse, 1974), the distribution of carbonate sediments in marine environments (Berner and Morse, 1974), flue gas desulfurization (Chan and Rochelle, 1982), the liming of acidified natural waters (Bjerle and Rochelle, 1982) and the design of limestone contactors. Limestone or calcite dissolution has been studied using rotating disks (Plummer et al., 1978; Sjöberg and Rickard, 1983), rotating cylinders (Wallin and Bjerle, 1989a; Schott et al., 1989), and agitated batch reactors containing crushed limestone particles (Plummer and Wigley, 1976).

The rate of carbonate mineral dissolution is determined by the physical and chemical characteristics of the stone, including the type and amount of impurities and the mineral crystallography. The chemistry and temperature of the solution are also important.

### 4.0.2 Impurities in Limestone

Natural limestones contain varying amounts of impurities (Boynton, 1980). Impurities can be classified as either homogeneous or heterogeneous. Homogeneous impurities are usually silt, sand or clay (or other forms of silica such as quartz) that entered the stone when it was first deposited and are therefore uniformly distributed throughout the formation. Heterogeneous

impurities are contaminants that have accumulated between the strata or are loosely embedded in the stone.

The most common impurities in limestone are silicon and aluminum followed by iron. Silicon is usually present as silica or with aluminum in alumino-silicate minerals. Aluminum may also be present as alumina. Iron may exist as an iron carbonate or iron oxide, distributed heterogeneously from minerals such as pyrite or limonite. Other, usually much less significant, contaminants include manganese, copper, titanium, sodium and potassium (Boynton, 1980).

Murray et al. (1954) analyzed 45 high-calcium limestone samples and found measurable amounts of silica, alumina, and magnesium oxide in each of them. Potassium, sodium and sulfur were detected in some samples. A spectrographic analysis of 25 of the 45 samples indicated that iron, barium, strontium and tin were also present.

Relatively pure limestones tend to develop a thin, light-covered crust when weathered. Impure varieties, especially those containing iron, weather yellowish or brown, and if there is much clay or sand, an obvious crust is formed. According to North (1930), weathering involves the removal to solution of the calcium carbonate fraction of the stone and, if much insoluble material is present, it tends to remain behind, forming a superficial layer usually different in color from the unweathered rock.

### 4.0.3 Mathematical Models of Dissolution Kinetics

A number of models have been developed for predicting the rate of calcium carbonate dissolution in aqueous systems. Some of these are entirely empirical (Sjöberg, 1976), and some have a partial basis in fundamental principles (Plummer et al., 1979; Bjerle and Rochelle, 1984). The potential for transport control of calcite dissolution has been recognized by many investigators (King and Liu, 1933; Tominaga et al., 1939; Kaye, 1957; Weyl, 1958; Nierode and Williams, 1971; Berner and Morse, 1974; Lund et

al., 1975; Plummer and Wigley, 1976; Bjerle and Rochelle, 1984; Chan and Rochelle, 1982; Wallin and Bjerle, 1989b; Haddad, 1986). There is some agreement that in neutral to alkaline solutions the dissolution of calcite is controlled by mixed kinetics in which the rate depends on both a surface chemical reaction and the transport of reactants and/or products to or from the reaction sites (Sjöberg and Rickard, 1983, 1984a,b, 1985; Berner and Morse, 1974; Plummer et al., 1978; Compton and Daly, 1984). Haddad (1986) concluded that predicting the rate of calcitic limestone dissolution in a packed-bed contactor requires knowledge of both the hydrodynamic mass transport properties of the mineral-water system and the kinetics of the heterogenous reaction at the calcite surface.

Most existing models of calcite dissolution are based on results obtained using large crystals of essentially pure calcite. For example, a number of studies have been done with Iceland spar. The direct application of these results to the dissolution of calcite crystals in limestone is questionable. Differences between limestone and pure calcite that may affect dissolution kinetics include: (a) impurities in the limestone such as silica, aluminum and iron, (b) crystal growth histories and defects, and (c) crystal grain sizes.

### 4.0.4 Effect of Stone Composition and Crystallography on Dissolution Kinetics

The effect of impurities on the dissolution rate of limestone has not been studied extensively. Research on silicate weathering has revealed the existence of a surface leached layer (Holdren and Berner, 1979; Schott et al., 1981; Berner and Schott, 1982; Schnoor, 1989). Studies of feldspar weathering by Chou and Wollast (1984) show the formation of a residue layer consisting mainly of aluminum and silica at the mineral surface. The rate of weathering of feldspar was found to be controlled by the existence and properties of the residue layer. As the layer increased in thickness, the rate of dissolution decreased rapidly

until it reached a quasi-steady state value. The quasi-steady state condition, it was suggested, is due to a balance between the rate of dissolution of the fresh feldspar (which depends on the diffusion of reactants and products through the residue layer) and the rate of dissolution of the residue layer. Schnoor (1989) has called this phenomenon "initial incongruent dissolution".

Weathering experiments by Sverdrup (1990) indicated that the dissolution rate of minerals containing aluminum, like feldspar, biotite and anorthite, is affected by the presence of aluminum if the solution aluminum concentration is greater than some limiting value. According to Sverdrup (1990), when aluminum is produced by chemical reaction at the mineral surface this rate is determined by the aluminum concentration gradient from the particle surface to the bulk solution. Sverdrup (1990) suggests that a similar mechanism could apply to cations such as Ca, Mg, K, Na, Fe, and Si that are released from the mineral surface during dissolution.

Differences in surface defect density, kink and step density, and the number of edges and corners per unit volume of a mineral can all combine to bring about significant differences in dissolution kinetics (Burton et al., 1951). For calcite this problem was addressed by Schott et al. (1989) who studied the dissolution of Iceland spar (high purity calcite) using rotating cylinders strained to a high defect density. They proposed that dissolution occurs preferentially at active sites such as lattice defects. Minerals with greater defect densities dissolve faster since their effective surface areas are greater than more perfect specimens of the same compound.

Compton and Daly (1984) found the rate of dissolution of Iceland spar was sensitive to the method of surface preparation. Surfaces obtained by misorienting the crystal face provided more sites at which dissolution could occur and thus dissolved faster than surfaces with ordinary cleavage planes.

Compton, Daly and House (1986) have shown that the dissolution rate of Iceland spar is influenced by surface

morphology and the method used to prepare the surface of the stone sample. Freshly cleaved crystals were essentially unreactive, but surfaces obtained by misorienting the crystal faces dissolved faster than the ordinary cleavage planes because, it was assumed, these provide more terrace sites at which dissolution can occur.

The relationship between dissolution rate and particle grain size for alkali feldspars was studied by Holdren and Speyer (1985, 1987). They observed that the dissolution rate increased linearly with decreasing grain size down to a critical range (approximately 50-100 μm). In this range, they hypothesized, the grain size and distance between adjacent reactive sites become roughly equivalent. For grain sizes below the critical region, rate and reactant surface area were not related, however, the rates for larger grain size minerals were reported as rates per unit area, where rate and area had a linear relationship.

The dissolution of dolomitic limestones ($CaMg(CO_3)_2$) was studied by Plummer and Busenberg (1982) in $CO_2$-$H_2O$-acid systems using a temperature range of 1.5 to 65°C. Their results show that in the early stages of dissolution the $CaCO_3$ component of dolomite dissolves faster than the $MgCO_3$ component, forming a Mg-enriched surface. After the initial period of enhanced $CaCO_3$ dissolution, Ca and Mg ions were released stoichiometrically.

Pure dolomite dissolves more slowly than pure calcite (Rauch and White, 1977; Palmer, 1991). In stones that are a mixture of $CaCO_3$ and dolomite, the dissolution rate has been shown to decrease in a regular way with increasing dolomite content of the rock (Rauch and White, 1977).

Herman and White (1985) studied the dissolution of dolomite samples and concluded that the dissolution rate increases with decreasing grain size. However, the difference between the initial rate of dissolution for a large single rhomb of dolomite and a microcrystalline rock was only a factor of 1.5.

4.0.5 Effect of Temperature on Dissolution Kinetics

The effect of temperature on the dissolution kinetics of limestones has received limited study. Rickard and Sjöberg (1983) showed that the experimentally observed rate constant for the dissolution of calcite in aqueous solutions is controlled by a surface reaction and a mass transfer resistance that act in series. They therefore concluded that the overall dissolution rate constant is likely to be a complex function of the temperature.

The temperature dependence of rate constants for heterogeneous reactions is usually quantified using the Arrhenius equation, i.e.,

$$\ln k = E_a/RT + \ln A \qquad (1)$$

where $E_a$ is the apparent activation energy, R is the gas constant (8.314 J $mol^{-1}K^{-1}$), k is the dissolution rate constant at the absolute temperature, T, and A is a constant.

The apparent activation energies for heterogeneous reactions have been used to discriminate between reactions showing transport control, surface chemical reaction control or mixed kinetics. The magnitude of $E_a$ for reactions controlled by transport processes is typically much less than values for surface and homogeneous chemical reactions, e.g., 10 to 20 kJ/mol versus 30 to 100 kJ/mol.

Rickard and Sjöberg (1983) concluded that at 25°C the rate of calcite dissolution in the $H^+$-dependent regime is controlled by mass transfer, which they assumed to be the diffusion of $H^+$ from the bulk solution through the mass transfer boundary layer to the stone surface. In the $H^+$-independent regime the surface chemical reaction controls and in the transition region between these limits the kinetics is a function of both the surface reaction and mass transfer. Lower temperatures cause the surface chemical reaction rate constant to become smaller and the extent of the transition region expands into the $H^+$-dependent region.

Lund et al., (1975) used a rotating cylinder to study the rate of dissolution of calcite in hydrochloric acid. The dissolution rate was limited by mass transfer at 25°C, even at high cylinder rotational speeds. At -15.6°C both mass transfer and surface reaction resistances were important.

4.0.6 Effect of Trace Species in Solution on Dissolution Kinetics

Another important factor that may affect the dissolution rate of calcite is the presence of trace species in solution that adsorb on the mineral surface. Inhibition can occur at very low levels of trace species as demonstrated by the strong retarding effect on calcite dissolution of micromolar concentrations of dissolved $Sc^{+4}$ (Terjesen et al., 1961) and orthophosphate (Berner and Morse, 1974). While modeling limestone dissolution in soils, Warfvinge and Sverdrup (1989) found that the rate of deactivation due to adsorbed impurities on the limestone surface had a significant influence on the model calculations. Fresh calcite was coated with rust colored precipitates when exposed to soil solutions or surface waters containing iron and dissolved organic carbon.

## 4.1 MODELING CALCITE DISSOLUTION IN LIMESTONE CONTACTORS

Haddad (1986) described the dissolution of calcite in limestone contactors by adapting the rate model derived by Rickard and Sjöberg (1983). Rickard and Sjöberg's model assumes that the dissolution of calcium carbonate in acidic solutions is controlled by a heterogenous reaction (see Appendix A), the rate of which is determined by a mass transfer resistance and a surface reaction acting in series. According to this assumption, the rate of calcium carbonate dissolution, r, is given by,

$$r = k_o \, a \, (C_{eq} - C) \qquad (2)$$

where $C_{eq}$ and C are the equilibrium and bulk fluid calcium ion concentrations, respectively, and a is the interfacial area of

calcium carbonate per unit volume of fluid. $k_o$ is the overall dissolution rate constant and is given by,

$$k_o = [(1/k_L) + (1/k_c)]^{-1} \quad (3)$$

where $k_L$ is the mass transfer rate constant for the calcium ion and $k_c$ is the first order surface reaction rate constant.

For a limestone contactor $C_{eq}$ is a function of the chemistry and temperature of the untreated water. In this study it was calculated using the chemical equilibrium model described in Appendix B, Equations 7B-9B. The quantity a is the interfacial area of calcium carbonate per unit volume of interstitial water and, for a limestone contactor with stone that is essentially 100 percent $CaCO_3$, is given by,

$$a = 6(1-\epsilon)/(d\epsilon\Psi) \quad (4)$$

where d and $\Psi$ are the volume-mean diameter and sphericity of limestone particles and $\epsilon$ is the bed porosity.

According to Haddad (Haddad, 1986; Letterman et al., 1991), for a packed bed of crushed limestone, the magnitude of $k_L$ can be determined using equations derived by Chu et al. (1953). Equation 5 was used for values of the modified Reynold's number (MRe) in the range $1 \leq MRe \leq 30$,

$$k_L = 5.7\ U_s\ (MRe)^{-0.87}\ (Sc)^{-2/3}, \quad (5)$$

and Equation 6 was used for values in the range $30 \leq MRe \leq 10{,}000$,

$$k_L = 1.8\ U_s\ (MRe)^{-0.44}\ (Sc)^{-2/3} \quad . \quad (6)$$

The modified Reynold's number is given by,

$$MRe = dU_s\ /(\nu(1-\epsilon)) \quad (7)$$

and the Schmidt number, Sc, by,

$$Sc = \nu/D \qquad (8)$$

where $\nu$ is the kinematic viscosity, D is the calcium ion diffusivity and $U_s$ is the superficial velocity of the fluid.

Haddad (1986) assumed that the magnitude of $k_c$ is determined by the chemistry of the solution at the $CaCO_3$ surface and used data from Sjöberg and Rickard (1984) to derive the following empirical relationship,

$$k_c \text{ (cm/s)} = 1.6 \times 10^{14} \{H_{eq}\}^{1.7} \qquad (9)$$

where $\{H_{eq}\}$ is the interfacial (equilibrium) hydrogen ion activity. In this study the magnitude of $\{H_{eq}\}$ was calculated with the chemical equilibrium model (Appendix B, Equations 7B-9B) and is related to the equilibrium calcium ion concentration ($C_{eq}$).

Haddad (1986) used the following version of the continuity equation to model the limestone dissolution process in a contactor operating at steady-state,

$$N_D \, d^2C/dZ^2 - \epsilon \, dC/dZ + r\Theta = 0 \qquad (10)$$

where $N_D$ is the dimensionless axial dispersion number, C is the calcium ion concentration, Z is the dimensionless depth, $\Theta$ is the mean fluid residence time and r is the calcium dissolution rate expression. Equation 2 was substituted for r into Equation 10 and the resulting expression was integrated over the depth of the column to obtain,

$$(C_{eq}-C_{bL})/(C_{eq}-C_{bo}) = \exp\{-k_o a L \epsilon/U_s + (k_o a L \epsilon/U_s)^2 \, N_D\} \qquad (11)$$

where $C_{bo}$ and $C_{bL}$ are the influent and effluent calcium concentrations and L is the overall depth of the contactor. This

equation assumes that the rate of dissolution at any point in the bed is constant with time and, therefore, factors such as residue layer formation and limestone particle shrinkage are insignificant. Haddad (1986) derived the following approximate equation for $N_D$ using data from a tracer response study,

$$N_D = 2(d/L). \qquad (12)$$

Equations 3 through 9 and 11 and 12 effectively predict the initial performance of a contactor filled with fresh limestone (Letterman et al., 1991). However, when an experimental contactor filled with limestone from Boonville, New York (the quarry where the SL sample of this study was taken) was operated continuously for several months, Haddad (1986) observed that the effluent pH and calcium ion concentration decreased with time (see Figure 4.1.1). Curve A was obtained using the steady state model, curve B is the simulation of non-steady-state when the stone diameter decreases and curve C is the simulation when stone diameter decreases and residue layer forms. The discrepancy between the values predicted by the steady-state model and the measured values increased with time.

Haddad (1986) used the steady-state model (Equations 3-9 and 11-12) to develop a time-step simulation program for predicting the performance of contactors during the non-steady-state behavior of long term operation. In this program the operational period is divided into short time intervals and the contactor bed is divided into thin layers. The steady-state model predicts the amount of calcium dissolved from each layer during each interval of time. After each interval, a new stone diameter is calculated for each of the layers using the amount of calcium dissolved. The results obtained from this simulation program showed that shrinkage of the limestone particles explained some but not all of the decrease in performance observed by Haddad in his long term column experiment (Curve B, Figure 4.1.1).

Haddad (1986) used x-ray energy spectroscopy to analyze the

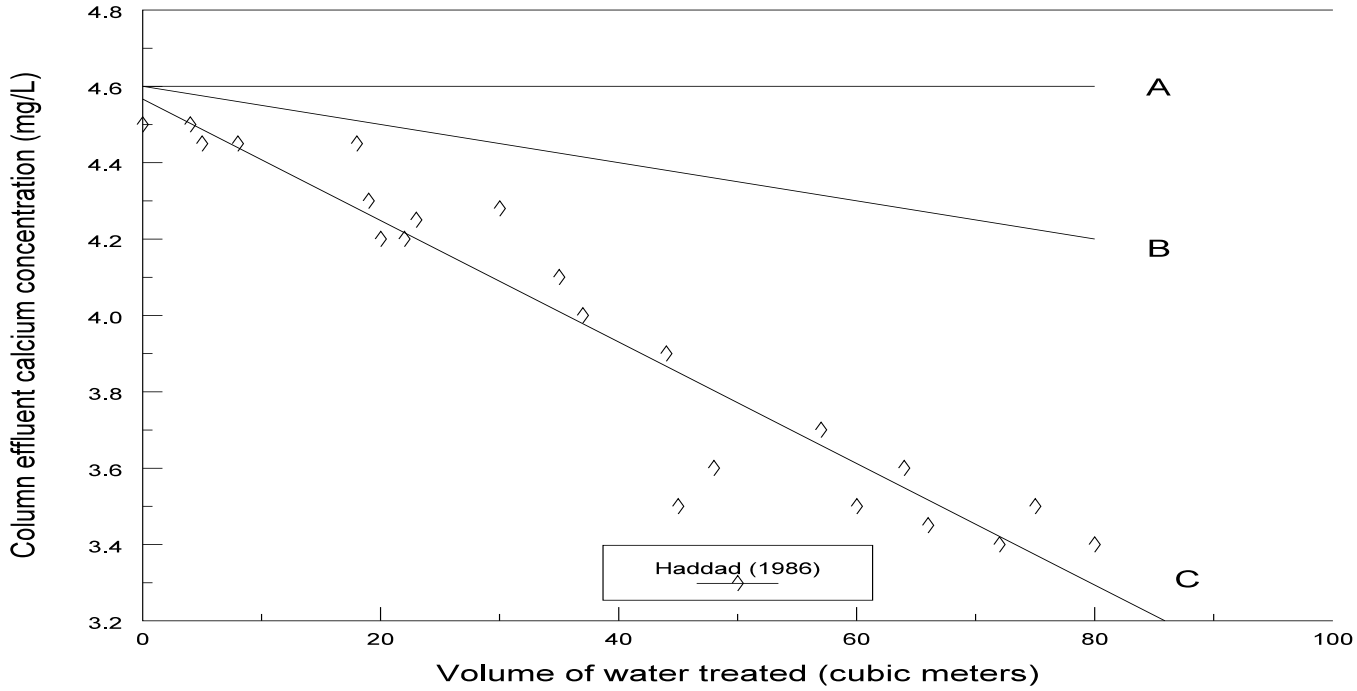


Figure 4.1.1 Calcium concentration is plotted as a function of volume water treated, using data from Haddad (1986).

surface of limestone particles from the contactor used in the long term experiment. He observed that the surface density of aluminum, silica and iron had increased during the experiment and concluded that a "residue layer" had formed as the $CaCO_3$ dissolved from the limestone matrix. As the residue layer increased in thickness, he assumed, it limited the transport of calcium ion away from the surface of the limestone and slowed the rate of dissolution.

The transport of calcium ions across the residue layer was modeled using,

$$k_f = D\epsilon_r/(\delta\tau_r) \qquad (13)$$

where $k_f$ is the residue layer mass transfer coefficient, $\epsilon_r$ and $\delta$ are the porosity and thickness of the residue layer, D is the diffusivity of the calcium ion in the bulk solution, and $\tau_r$ is the pore length (tortuosity) factor. An expression for $\delta$ was derived by assuming that the thickness of the residue layer was much less than the diameter of the particle and that it increased as calcium dissolved from the surface of the limestone, i.e.,

$$\delta = [M(1-ß)(f)]/[0.4ß\rho_s(1-\epsilon_r)] \qquad (14)$$

where M is the cumulative mass of calcium dissolved per unit area of stone, ß is the mass fraction of $CaCO_3$ in the stone, $\rho_s$ is the mass density of the residue solids and f is the fraction of the total residue solids that remains on the stone surface.

The following equation for $k_f$ is obtained by substituting Equation 14 into Equation 13,

$$k_f = 0.4ßDK/[M(1-ß)]. \qquad (15)$$

The coefficient K in Equation 15 includes all the parameters that Haddad (1986) could not measure experimentally and is given by,

$$K = \rho_s(1-\epsilon_r)(\epsilon_r)/[(f)(\tau_r)]. \qquad (16)$$

The residue layer mass transfer coefficient, $k_f$, was included in the calculation of the overall dissolution rate constant by expanding Equation 3 as follows,

$$k_o = [(1/k_L) + (1/k_c) + (1/k_f)]^{-1}. \qquad (17)$$

Haddad calibrated the non-steady-state simulation program (with the residue layer resistance) by finding that K = 0.6 gave good agreement between the measured and model predicted effluent calcium concentrations. This value of K was in reasonable agreement with a value of K calculated using rough estimates of the magnitudes of the parameters in Equation 16.

# CHAPTER 5
# EXPERIMENTAL METHODS AND MATERIALS

## 5.0 EXPERIMENTAL MATERIALS

The study was conducted using 13 samples of limestone including a white marble (sample WM) from a quarry in Proctor, Vermont, a sedimentary limestone (sample SL) from a quarry near Boonville, New York, Black River limestone (sample BR) from a quarry near Watertown, New York and 10 samples (samples A-J) from a dolomite quarry near York, Pennsylvania.

The SL stone was selected for the study because it is from the quarry where Haddad (Haddad, 1984, 1986; Letterman et al., 1991) obtained his samples. The Vermont marble sample (sample WM) was used to compare the behavior of marble with that of sedimentary limestones. The Black River limestone was selected because of its unusual black color. A black color in limestone is usually caused by small amounts of organic material (Boynton, 1980). The 10 samples from the dolomite quarry in Pennsylvania were selected to study the effect of the dolomite content on dissolution kinetics. The dolomite content of these stones ranged from essentially zero to 100 percent. Their physical and chemical characteristics are discussed below.

### 5.0.1 Limestone - Physical Characteristics

A qualitative assessment of the mineral content of five of the limestone samples (samples WM, SL, C, F and I) was made by observing thin sections of stone under polarized light using a Zeiss petrographic microscope. The thin sections were prepared by gluing samples of stone to a glass slide and then cutting and grinding them to a thickness of about 3 microns. Photomicrographs

of the sections are shown in Figures 5.0.1-5.0.5. According to this analysis the WM sample consisted of coarse grains of calcium carbonate and included about 20% quartz. The SL sample was gray in color and fine-grained. The photomicrograph of the SL sample (Figure 5.0.2) shows that this stone was derived from calcareous mud called micrite (microcrystalline calcite). Some fossil debris and small quartz grains are evident in the sample.

Figure 5.0.3 shows that stone I is a high magnesium calcite dolomicrite. It is finely crystalline and brecciated and consists of angular fragments up to 50 mm wide separated by thin calcite cemented fractures. In sample C (Figure 5.0.4) calcite has cemented and replaced dolomicrite breccia. This sample is similar to sample I except that calcite has replaced dolomite in large areas as well as in the fractures. Sample F (Figure 5.0.5) is a low magnesium limestone. It has finely crystalline micrite with

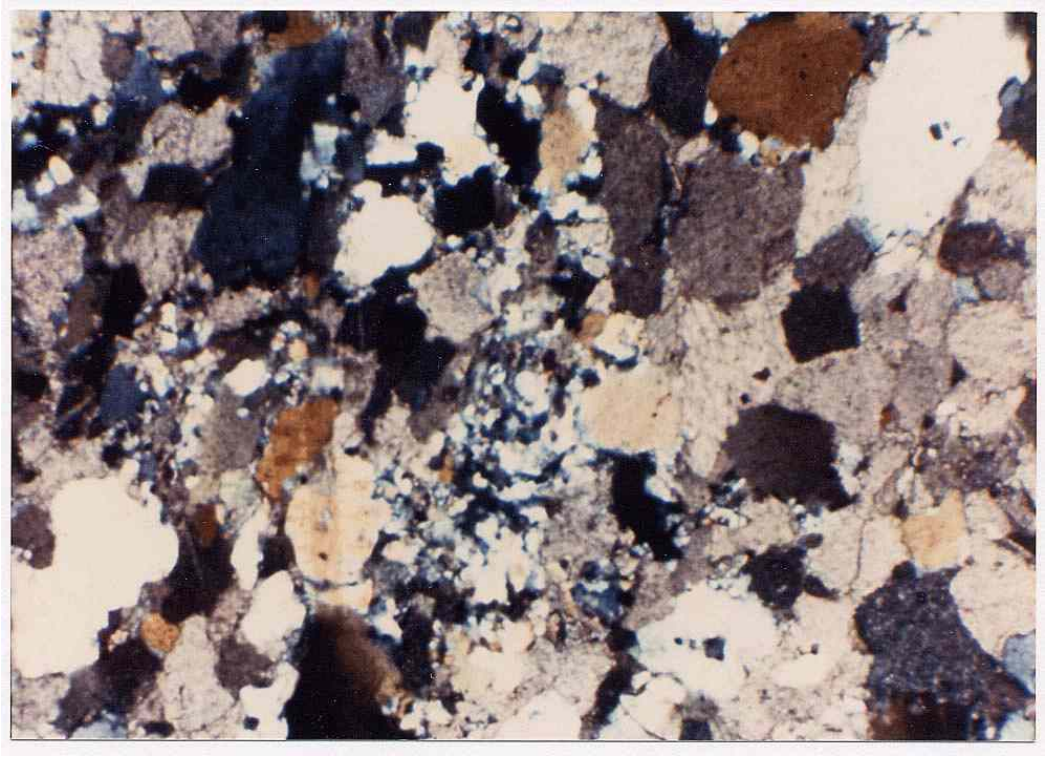

Figure 5.0.1 Photomicrograph of a thin section cut from undissolved stone sample WM.

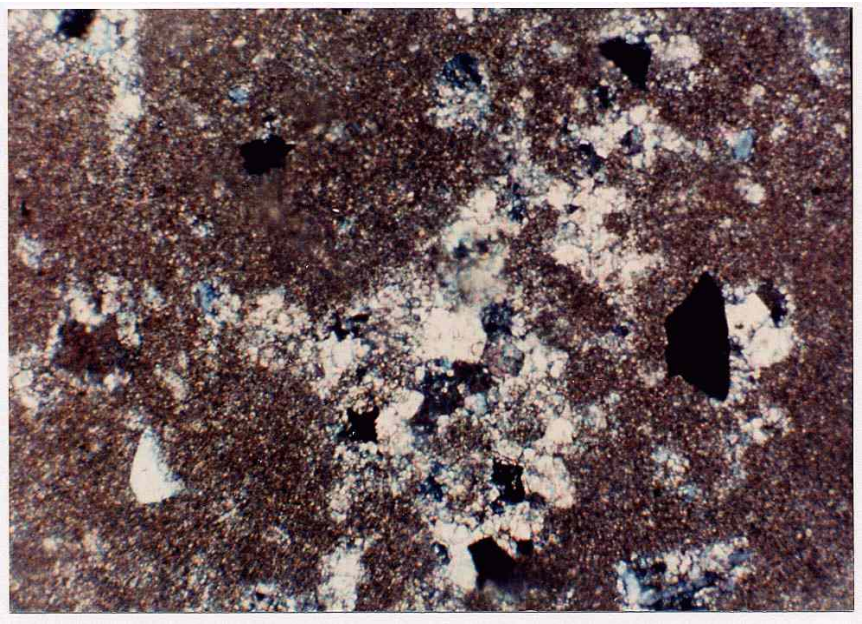

Figure 5.0.2 Photomicrograph of a thin section cut from undissolved stone sample SL.

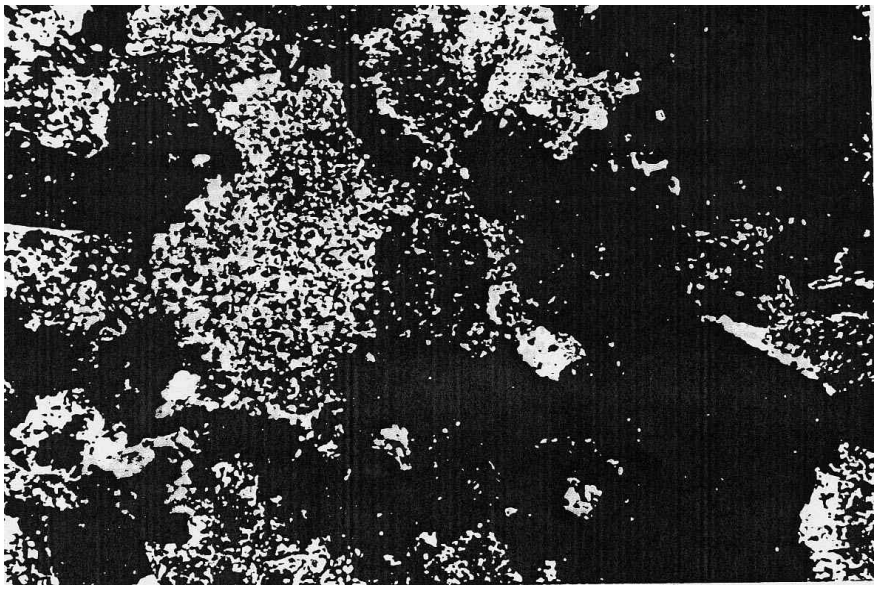

Figure 5.0.3 Photomicrograph of a thin section cut from undissolved stone sample C.

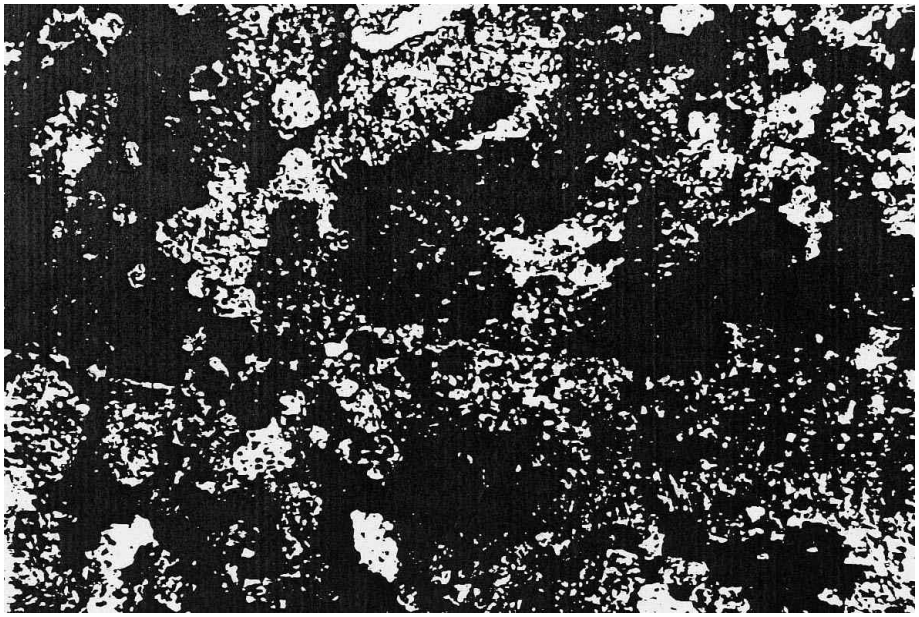

Figure 5.0.4 Photomicrograph of a thin section cut from undissolved stone sample F.

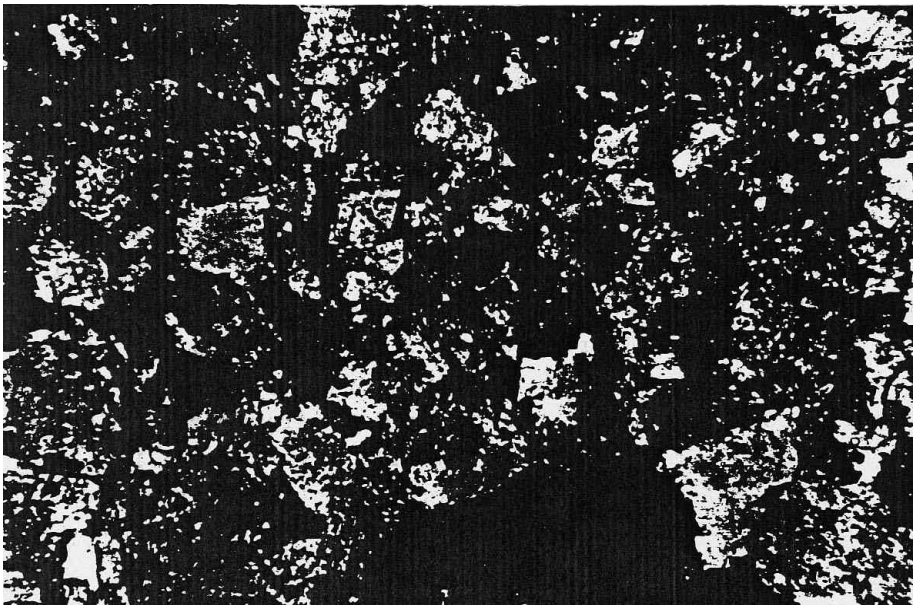

Figure 5.0.5 Photomicrograph of a thin section cut from undissolved stone sample I.

fossil forminifera and some blocky secondary calcite. X-ray diffraction analysis was done on stones samples I, C and F using a Philips APD 3520 x-ray diffraction apparatus. According to the results in Figure 5.0.6, the 2Θ angle for calcite is 29.55 degrees for samples C and F and 29.5 degrees for sample I. The dolomites are ordered and the 2Θ angle is 31.5 degrees for samples C and F and 31.1 for sample I. According to Figure 5.0.6, stone I is essentially dolomite, stone C is dolomicrite and stone F is low magnesium calcite.

5.0.2 Limestone - Chemical Characteristics

Samples of each of the stones (BR, SL, WM and A-J) were powdered using a mortar and pestle. The stone samples were core sections that had been located next to the wafers cut for the rotating disk apparatus. A 0.1 g quantity of each powdered sample was dissolved in concentrated hydrochloric acid overnight. For a number of the samples some translucent material, probably quartz, remained after 2 days of dissolution. The acidified samples were then diluted to 50 mL using DI water. After 2 days, 1 mL of the sample solution was diluted to 50 mL with DI and duplicates of both the diluted and undiluted samples were analyzed with a Perkin Elmer Model PE 3030B atomic absorption spectrophotometer (AAS). The calcium, magnesium, iron and aluminum content of the samples was determined by averaging the duplicate measurements for the diluted samples. The results are listed in Table 5.0.1.

The atomic absorption spectrophotometer was calibrated using 1000 ppm Ca, Mg, Al and Fe reference solutions (certified Fisher Scientific atomic absorption standards). For Ca and Mg, interference from phosphates, silica, and aluminum was minimized by adding 1% lanthanum chloride (1 mL $LaCl_2$ solution to 10 mL solution) to the standards and samples. The AAS was operated using a wavelength of 422.7 nm and a slit width of 7 nm (normal).

The Ca, Mg, Fe and Al results for samples A-J (Table 5.0.1) were compared with measurements made by the quarry in York, PA that had sent the cores. The quarry's results and the values

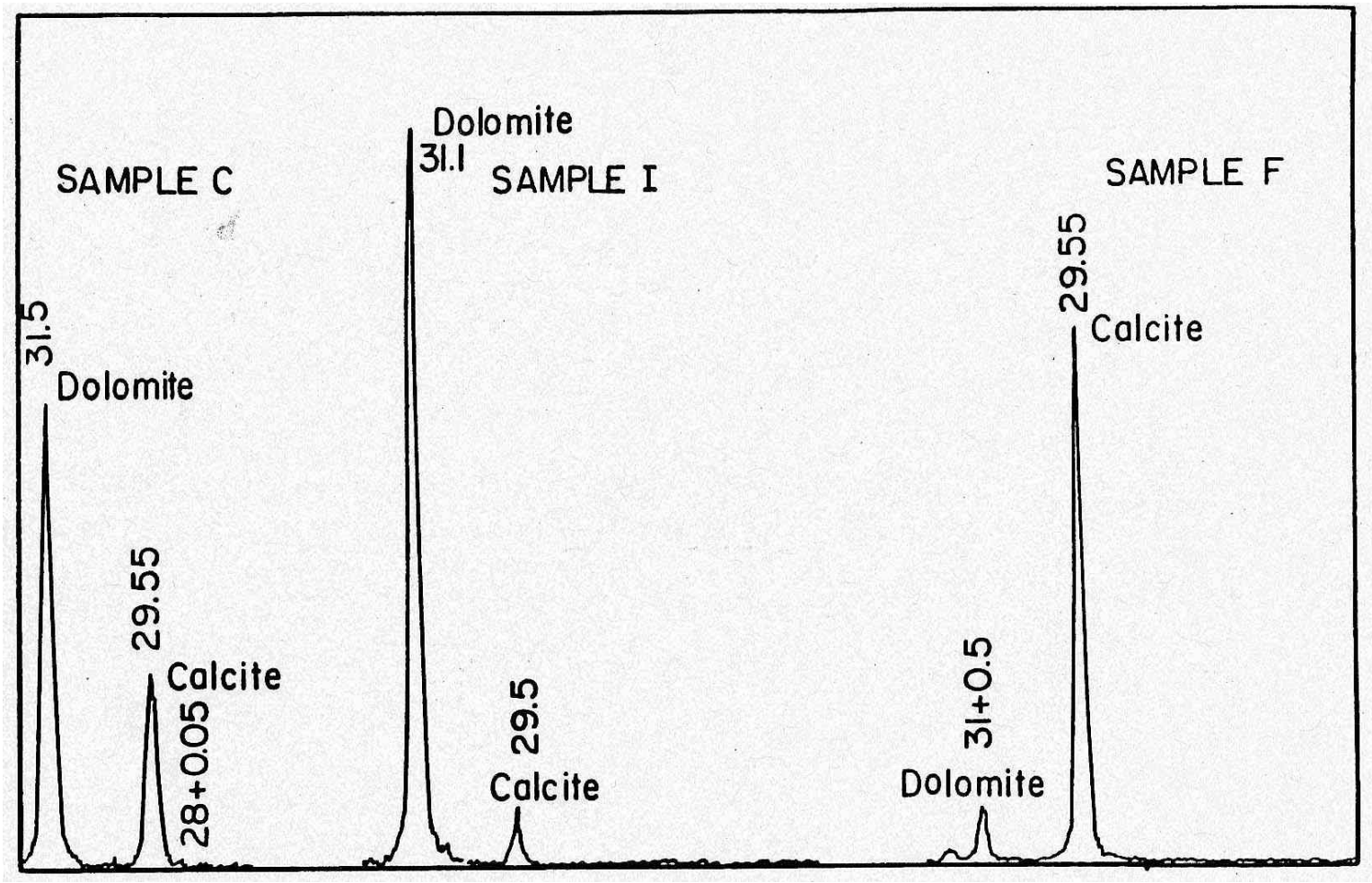


Figure 5.0.6 X-ray diffraction analysis results for undissolved stone samples C, F and I.

Table 5.0.1 RESULTS OF STONE ANALYSIS

| Limestone Composition (g/100g) | | | | |
|---|---|---|---|---|
| Stone ID | Ca | Mg | Fe | Al |
| WM | 25.6 | 0.09 | 0.071 | 0.034 |
| SL | 37.5 | 0.49 | 0.101 | 0.114 |
| BR | 40.0 | 0.23 | 0.019 | 0.044 |
| | | | | |
| A | 39.0 | 2.1 | 0.024 | 0.012 |
| B | 37.8 | 0.58 | 0.029 | 0.001 |
| C | 21.2 | 8.9 | 0.189 | 0.093 |
| D | 35.4 | 2.3 | 0.040 | 0.037 |
| E | 34.6 | 3.8 | 0.041 | 0.025 |
| F | 37.5 | 1.1 | 0.015 | 0.005 |
| G | 22.0 | 7.8 | 0.294 | 0.129 |
| H | 26.8 | 7.0 | 0.154 | 0.134 |
| I | 23.6 | 12.2 | 0.377 | 0.032 |
| J | 19.4 | 13.6 | 0.189 | 0.010 |

listed in Table 5.0.1 were compared using the mean relative difference parameter (MRD), $\Sigma\{(|Q_i-S_i|)/[(Q_i+S_i)/2]\}$, where $Q_i$ is the quarry's result for a given element and a given sample and $S_i$ is the corresponding value from Table 5.0.1. The MRD values were 10% for calcium, 45% for magnesium, 56% for iron and 136% for aluminum. It could not be determined if the quarry's analytical samples were from the same location in each core as the ones sent, therefore, it is likely that the higher values of the MRD for Al and Fe, and to a certain extent for Mg, reflect spatial differences in the Al, Fe, and Mg content of the stone.

The analytical results listed in Table 5.0.1 were used to estimate the calcite, dolomite and insoluble residue content of the samples. In these calculations the magnesium was assumed, based on the x-ray diffraction and thin-section photomicrography results, to be associated only with dolomite. The dolomite

content in grams per 100 grams was calculated using the magnesium concentration from Table 5.0.1, $C_{Mg}$, and

$$\text{dolomite content} = C_{Mg} \times (184.3/24.3) \qquad (18)$$

The calcite content was determined by subtracting the calculated amount of calcium in the dolomite from the total amount of calcium in the sample, $C_{Ca}$, listed in Table 5.0.1, i.e.,

$$\text{calcite fraction} = [(C_{Ca} - (C_{Mg} \times 40/24.3)] \times (100/40) \qquad (19)$$

The insoluble residue was assumed to be the mass fraction of the stone not attributable to either calcite or dolomite,

$$\text{insoluble residue} = 100\text{g}/100\text{g} - (\text{calcite} + \text{dolomite}) \qquad (20)$$

The results of these calculations are listed in Table 5.0.2. In several cases, as a result of measurement error, the sum of the calcite and dolomite fractions is greater than 100g/100g of stone. In these cases the insoluble residue content was set equal to zero.

The results in Tables 5.0.1 and 5.0.2 indicate that samples WM, SL and BR as well as a number of the samples from the York, Pennsylvania dolomite quarry (samples A, B, D, E and F) are high calcium limestones. A number of the York samples (samples C, G, H, and I) are predominately dolomite and sample J is essentially pure dolomite.

The WM sample had the highest insoluble residue content (36 g/100g) but relatively low amounts of iron and aluminum (34 mg Al/100g and 71 mg Fe/100g of stone). It is likely that the insoluble residue in this sample is quartz. Sample I, from York, Pennsylvania, had the highest amount of iron (377 mg Fe/100g) and sample H had the highest amount of aluminum (134 mg Al/100g).

Table 5.0.2 ESTIMATED MINERAL CONTENT OF THE STONE SAMPLES

| Major Stone Constituents (g/100g) | | | |
|---|---|---|---|
| Stone ID | Calcite | Dolomite | Insoluble |
| WM | 64 | 1 | 35 |
| SL | 92 | 4 | 4 |
| BR | 99 | 2 | 0 |
| | | | |
| A | 89 | 16 | 0 |
| B | 92 | 4 | 4 |
| C | 17 | 68 | 15 |
| D | 79 | 18 | 3 |
| E | 71 | 29 | 0 |
| F | 89 | 9 | 2 |
| G | 23 | 59 | 18 |
| H | 38 | 53 | 9 |
| I | 9 | 93 | 0 |
| J | 0 | 100 | 0 |

5.0.3 Rotating Disk Solution Characteristics

All solutions used in the rotating disk experiments were made with distilled and deionized (DI) water that had been boiled for a few minutes, several hours before use, to remove carbon dioxide. Fisher analytical grade (ACS Certified) chemicals were used (KCl, N/10 HCl). The background electrolyte was 0.079 M KCl.

5.1 ROTATING DISK APPARATUS

Transport to or from a rotating disk in a batch reactor is affected by the disk diameter, the vessel size and geometry, and the disk rotational speed. According to Riddiford (1966), the disk radius, $r_0$, should be much greater than the thickness of the diffusion boundary layer at the face of the disk, i.e,

$$(2.8/r_0)(\nu/\omega)^{1/2} \leq 0.03 \qquad (21)$$

where $\nu$ is the kinematic viscosity in $cm^2/sec$ and $\omega$ is the angular velocity in radians/sec.

The condition expressed by Equation 21 was met in all experiments by choosing a disk diameter of 4.45 cm.

According to Riddiford (1966) the effect of the vessel walls on fluid motion at the disk is minimized if the minimum distance between the rotating disk and the walls of the reactor is greater than 0.5 cm. In this apparatus the reactor diameter was 14 cm and the clearance between the disk and the walls of the vessel was greater than 4 cm. The disk was centered about 3 cm above the bottom of the vessel (see Figure 5.1.1).

The disk was rotated by an adjustable-speed, DC motor. A bench tachometer (Amtek Model 1723) was used to set and monitor the rotational speed which was varied over the range 200 to 1200 rpm.

The reactor was constructed with double glass walls. A Haake Model A80 water bath was used to circulate water between the walls to maintain the reactor contents at preselected temperatures in the range 4 to 25 ± 0.2°C. The plexiglass cover on the reactor had holes for the insertion of the rotating shaft, pH electrode and wetted nitrogen inlet tube. Additional holes were provided for measuring the temperature and pipetting samples for the calcium measurement.

The pH was measured using a Ross "Sure-Flow™" combination pH electrode (Orion) connected to an Orion Expandable Ion Analyzer, Model EA940. The bulb of the pH electrode was located 1.5 cm from the rotating disk and 3 cm above the bottom of the vessel. To monitor the pH measurements, the ion analyzer was interfaced with a microcomputer.

### 5.1.1 Stone Disk Preparation

The SL sample was prepared by cutting a 3.10 cm diameter, cylindrical core from a piece of rock collected at the quarry. The WM and BR samples were cut from existing 3.68 cm and 2.45 cm

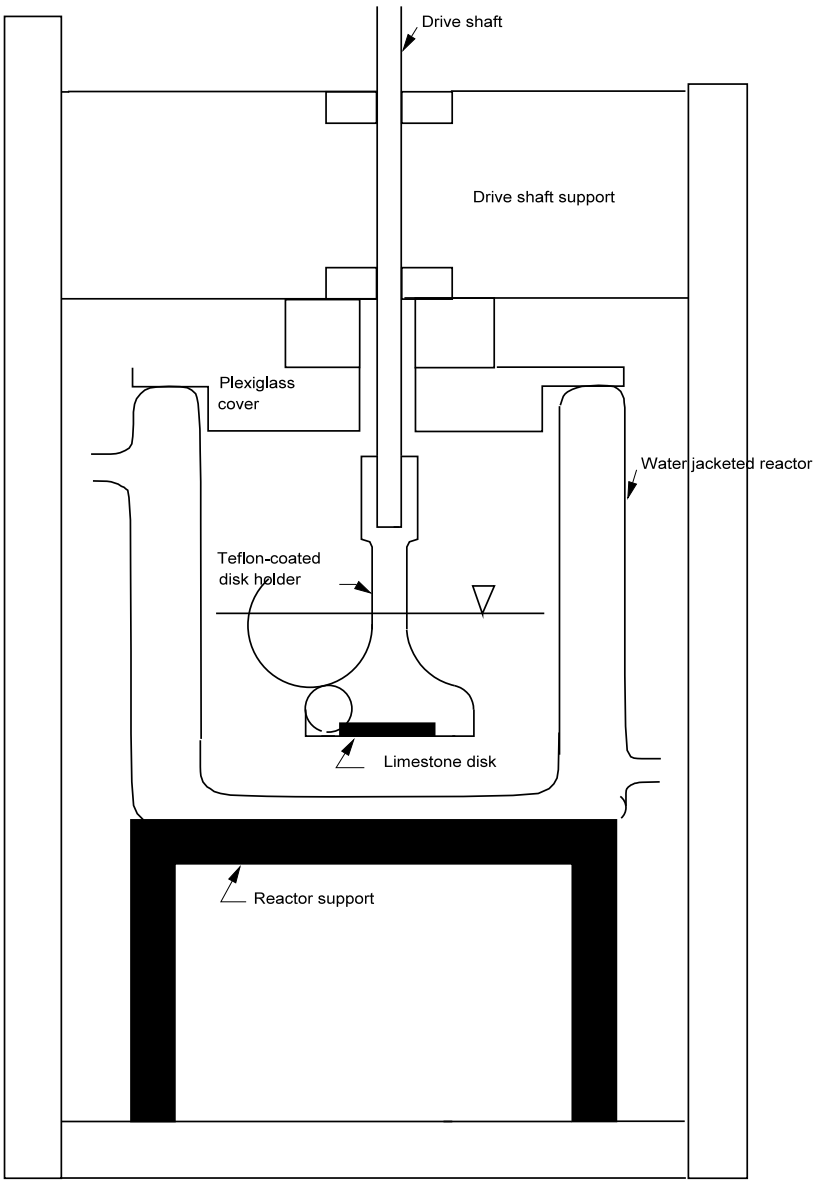


Figure 5.1.1 Schematic diagram of the rotating disk apparatus

diameter cores, respectively. The ten samples from the York, Pennsylvania quarry were cut from existing 3.65 cm diameter cores. Each core was cut into a number of 3 mm thick disks using a rock saw. The disk faces were smoothed and polished on a lapwheel using 400 (38 micron) and then 600 (25 micron) grit size

silicon carbide.

The back face and edge of the disks were coated with plastic so that only the polished face was available for dissolution. Each disk was mounted in a teflon-coated brass holder as shown in Figure 5.1.1. The WM sample and samples A-J were glued, as is, in the 3.7 cm diameter x 4 mm deep well in the bottom of the holder. For the 3.1 cm diameter SL and the 2.45 cm diameter BR samples, 3 mm thick plexiglass rings were used as fillers to center the stone disks in the holder.

## 5.2 EXPERIMENTAL PROCEDURE

A free-drift method, in which the pH was allowed to increase as the carbonate minerals dissolved from the stone, was used in all experiments. Each experimental solution (600 mL) was prepared as needed by adding KCl and the required volume of acid to boiled water and then transferring this to the reactor.

Ultra-pure nitrogen gas, saturated with water vapor, was bubbled continuously through the solution for a few minutes before the experiment was started. During the experiment, humidified nitrogen flowed through the headspace above the solution to minimize exchange of $CO_2$ with the atmosphere. The nitrogen flowrate was approximately 1 L/min. Sjöberg and Rickard (1983) have shown that the use of low $CO_2$ nitrogen gas in this way causes negligible loss of dissolved inorganic carbon from the reactor during the dissolution experiment, apparently because of the low rate of gas-solution exchange of $CO_2$.

The pH measurement was standardized with Fisher™ pH 4 and 7 buffer solutions that had been adjusted to the temperature of the reactant solution. A series of experiments (described in Appendix C) was conducted using methyl red dye and a fiber optic probe colorimeter to verify that the solution in the vessel was well mixed and that the response time of the pH electrode was not affecting the accurate measurement of the time-varying pH.

Each experiment was started by raising the vessel and solution into place beneath the rotating disk and against the

plexiglass cover. Samples of solution (either 2 or 5 ml volume) were withdrawn from the vessel at 6 or 9 minute intervals for a period of 1.5 hours using a Finnpipette (1-5 ml). The samples were stored in polyurethane disposable test tubes at 4°C for no longer than 2 days before the ion concentrations were measured by AAS.

The total calcium and magnesium ion concentrations in each sample were measured with a Perkin Elmer Model PE 3030 atomic absorption spectrophotometer. After a run, the disk was either rinsed with DI water and stored in a known volume of DI water or the surface of the disk was "aged" with an acidic solution. The aging procedure is discussed below.

In the experiments on the effect of temperature, the disk holder and the disk were brought to the temperature of the solution by wrapping the disk holder in Saran plastic wrap and immersing it in the water bath before it was attached to the drive shaft and inserted in the solution for the rate experiment.

### 5.2.1 "Aging" the Limestone Disk Surface

A special procedure was used to dissolve controlled amounts of calcium and, for some dolomitic stones, magnesium from the disks between rotating disk experiments. This is referred to as "aging" the disk surface. Each disk and its holder was placed in a beaker containing a measured volume of acidified solution (0.1 meq/L acid, initial pH≈4). The solution was stirred continuously with a magnetic stirrer. At the conclusion of this procedure, a sample was taken for determining the calcium and magnesium concentrations and the volume of the solution was recorded. The measured calcium concentration was used with the volume of this solution to determine the mass of calcium dissolved ($Ca_s$). The remaining solution was discarded, the disk was placed in fresh pH 4 solution, and the process was repeated until the desired mass of calcium had been dissolved from the disk.

The total mass of calcium dissolved per unit area of the disk surface, $Ca_d$, was obtained by dividing the sum of the mass

of calcium dissolved during aging ($\Sigma Ca_s$) and the mass of calcium dissolved during all the earlier rate experiments ($\Sigma Ca_r$) by the surface area of the disk (A).

$$Ca_d = (\Sigma Ca_s + \Sigma Ca_r)/A \qquad (22)$$

5.2.2 Calcium and Magnesium Determination by Atomic Absorption Spectrophotometry

The standards used to calibrate the AAS were made by diluting 1000 ppm calcium reference solution (certified Fisher Scientific atomic absorption standard) with background electrolyte solution (0.079 M KCl). The calcium concentrations in the standards ranged from 0.5 to 5 ppm. To minimize interference from phosphates, silica and aluminum, 1% lanthanum chloride was added to the standards and samples using 1 mL $LaCl_2$ solution to 10 mL solution. The AAS was operated using a wavelength of 422.7 nm and a slit width of 7 nm (normal).

The standards were used to obtain a linear calibration curve of absorbance versus the calcium concentration. The standards were then run as samples to verify the calibration. After this verification step, the AAS was calibrated again and the samples were analyzed a second time. The difference between the first and second measurement was always less than 4 percent.

5.2.3 Agreement Between Calculated and Measured Calcium Concentrations

To check for consistency between the measured pH and the measured calcium ion concentration, Equation 11B in Appendix B was used to calculate the theoretical amount of calcium dissolved as a function of the measured pH. Good agreement was obtained between the measured and calculated calcium concentrations when it was assumed that the solution contained $1.28 \times 10^{-5}$ moles/L of initial dissolved inorganic carbon (see Appendix D). This suggests that the procedures used to minimize the amount of

carbon dioxide in the rotating disk solutions were not entirely effective.

5.2.4 Alkalinity Measurements

Alkalinity measurements were used occasionally as an approximate check of the measured calcium concentrations (see Appendix D). The alkalinity was determined using strong acid titration to an equivalent endpoint determined by Gran plot analysis. A 75 ml sample was titrated to a pH of 3.2 using 0.1 N HCl and a computer controlled Metrohm Dosimat 655 automatic titrator. Two DI water blanks were analyzed before titrating the samples. The error in duplicates analyzed was less than 0.3%.

5.2.5 Solubility Product Determination

A set of long duration experiments was performed to estimate the solubility product of the calcium carbonate in the limestone samples. The calcium and magnesium concentrations and the pH and alkalinity at the end of the experiment were used with the relationships presented in Appendix E to calculate the solubility product. Effective solubility products for calcite and calcite combined with dolomite were determined for samples WM, SL, A, C, F, and I. The results are listed in Table 5.2.1.

Table 5.2.1 EFFECTIVE SOLUBILITY PRODUCTS FOR CALCIUM CARBONATE AND CALCIUM-MAGNESIUM CARBONATE IN SELECTED LIMESTONE SAMPLES. VALUES ARE FOR 25°C AND INFINITE DILUTION.

| Stone sample ID | Negative log of the effective solubility product |
|---|---|
| WM | 8.20 ± 0.07 |
| SL | 8.35 ± 0.06 |
| A | 8.76 ± 0.09 |
| C | 8.72 ± 0.07 |
| F | 8.88 ± 0.05 |
| I | 8.89 ± 0.04 |

### 5.2.6 Glassware

All glassware used in sampling and the preparation of standards was soaked overnight in 1 N HCl and then rinsed three times with DI water. The glassware was then soaked in DI water for a day and rinsed with fresh DI water before use.

# CHAPTER 6
# EXPERIMENTAL RESULTS AND DISCUSSION

## 6.0 DISSOLUTION RATE DETERMINATION

The calcium concentration and pH change with time in a typical rotating disk experimental run are shown in Figures 6.0.1 and 6.0.2. In this example, the WM stone sample was used, the rotational speed was 600 rpm and the initial acidity was 0.01 meq/L. At the end of the experiment the pH was 9.04 and the calcium concentration was 1.71 mg/L. For an initial acidity of 0.01 meq/L and with no calcium in the solution at t = 0, the calculated equilibrium calcium concentration is 11.6 mg/L and the calculated equilibrium pH is 10.02 (see $pK_{sp}$ for sample WM, Table 5.2.1, and Equations 7B-9B, Appendix B).

The initial rate of dissolution in this study ranged from 8 x $10^{-10}$ moles Ca/$cm^2$s to 1 x $10^{-9}$ moles Ca/$cm^2$s. These values lie within the range of values (1 x $10^{-10}$ moles Ca/$cm^2$s to 2 x $10^{-9}$ moles Ca/$cm^2$s) reported in the literature (see Table 6.0.1).

The overall dissolution rate constant, $k_o$, was determined for each experimental run using the measured calcium concentrations and, in some cases, the measured magnesium concentrations. For the stones that released negligible amounts of magnesium, the calcium concentrations ($C_t$) were substituted in the relationship,

$$Ln/a = \ln \{(C_{eq} - C_t)/(C_{eq} - C_o)\}(V_t/A) \qquad (23)$$

where $C_{eq}$ and $C_o$ are the equilibrium and initial calcium concentrations, respectively, and A is the surface area of the stone sample disk exposed to the solution. $C_o$ was zero in all experiments. $V_t$ is the volume of the solution in the rotating

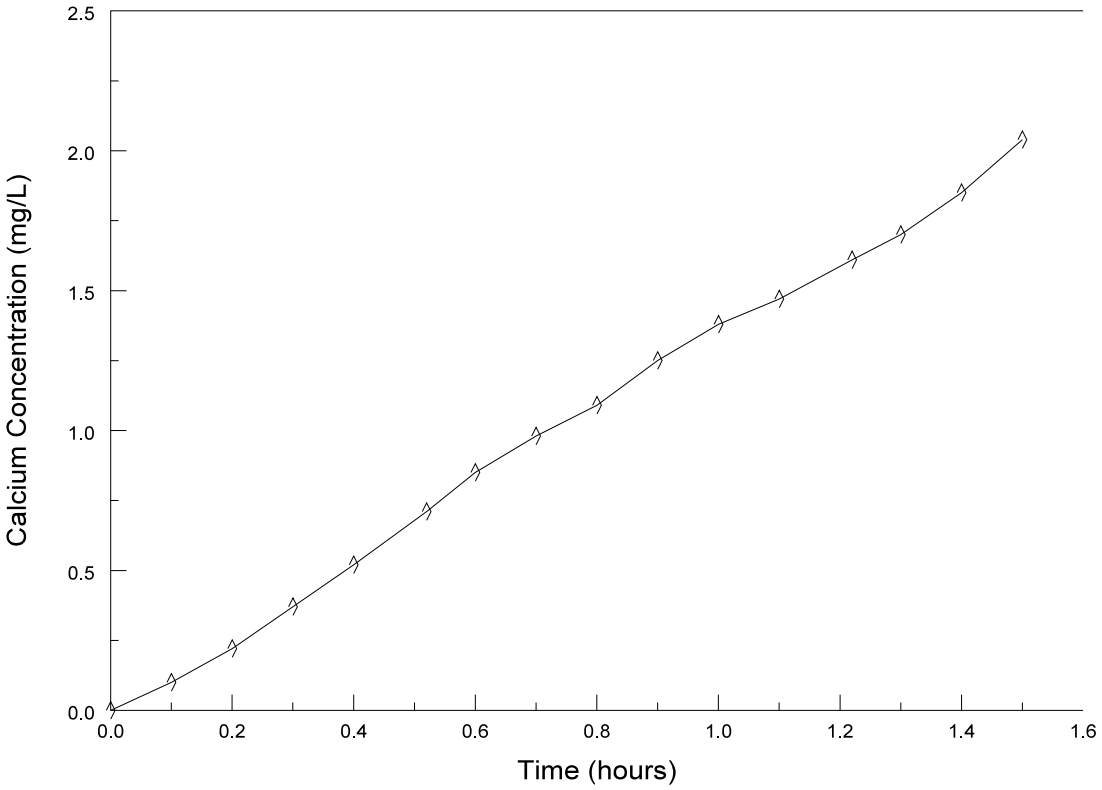


Figure 6.0.1 Calcium concentration in the rotating disk apparatus as a function of time; WM sample; w = 600 rpm and initial acidity of 0.01 meq/L.

disk apparatus. For sample WM and samples A-J the limestone disk was 3.6 cm in diameter and, therefore, A was 10.17 $cm^2$. For the 3.1 cm diameter SL sample and the 2.5 cm diameter BR sample, A was 7.91 $cm^2$ and 4.71 $cm^2$, respectively.

The magnitude of $C_{eq}$ was determined for each experimental run using the equilibrium model described by Equations 7B-9B in Appendix B and the effective solubility products listed in Table 5.2.1. For the stone samples that were not included in the solubility product experiments, i.e., samples B, D, E, G, H and J, the average value of the effective solubility products for the samples from the same quarry ($pK_{sp}$ = 8.81) was used. $pK_{sp}$ = 8.35 was used for sample BR because of its similarity to sample SL.

As samples were withdrawn during an experiment, the

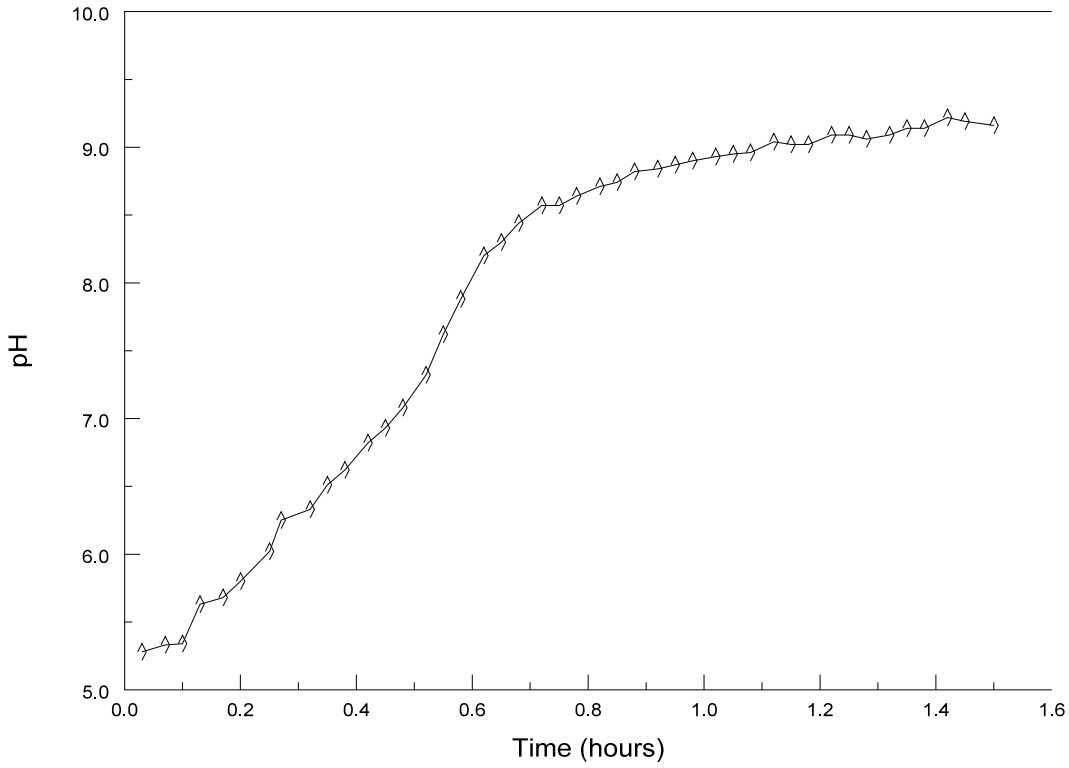


Figure 6.0.2 pH vs time for the rotating disk experiment of Figure 6.0.1.

Table 6.0.1 REPORTED INITIAL RATES OF CALCITE DISSOLUTION AT 25°C

| Reference | Type of System Used | Rate x $10^{10}$ moles $Ca/cm^2s$ |
|---|---|---|
| Wallin and Bjerle (1989a) | Rotating Cylinder | 1 to 5 |
| Sjöberg and Rickard (1983) | Rotating Disk | 5 to 20 |
| Plummer et al. (1978) | Stirred Suspensions | 10 to 20 |

magnitude of $V_t$ decreased. A value of $V_t$ was calculated for each value of $C_t$ using the relationship,

$$V_t = V_o - nv \qquad (24)$$

where $V_o$ is the volume of the solution in the reactor at the start of the experiment, v is the volume of each sample withdrawn for the calcium and magnesium measurements and n is the total number of samples withdrawn from the reactor up to that sample. In the dissolution rate experiments, $V_o$ was 600 mL and v was either 2 or 5 mL.

A straight line was fitted to the Ln/a versus time points using the method of least squares. The negative slope of this line is equal to the overall dissolution rate constant, $k_o$.

Figure 6.0.3 is a Ln/a versus time plot for a fresh sample of WM stone. In this experiment the disk rotational speed was 600 rpm, the water temperature was 25°C and the initial acidity was 0.01 meq/L. The negative slope of the least squares line in Figure 6.0.3 yields an overall dissolution rate constant of 3.3 x $10^{-3}$ cm/s.

## 6.1 EFFECT OF DOLOMITE CONTENT ON $k_o$

Significant amounts of magnesium were dissolved from the high dolomite content stones (samples I and J with approximately 93 and 100 percent dolomite, respectively) during the rate experiments and during the batch aging process and the solubility product experiments of Appendix E. The average calcium to magnesium mass ratios for each of the solutions used in the batch aging process was 0.51 for stone I and 0.54 for stone J. For the stoichiometric dissolution of pure dolomite the theoretical Mg/Ca mass ratio is 0.61.

For stone samples I and J, an effective value of $k_o$ was determined using an "equivalent" calcium concentration, $C'_t$, in place of $C_t$ in Equation 23. The magnitude of $C'_t$ was calculated for each sample from the reactor by adding the measured concentrations of calcium and magnesium (expressed in equivalents per liter) and then multiplying this sum by the equivalent weight of calcium.

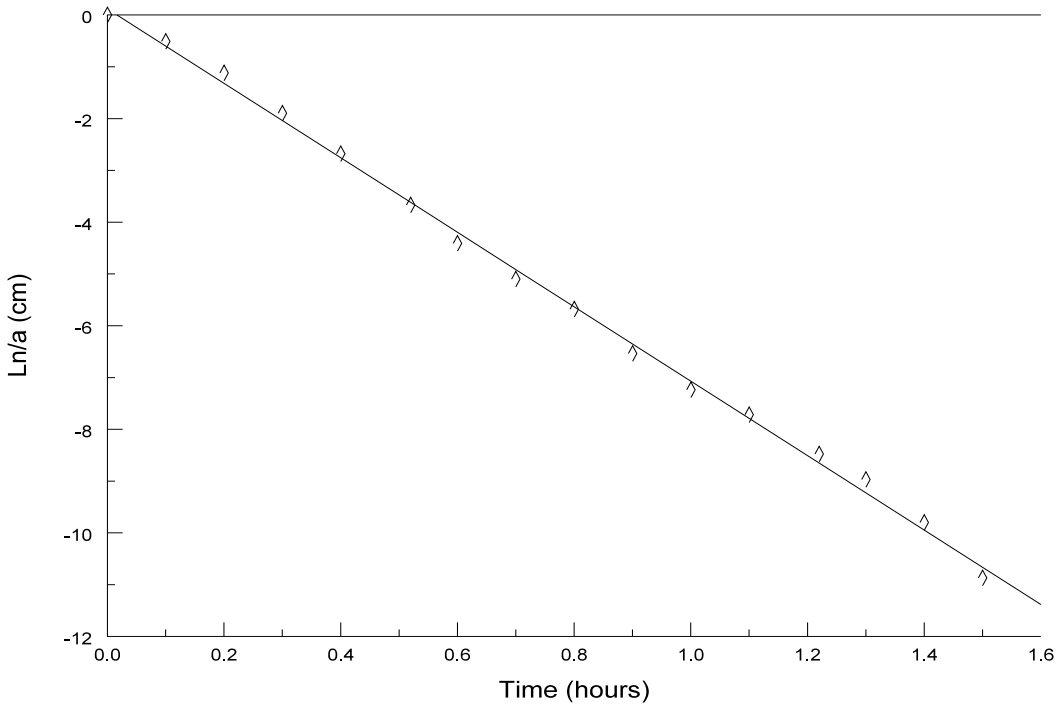


Figure 6.0.3 Dissolution rate experiment for the WM stone sample. Initial acidity = 0.01 meq/L and w = 600 rpm. In this example, $k_o$ = 0.0033 cm/s.

Figure 6.1.1 shows the calcium and magnesium concentrations and the calculated equivalent calcium concentrations plotted versus time for an experiment with sample J. The Ln/a versus time points (calculated using the equivalent calcium concentrations) are plotted in Figure 6.1.2. An "effective" equilibrium calcium concentration of 6.48 mg/L was used in place of $C_{eq}$ in Equation 23. This value was calculated using an effective solubility product of $pK_{sp}$ = 8.81 and the equilibrium relationships described in Appendix B.

A significant y-axis intercept for the line fitted to the Ln/a versus time data (see Figure 6.1.2) was typical for the first rate experiments conducted with new disks of stones I and J. For fresh samples of stones I and J, there was always an initial period with a high rate of dissolution. This period is apparently the cause of the significant y-axis intercept of the

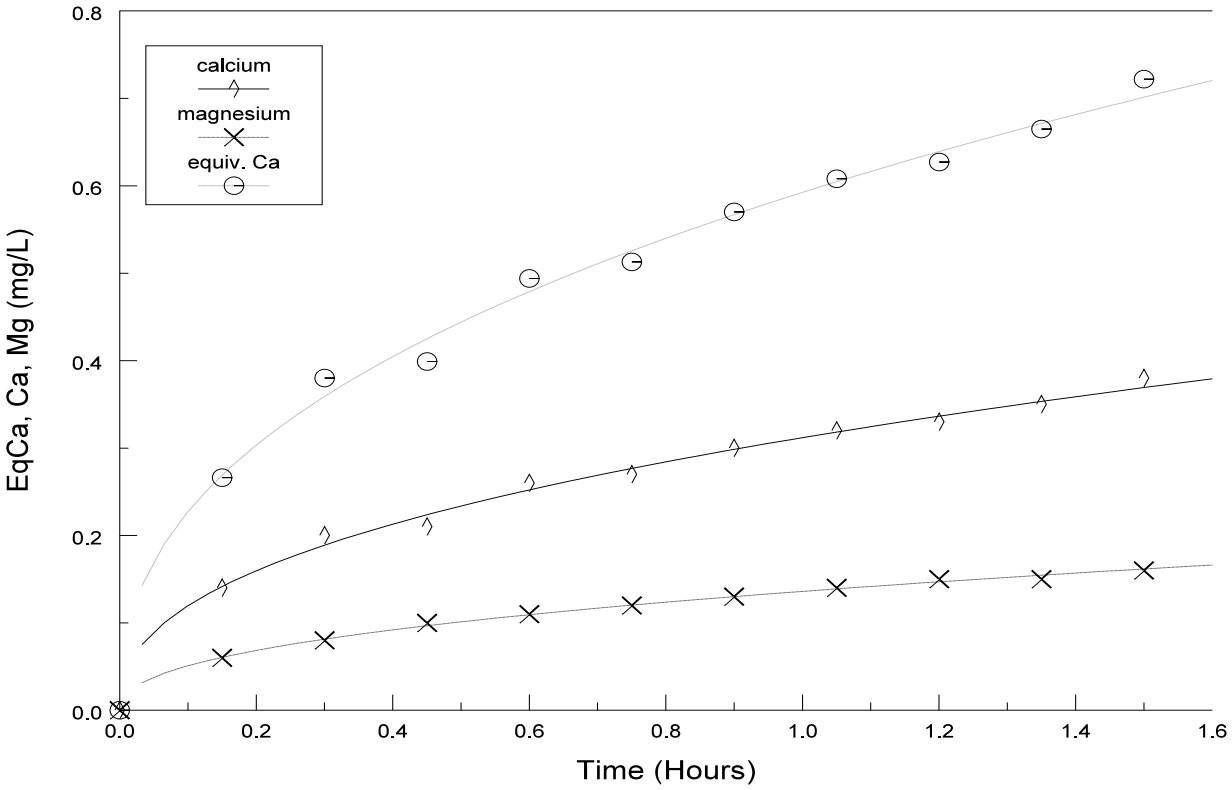


Figure 6.1.1 Calcium, magnesium and calculated equivalent calcium concentration for a rotating disk experiment with stone sample J and 600 rpm.

least-squares fitted line.

The high initial rate of dissolution for stones I and J is consistent with the observations of Plummer and Busenberg (1982) who, in their study of dolomite dissolution, observed that initially the calcium carbonate component of dolomite dissolved faster than the magnesium carbonate component, forming a Mg-enriched surface on the disk. After this initial period the dissolution of Ca and Mg became slower and more consistent (stoichiometrically) with the composition of the solid.

For all stone samples except I and J, the highest concentration of magnesium measured during a rate experiment was always less than 0.03 mg/L. Figure 6.1.3 shows the calcium and magnesium concentrations plotted versus time for stone sample C.

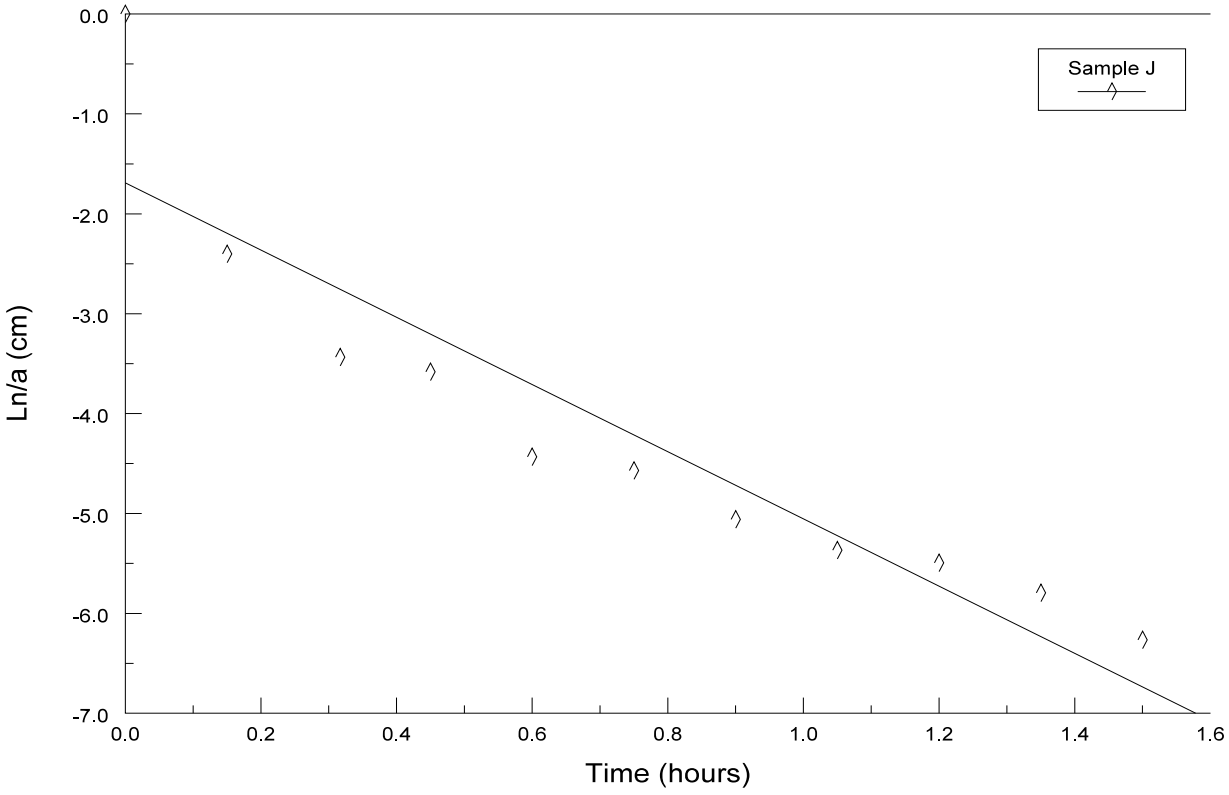


Figure 6.1.2 Dissolution rate experiment results for stone sample J. Ln/a calculated using the equivalent calcium concentrations in Figure 6.1.1.

Sample C had 17% calcite and 68% dolomite.

## 6.2 EFFECT OF INSOLUBLE RESIDUE CONTENT ON THE INITIAL RATE OF CALCITE DISSOLUTION

It was observed that the overall dissolution rate constant for fresh calcitic stones (stones with low dolomite content) tended to decrease as the estimated amount of insoluble residue in the stone increased. It is reasonable to conclude that the insoluble impurities reduce the area of calcite exposed to the solution. To test this hypothesis, it was assumed that the area of exposed calcite is proportional to the mass percent of calcite in the stone. The rate constants were "corrected" for the residue content by dividing them by the mass percent of calcite in the

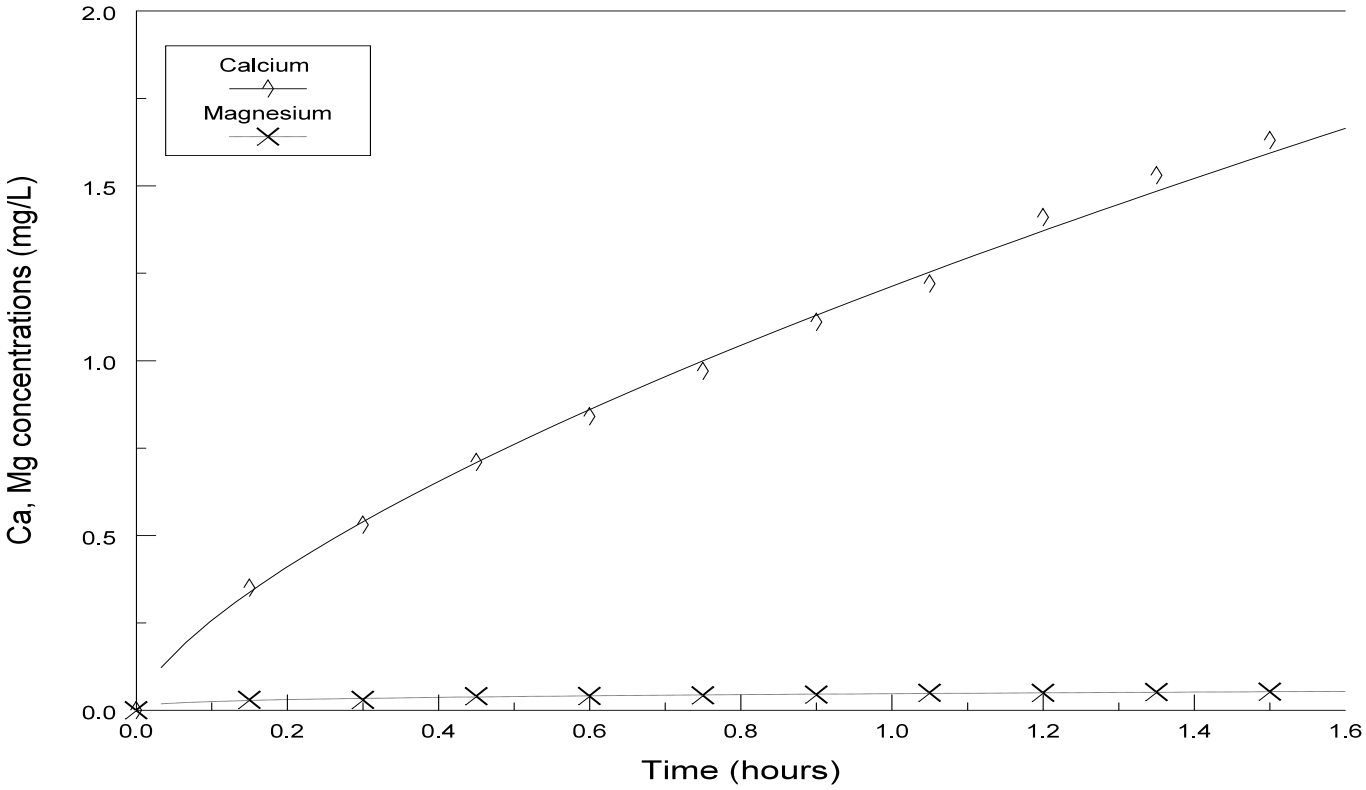


Figure 6.1.3 Calcium and magnesium concentrations for rotating disk experiment with stone sample C at 600 rpm.

stone. The results of this calculation, listed in the right-hand column of Table 6.2.1, show that this correction reduces the effect of the residue content on $k_o$.

The corrected overall dissolution rate constant for the coarse-grained WM sample ($3.12 \times 10^{-3}$ cm/s) is somewhat less than the values of $3.51 \times 10^{-3}$ and $3.75 \times 10^{-3}$ cm/s for the fine-grained SL and BR samples. This difference is consistent with the observation of Holdren and Speyer (1985) that stones with smaller grain size have higher rates of dissolution.

## 6.3 VARIATION OF $k_o$ WITH THE $CaCO_3$ CONTENT OF THE STONE

In Figure 6.3.1 the experimental values of $k_o$ for the fresh stone samples, $k_{oi}$, are plotted versus the approximate calcite

Table 6.2.1 COMPARISON OF EXPERIMENTAL AND CORRECTED OVERALL DISSOLUTION RATE CONSTANTS FOR ESSENTIALLY FRESH LIMESTONE DISKS

(Small amounts of calcium had been dissolved from samples WM, SL and BR before the first rate constants were determined).

| Stone | Mass % Calcite | Experimental $k_o \times 10^3$ (cm/s) | Corrected $k_o \times 10^3$ (cm/s) |
|---|---|---|---|
| $Ca_d$ = 0.2 mg Ca/cm$^2$ | | | |
| WM | 64 | 1.99 | 3.12 |
| SL | 92 | 3.26 | 3.51 |
| BR | 100 | 3.75 | 3.75 |
| $Ca_d \approx$ 0 mg Ca/cm$^2$ | | | |
| B | 92 | 4.39 | 4.77 |
| F | 89 | 3.46 | 3.89 |

content of the stone (CAL) in grams of $CaCO_3$ per 100 grams of stone (see Table 5.0.2). The magnitude of CAL ranges from 92 g/100 g for sample B to 0 g/100g for the essentially pure dolomite stone (sample J).

According to the results plotted in Figure 6.3.1, the magnitude of $k_{oi}$ for fresh stone decreases by approximately 60% as the calcite content of the stone decreases from 92 to 9 g $CaCO_3$/100 g. The y-axis intercept of the line fitted to these points by the method of least-squares is an extrapolated value of $k_{oi}$ for pure dolomite (CAL=0). The value of this intercept for the data plotted in Figure 6.3.1 is 2.58 x $10^{-3}$ cm/s, which is significantly greater than the observed value of $k_{oi}$ ($k_{oi}$ = 0.93 x $10^{-3}$ cm/s) for the fresh sample of pure dolomite. This result suggests that the presence of calcite in stones with high dolomite content enhances the rate of dolomite dissolution. Since the Mg concentrations measured in the rate experiments were negligible for all stone samples except I and J, it appears that

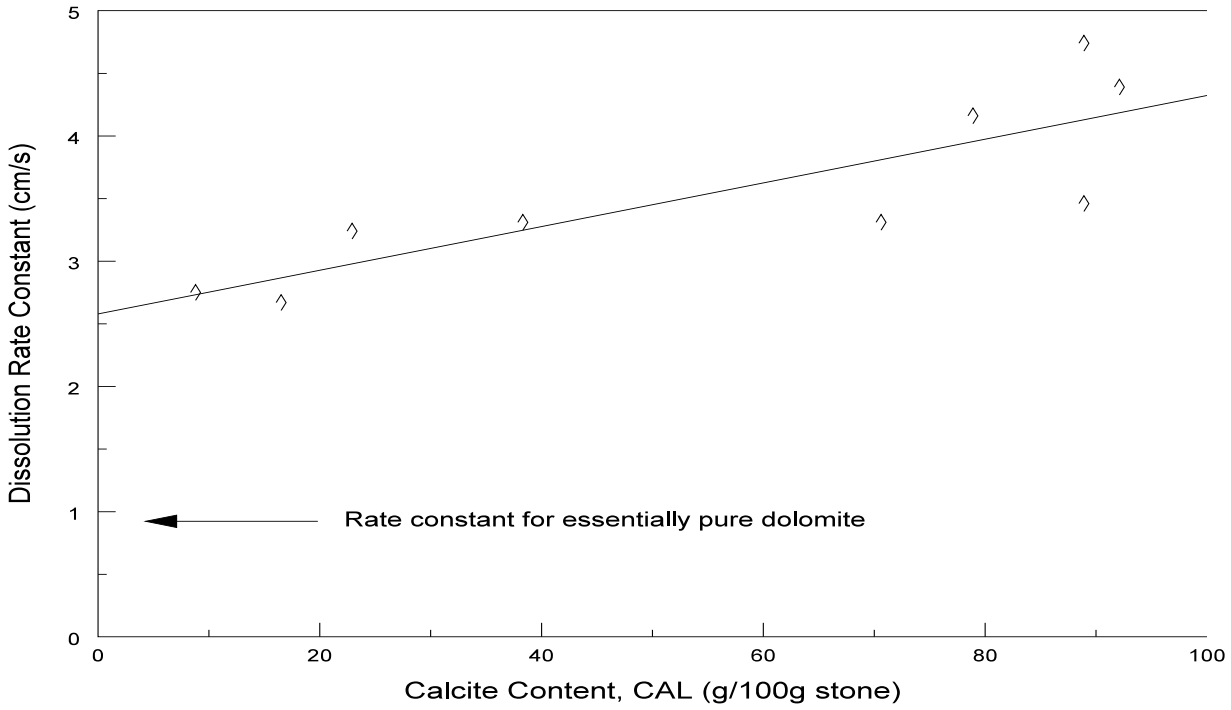


Figure 6.3.1 Effect of the calcite content of the stone sample on the initial value of the dissolution rate constant.

the dissolution of dolomite in all but the essentially pure dolomite samples occurred, as observed by Plummer and Busenberg (1982), by the dissolution of calcium and carbonate from the dolomite fraction of the stone.

## 6.4 EFFECT OF IRON AND ALUMINUM ON THE DISSOLUTION RATE

It was observed that the extent to which the dissolution of calcium from the stone surface reduces the overall dissolution rate constant depends on the aluminum and iron content of the stone.

Figure 6.4.1 shows the normalized overall dissolution rate

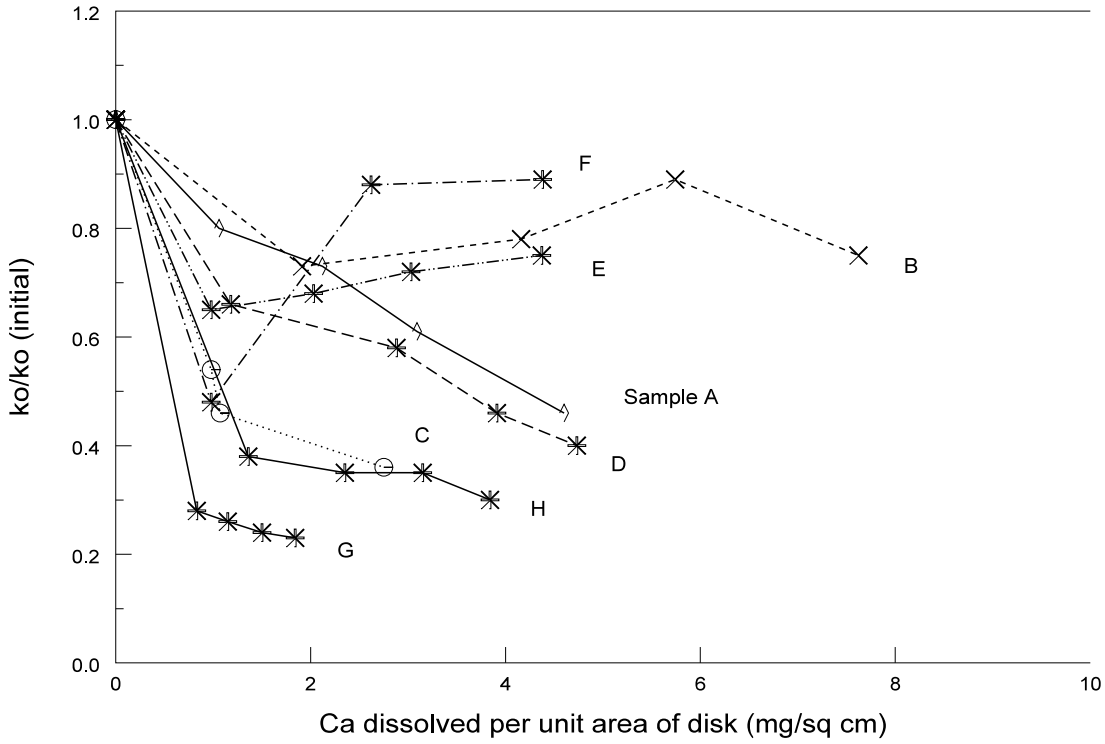


Figure 6.4.1 Effect of amount of calcium dissolved on the fractional decrease in the overall dissolution rate constant.

constant (i.e., the measured value divided by the initial, fresh stone, value, $k_o/k_{oi}$) plotted versus the amount of calcium dissolved from the surface of the stone, $Ca_d$, for stones A-D, F, G, I and J (see Equation 22). For stones D, G and I, $k_o$ decreased by more than 60 percent as the amount of calcium dissolved increased from 0 to 4 mg Ca/cm$^2$. For stones F, B and J the decrease was less than 30 percent.

Values of $k_o/k_{oi}$ were interpolated from Figure 6.4.1 at $Ca_d$ = 2 mg Ca/cm$^2$ and then listed in Table 6.4.1 in rank order, from the highest ($k_o/k_{oi}$ = 0.90 for stone F) to the lowest ($k_o/k_{oi}$ = 0.23 for stone G). The stones with the highest aluminum content (> 25 mg Al/100g of stone) had the greatest decrease in $k_o$ for

Table 6.4.1 EFFECT OF THE IRON AND ALUMINUM CONTENT ON THE FRACTIONAL DECREASE IN THE OVERALL DISSOLUTION RATE CONSTANT AT $Ca_d$ = 2 mg CALCIUM DISSOLVED PER SQUARE CENTIMETER OF LIMESTONE SURFACE.

| Stone ID | % Calcite | $k_o$ x $10^3$* (cm/s) | $k_o/k_{oi}$ | Fe (mg Fe/100g) | Al (mg Al/100g) |
|---|---|---|---|---|---|
| F | 88.9 | 3.5 | 0.90 | 15 | 5 |
| A | 88.9 | 4.7 | 0.74 | 24 | 12 |
| B | 92.1 | 4.4 | 0.73 | 29 | 1 |
| J | 0 | 0.9 | 0.70 | 189 | 10 |
| E | 70.7 | 3.3 | 0.65 | 41 | 25 |
| D | 78.9 | 4.2 | 0.61 | 40 | 37 |
| C | 16.5 | 2.7 | 0.43 | 189 | 93 |
| I | 8.8 | 2.8 | 0.36 | 377 | 32 |
| H | 38.3 | 3.3 | 0.35 | 154 | 134 |
| G | 22.9 | 3.2 | 0.23 | 294 | 129 |

*interpolated from Figure 6.4.1 at $Ca_d$ = 2 mg Ca/$cm^2$.

this amount of calcium dissolved. For several stones, especially stone I with $k_o/k_{oi}$ = 0.36, the iron content seemed to be an additional factor.

Since both the iron and aluminum content of the stone seem to determine how sample aging affects the overall dissolution rate constant, a composite parameter that includes a weighted combination of the iron and aluminum concentrations ($aC_{Al} + bC_{Fe}$) was derived, where $C_{Al}$ is the aluminum concentration in mg Al/100 g and $C_{Fe}$ is the iron concentration in mg Fe/100 g.. The highest linear correlation between $k_o/k_{oi}$ and the parameter ($r^2$ = 0.92) was obtained with weighting factors a = 1 and b = 0.3, i.e., ($C_{Al}$ + 0.30 $C_{Fe}$), The quantity $k_o/k_{oi}$ and corresponding values of ($C_{Al}$ + 0.30 $C_{Fe}$) are listed in Table 6.4.2.

According to the results in Table 6.4.2, the effect of iron and aluminum on the overall dissolution rate constant will be minimized if the quantity $C_{Al}$ + 0.30 $C_{Fe}$ for the stone is less

Table 6.4.2 EFFECT OF THE WEIGHTED SUM OF IRON AND ALUMINUM IN THE LIMESTONE ON THE FRACTIONAL DECREASE IN THE OVERALL DISSOLUTION RATE CONSTANT AT 2 mg CALCIUM PER SQUARE CENTIMETER OF LIMESTONE SURFACE

| Stone ID | $k_o/k_{oi}$ | $C_{Al} + 0.30\ C_{Fe}$ (mg/100g) |
|---|---|---|
| F | 0.90 | 10 |
| A | 0.74 | 19 |
| B | 0.73 | 10 |
| J | 0.70 | 67 |
| E | 0.65 | 37 |
| D | 0.61 | 49 |
| C | 0.43 | 149 |
| I | 0.36 | 145 |
| H | 0.35 | 180 |
| J | 0.23 | 217 |

than about 10 mg/100g.

6.4.1 Residue Layer Resistance

Haddad (1986) assumed that when limestone contains impurities such as alumino-silicates, iron and aluminum, the dissolution of calcium carbonate from the limestone matrix leads to the formation of a residue layer on the exposed limestone surface. With a significant residue layer resistance, the overall dissolution rate constant can be assumed to be given by Equation 17. When the residue layer is negligible and $k_f$ is large, Equation 3 is used to calculate the overall dissolution rate constant.

Scanning electron micrographs of the surfaces of the WM and SL stones are shown in Figures 6.4.2A-6.4.2C and 6.4.3A-6.4.3E. These electron micrographs show that the appearance of the disk surface changed significantly due to dissolution. According to Figure 6.4.2A, freshly polished WM stone is relatively smooth and


Figure 6.4.2A Scanning electron micrograph of freshly prepared WM stone sample.

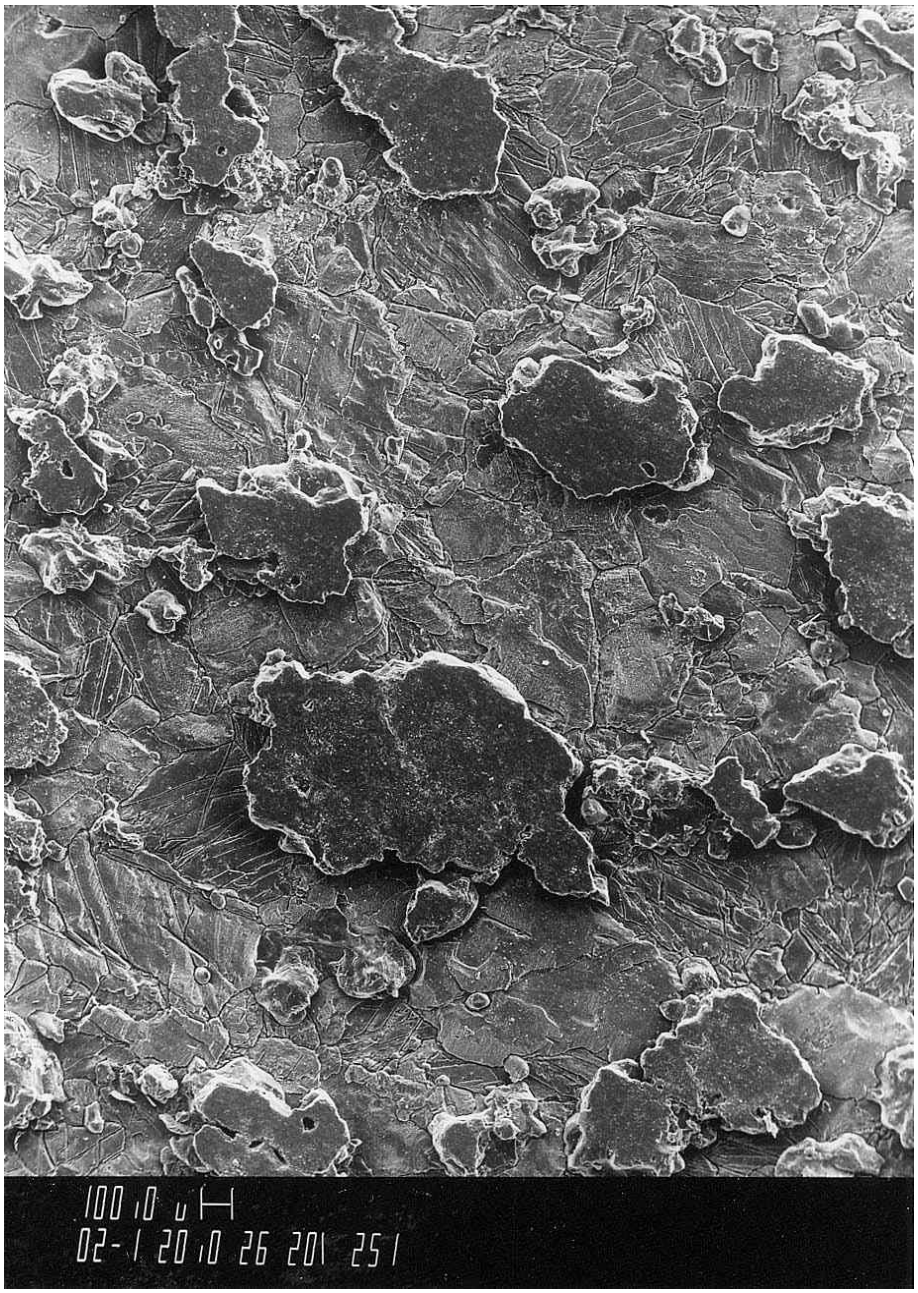

Figure 6.4.2B SEM image of WM stone sample after dissolving 6 mg Ca/cm$^2$ from the surface of the stone. Undissolved elevated regions are silica.

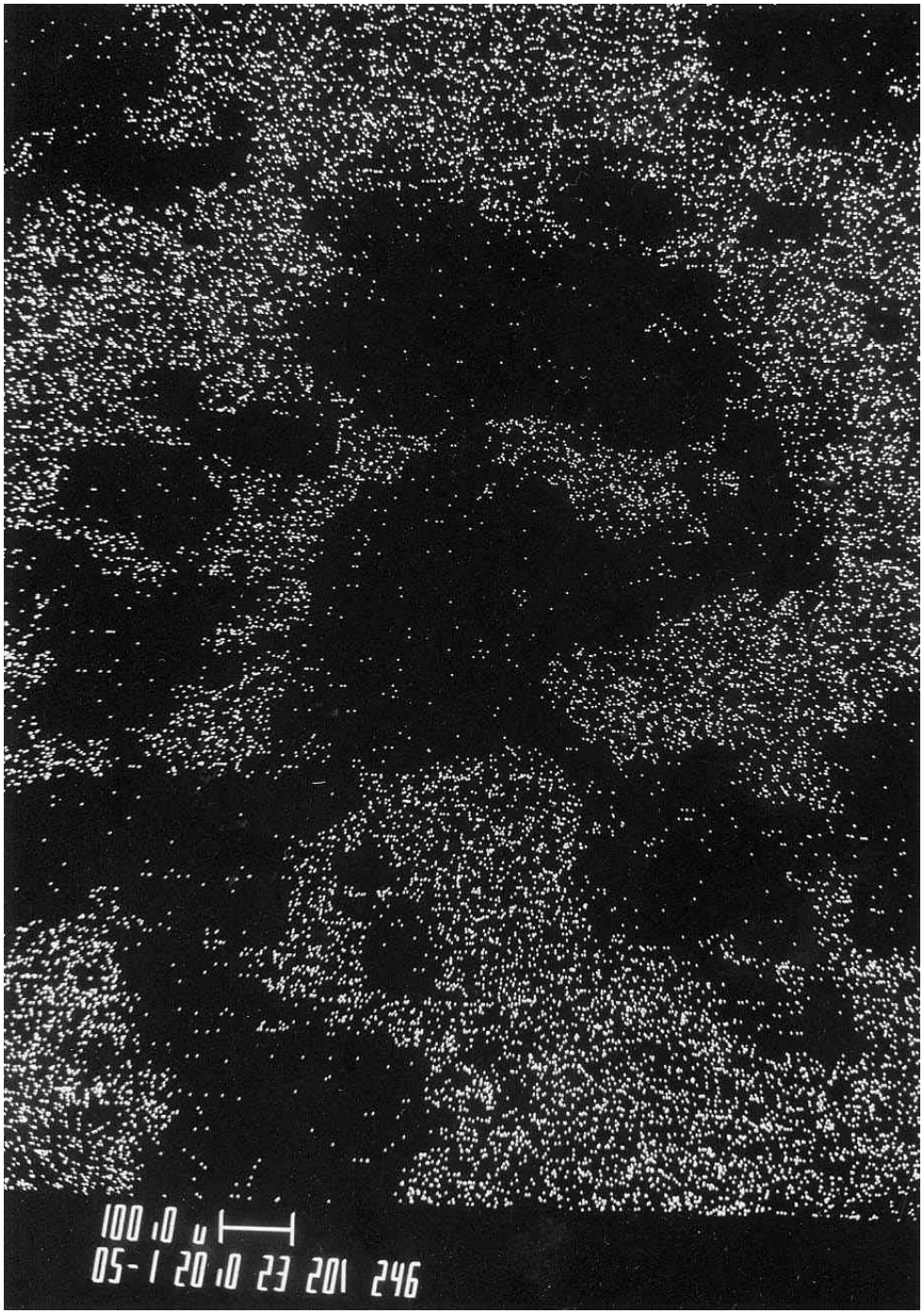


Figure 6.4.2C XES map of calcium distribution in fresh sample of the WM stone.


Figure 6.4.3A Scanning electron micrograph of the surface of a fresh SL sample.

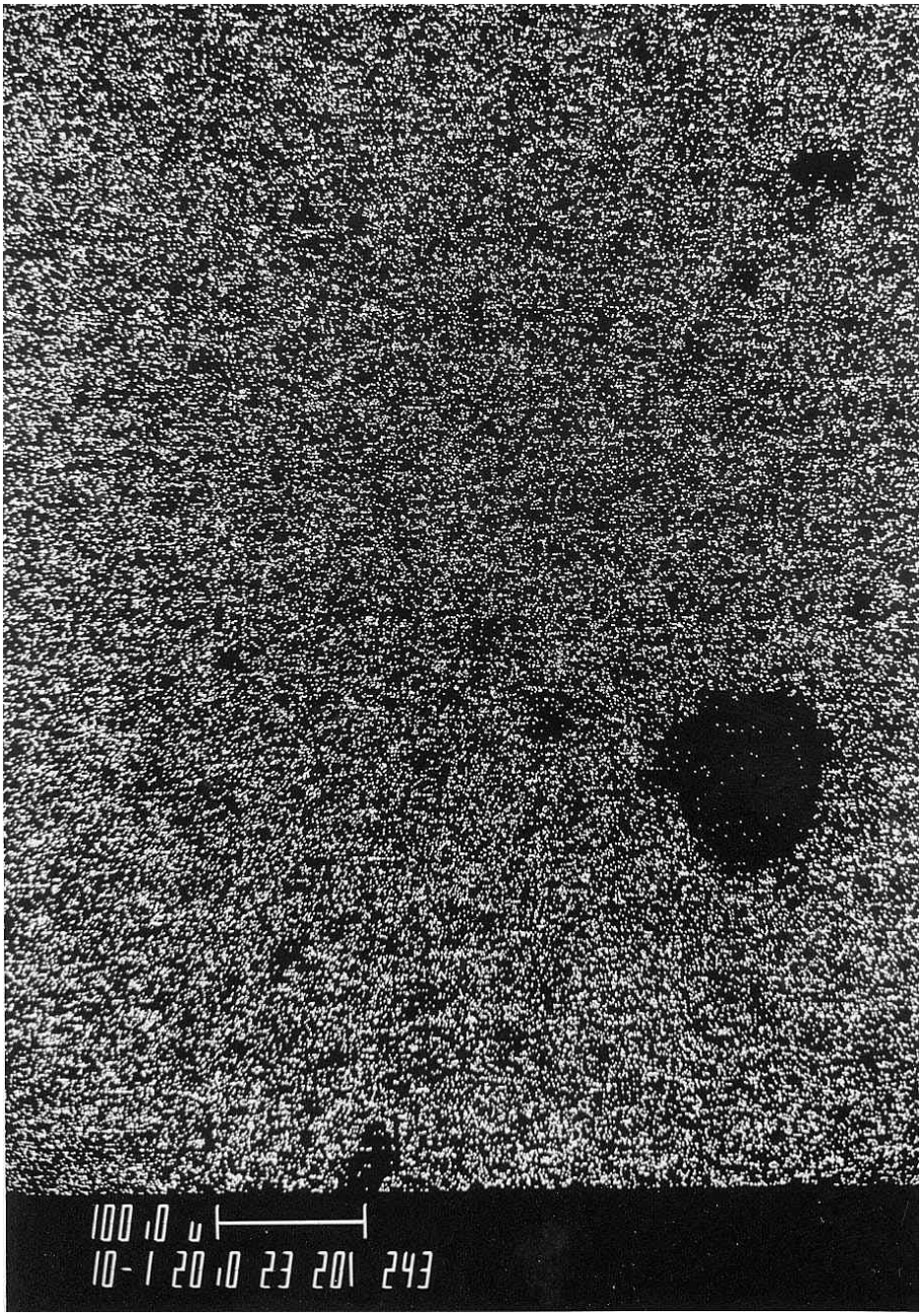


Figure 6.4.3B XES map of the distribution of calcium on the fresh SL sample.


Figure 6.4.3C XES map after dissolving calcium from the surface of fresh SL sample. The abundance of calcium has decreased significantly compared to Figure 6.4.3B.


Figure 6.4.3D XES map showing the distribution of silica SL sample after calcium was dissolved from the surface.

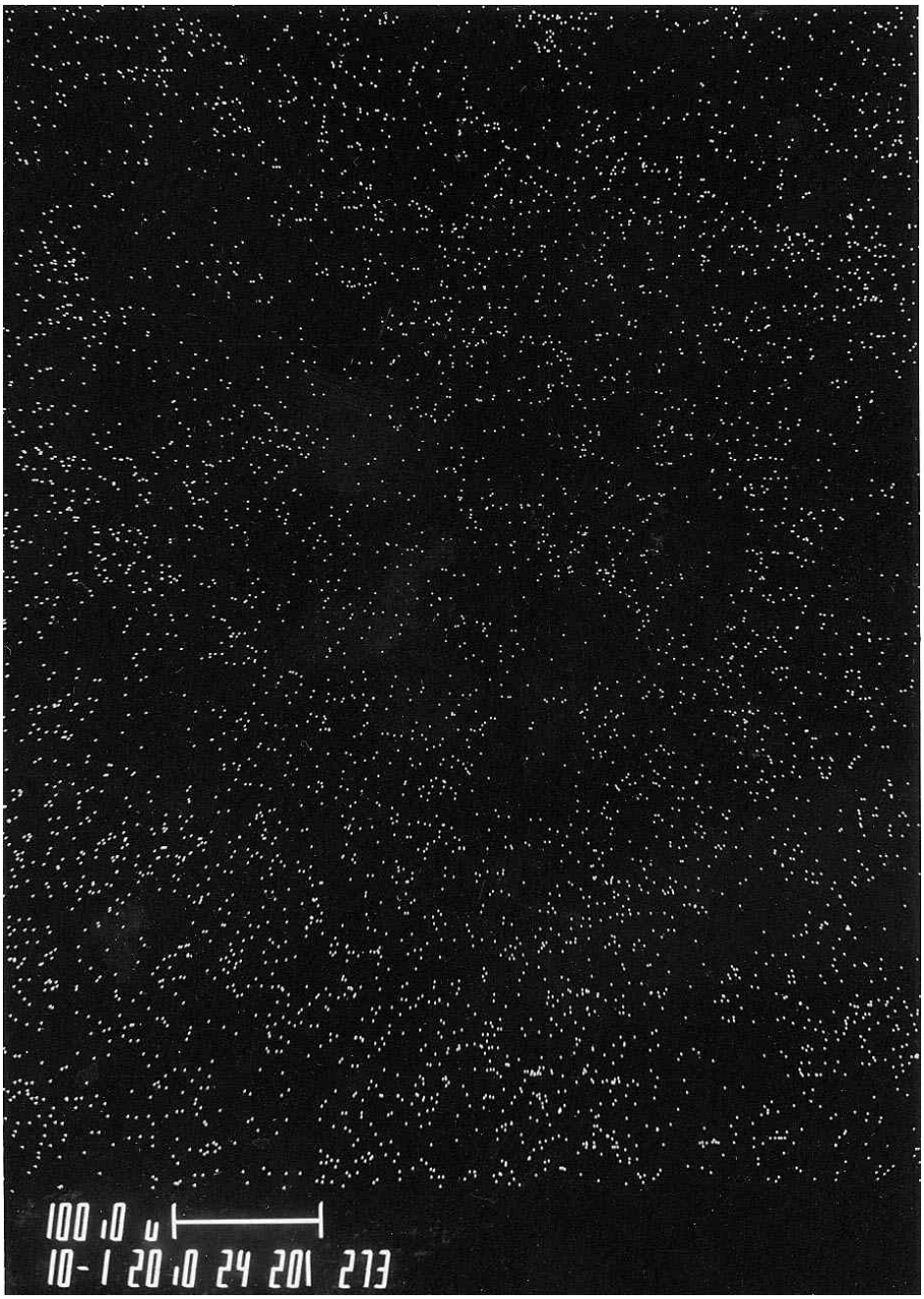


Figure 6.4.3E XES map showing the distribution of aluminum on the dissolved SL sample.

featureless. Analysis of the surface by an x-ray energy spectrometer (XES) indicated that it was mostly calcium and silica (see Figure 6.4.2B). As $CaCO_3$ was dissolved, significant pitting and roughening of the surface became apparent. Areas of silica remained and formed plateau-like structures on the surface of the disk (Figure 6.4.2C).

For the SL stone, dissolution of $CaCO_3$ produced a brownish-white residue layer on the surface. The SEM/XES analysis indicated that this layer consisted of aluminum, silica and iron (Figures 6.4.3D and 6.4.3E). The impurities measured in the SL sample (Table 5.0.2) are consistent with these observations.

Values of $k_o$ plotted as a function of $Ca_d$, the mass of calcium dissolved per unit area of stone (in $mg/cm^2$), are shown in Figure 6.4.4 for the SL, WM and BR samples. $k_f$ values for different amounts of calcium dissolved from the surface of the SL stone are given in Table 6.4.3.

To calculate $k_f$, experimentally determined values of $k_o$, $k_L$ and $k_c$ were substituted in Equation 17. As increasing amounts of calcium are dissolved, $k_f$ becomes smaller and, eventually controlling. Also included in Table 6.4.3 are the $k_f$ values calculated using the empirical equation (Equation 13) derived by Haddad (1986) for his non-steady-state simulation model.

The WM stone contains less calcium than the SL and BR stones (Table 5.0.2). It also contains the greatest amount of silica (as indicated by the analysis of thin sections). This stone provides limited evidence that the silica content does not by itself establish that a residue layer will be formed. Repeated experiments with the same WM stone did not produce a significant decrease in the dissolution rate. Even after $Ca_d$ was 5.7 $mgCa/cm^2$ the dissolution rate was essentially equal to the initial value.

SL stone, on the other hand, is 93% $CaCO_3$ (see Table 5.0.2) but it also contains more of the elements (aluminum and iron) that seem to be critical for the formation of a residue layer, $(C_{Al} + 0.3\ C_{Fe}) = 114$ mg/100g. As calcium was dissolved from the surface of the SL stone the overall dissolution rate constant

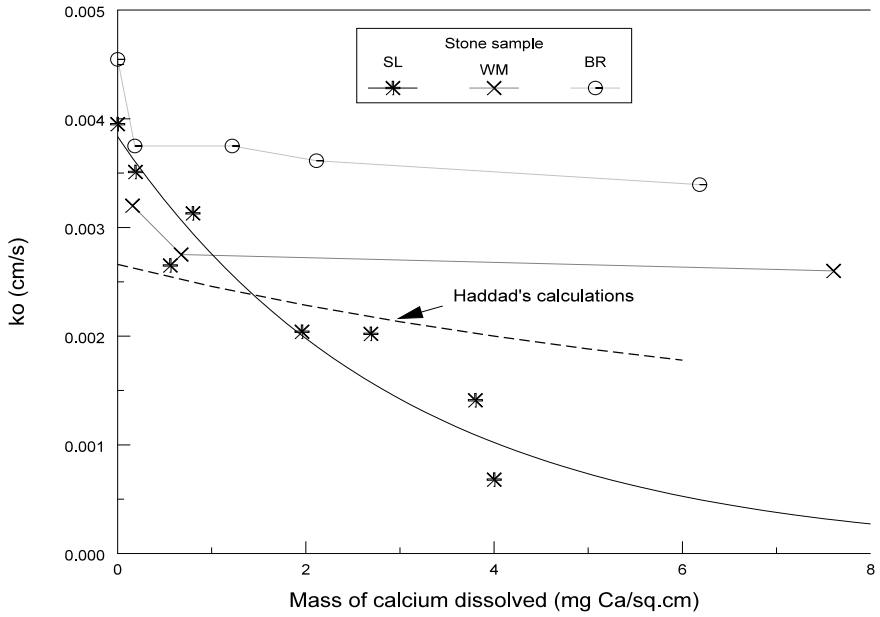


Figure 6.4.4 Variation in the overall dissolution rate constant, $k_o$, with the amount of calcium dissolved from the disk surface. The dashed line curve is the relationship used by Haddad (1986) in his simulation program.

Table 6.4.3 RESIDUE LAYER MASS TRANSFER COEFFICIENT FOR SL SAMPLE

| Calcium dissolved (mg Ca/cm$^2$) | $k_o$ x $10^3$ Experimental (cm/sec) | $k_f$ x $10^3$ From exp. $k_o$ (cm/sec) | $k_f$ x $10^3$ Haddad (cm/sec) |
|---|---|---|---|
| 0.00 | 3.95 | -- | -- |
| 0.19 | 3.51 | -- | 169 |
| 0.56 | 2.65 | 640.57 | 57 |
| 0.80 | 3.13 | -- | 40 |
| 1.96 | 2.04 | 8.74 | 16 |
| 2.69 | 2.02 | 8.38 | 12 |
| 3.80 | 1.41 | 2.99 | 8.4 |
| 4.00 | 0.68 | 0.91 | 8.0 |

decreased, from 3.50 x $10^{-3}$ cm/s at $Ca_d$=0.2 to 0.68 x $10^{-3}$ cm/s at

$Ca_d$=4.0 mgCa/cm$^2$.

BR stone has the highest calcium content (99% $CaCO_3$, Table 5.0.2) and small amounts of aluminum and iron ($C_{Al}$ + 0.3 $C_{Fe}$ = 50 mg/100g). The dissolution rate decreased slightly from 3.75 x $10^{-3}$ to 3.39 x $10^{-3}$ cm/s as the amount of calcium dissolved increased from $Ca_d$ = 0.2 to $Ca_d$ = 6.2 mg Ca/cm$^2$. The BR stone was essentially black in color, possibly from the presence of trace amounts of organic matter.

The residue layer that formed on the SL disk was scraped into concentrated nitric acid, ultrasonicated and the solution was analyzed for total soluble aluminum. The soluble aluminum expressed as the amount per area of disk was 0.97 µmoles/cm$^2$ (26 µg/cm$^2$). The scraped residue did not dissolve completely in acid suggesting the presence of alumino-silicates. The overall dissolution rate constant for SL stone increased to 90% of its original value when the residue layer was removed by scraping the disk surface (see Figure 6.4.5).

## 6.5 EFFECT OF TEMPERATURE ON $k_o$

The effect of temperature on the rate of calcite dissolution was studied by conducting rotating disk experiments at 5, 12, 18 and 25°C. Stone sample B was used for these experiments because it had a high calcite content and low amounts of impurities ($C_{Al}$ + 0.3 $C_{Fe}$ = 10 mg/100g). The background electrolyte was 0.079 M KCl, the disk rotational speed was 600 rpm and the initial acidity was 0.01 meq/L.

Figure 6.5.1 shows plots of Ln/a versus time for 12°C and 18°C. The equilibrium calcium concentration, $C_{eq}$, used to calculate values of Ln/a was determined for each temperature using the chemical equilibrium model described in Appendix B and an effective solubility product of 1.55 x $10^{-9}$ ($pK_{sp}$ = 8.81). The procedure used to estimate the effective solubility product is described in Appendix E. Table 6.5.1 lists the calculated values of $C_{eq}$ and the experimental values of $k_o$ for each temperature.

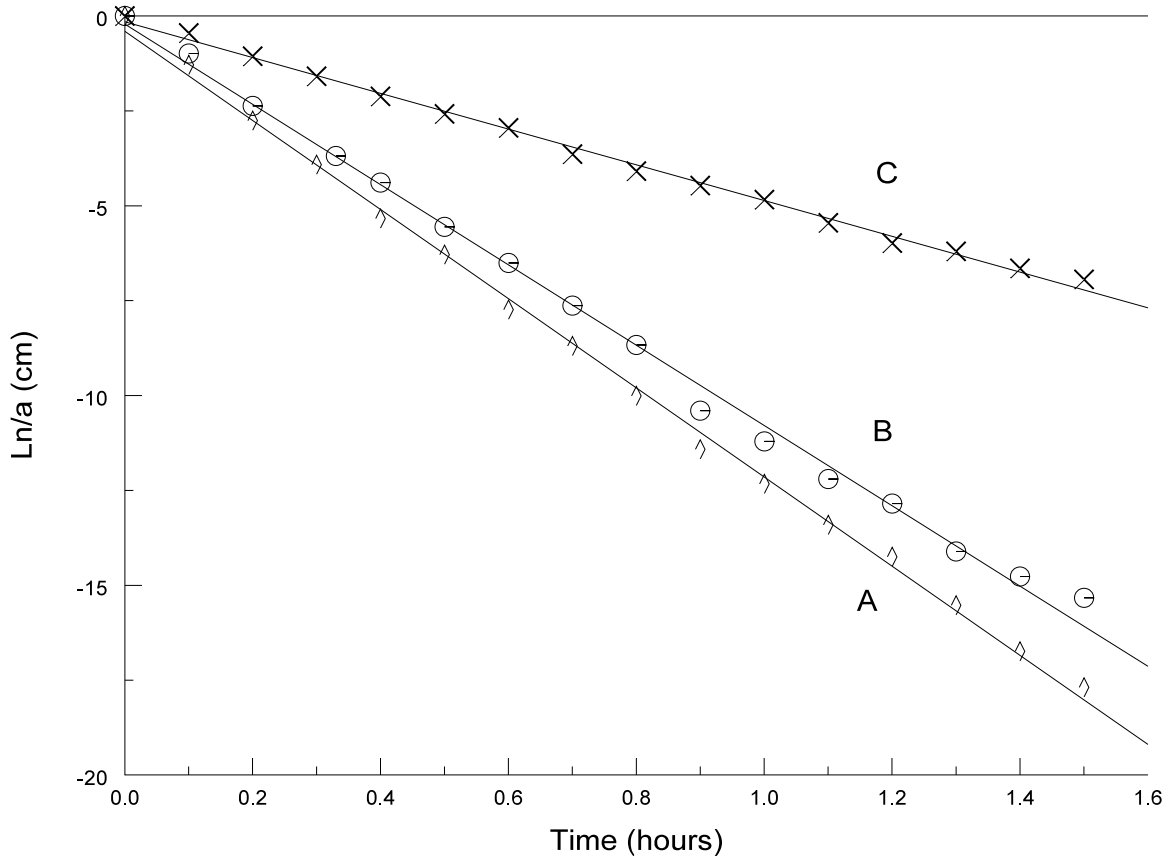


Figure 6.4.5 Plots of ln{(Ceq-C)/Ceq}V/A versus time for SL sample; 0.01 meq/L of initial acidity and 600 rpm. Curve A and C are for 0.2 and 3.8 mg/cm$^2$ of calcium dissolved from the surface of SL sample. Curve B was obtained after scraping the residue.

## 6.6 EFFECT OF TEMPERATURE ON $k_c$ AND $k_L$

The experimental values of $k_o$ listed in Table 6.5.1 were used to determine the effect of temperature on the surface reaction rate constant, $k_c$, for stone B and on the mass transfer constant, $k_L$, for the calcium ion. For heterogeneous reactions, the overall dissolution rate constant is related to $k_L$ and $k_c$ by,

$$k_o = k_L\ k_c/(k_L + k_c) \qquad (25)$$

The magnitude of $k_L$ for the surface of a rotating disk is

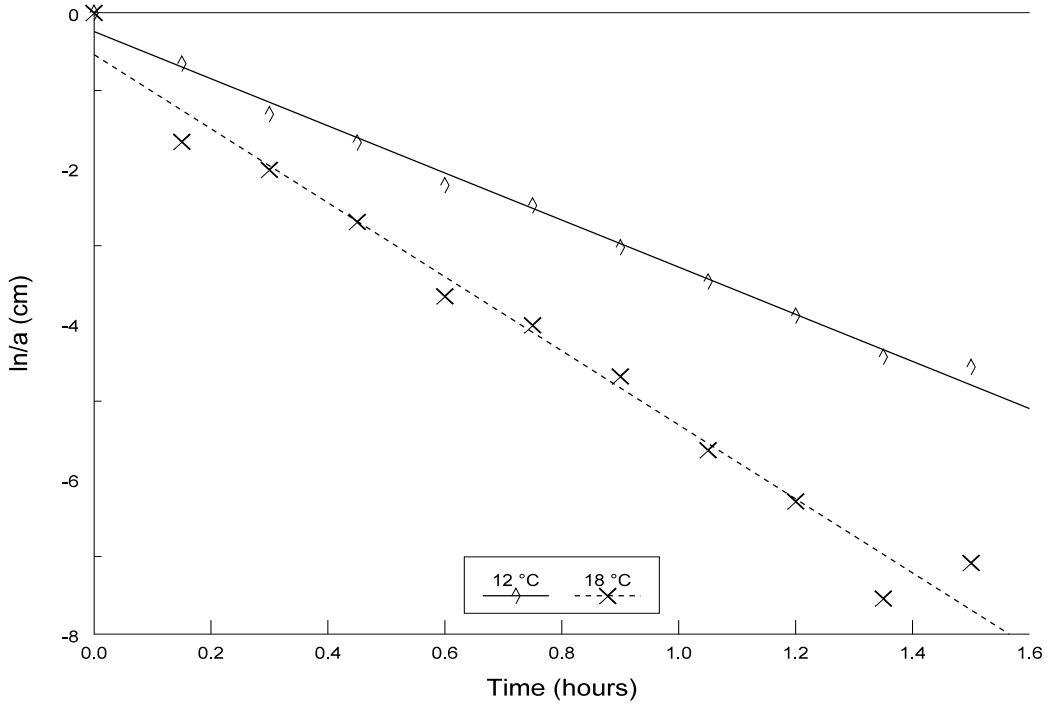


Figure 6.5.1 Plot of ln{(Ceq-C)/(Ceq-Co)}/(V/A) versus time for 12 and 18°C and sample B. Initial acidity is 0.01 meq/L and rotational speed is 600 rpm.

Table 6.5.1 EFFECT OF TEMPERATURE ON THE CALCULATED VALUES OF THE EQUILIBRIUM CALCIUM CONCENTRATION AND EXPERIMENTAL VALUES OF THE DISSOLUTION RATE CONSTANT

| Temperature °C | $C_{eq}$* mg/L | $k_o \times 10^3$ (cm/s) |
|---|---|---|
| 5 | 6.04 | 0.38 |
| 12 | 6.16 | 0.84 |
| 18 | 6.00 | 1.3 |
| 25 | 6.60 | 2.8 |
| 25 | 6.60 | 2.83 |

*based on $pK_{sp}$ = 8.81 at 25°C

$$k_L = 0.62\ D^{2/3}\ \nu^{-1/6}\ \omega^{-1/2} \qquad (26)$$

given by the theoretical expression, where D is the diffusivity of the calcium ion, $\nu$ is the kinematic viscosity and $\omega$ is the rotational velocity of the disk. The assumed magnitude of D at 25°C ($D_{25}$ = 0.8 x $10^{-5}$ $cm^2/s$, See Appendix F) was used with Equation 27 to calculate values of D for the other temperatures, i.e.,

$$D_T = (D_{25}\ \nu_{25}/298)\ x\ [(T+273)/\nu_T)] \qquad (27)$$

where T is the temperature in degrees Celsius. Solving Equation 25 for $k_c$ yields,

$$k_c = k_o\ k_L/(k_L - k_o). \qquad (28)$$

Equations 26 and 28 were used with the values of D and $\nu$ listed in Table 6.6.1 to calculate the values of $k_L$ and $k_c$ listed in Table 6.6.2.

Table 6.6.1 EFFECT OF TEMPERATURE ON THE CALCIUM ION DIFFUSIVITY AND KINEMATIC VISCOSITY

| Temperature °C | D x $10^5$ ($cm^2/s$) | $\nu$ |
|---|---|---|
| 5 | 0.44 | 1.521 |
| 12 | 0.55 | 1.238 |
| 18 | 0.65 | 1.061 |
| 25 | 0.80 | 0.894 |

## 6.7 APPARENT ACTIVATION ENERGY FOR $k_L$ AND $k_c$

Values of the apparent activation energy ($E_a$) were determined for $k_c$ and $k_L$ by plotting the natural log of the quantities listed in Table 6.6.2 versus the reciprocal of the absolute temperature (see Figure 6.7.1). The slopes of the

TABLE 6.6.2 EFFECT OF TEMPERATURE ON THE MASS TRANSFER COEFFICIENT, $k_L$, AND THE SURFACE REACTION CONSTANT, $k_C$

| Temperature °C | $k_L$ x $10^3$ (cm/s) | $k_c$ x $10^3$ (cm/s) |
|---|---|---|
| 5 | 2.63 | 0.44 |
| 12 | 3.17 | 1.14 |
| 18 | 3.65 | 2.02 |
| 25 | 4.26 | 8.17 |
| 25 | 4.26 | 8.43 |

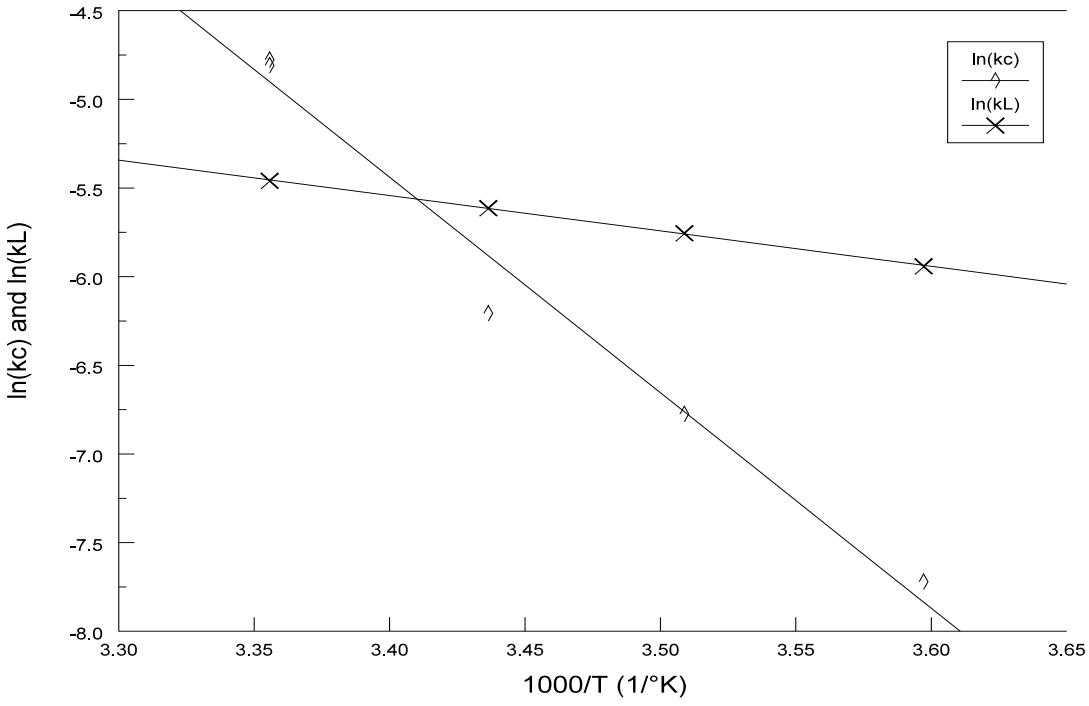


Figure 6.7.1 Arrhenius plot for the mass transfer ($k_c$) and surface reaction constants ($k_L$).

straight lines fitted to these points are equal to $E_a/R$ where R is the gas law constant, 8.314 J/mol°K. The correlation coefficients ($r^2$) for the lines fitted to points in Figure 6.7.1

are greater than 0.98.

For $k_c$, Figure 6.7.1 yields $E_a$ = 101 ± 8 kJ/mol, a value that is significantly larger than the literature values listed in Table 6.7.1 for surface reaction controlled kinetics. For $k_L$, $E_a$ = 17 ± 0.3 kJ/mol was obtained. This quantity, as expected, is in good agreement with the values listed in Table 6.7.1 for mass transfer controlled kinetics.

TABLE 6.7.1 APPARENT ACTIVATION ENERGIES FOR THE LIMESTONE Overall dissolution rate constant WHEN DISSOLUTION IS CONTROLLED BY a) SURFACE REACTION AND b) MASS TRANSFER.

| Predominant Mineral | Stone Characteristics | Apparent Activation Energy, $E_a$ | Reference |
|---|---|---|---|
| a) surface reaction control | | | |
| Calcite | Iceland spar | 46 ± 4 kJ/mol | (1) |
| Calcite | Carrara marble | 54 ± 4 kJ/mol | (1) |
| Dolomite | Coarsely crystalline | 62 kJ/mol | (2) |
| Calcite | Vermont marble | 63 kJ/mol | (3) |
| b) mass transfer control | | | |
| Calcite | Iceland spar and Carrara marble | 13 kJ/mol | (1) |
| Calcite | Limestone | 15 kJ/mol | (4) |
| Calcite | Iceland spar | 41 kJ/mol | (5) |

(1) Sjöberg and Rickard (1984), Rotating disk experiments conducted at constant pH

(2) Lund et al. (1973), Rotating disk experiments with pH free-drift

(3) Lund et al. (1975), Rotating disk experiments with pH free-drift

(4) Barton and Vatanatham (1976)

(5) Plummer, Wigley and Parkhurst (1978)

REFERENCES


1. Letterman, R.D., Driscoll, C.T., Haddad, M., and Hsu, H.A. Limestone bed contactors for control of corrosion at small water utilities. A Report for the Water Engineering Research Laboratory, Office of Research and Development-USEPA, 1987.

2. Letterman, R D., Haddad, M., and Driscoll, C.T. Limestone contactors-steady-state design relationships, J. Env. Eng., ASCE, 117: 339-358, 1991.

3. Haddad, M. Modeling of limestone dissolution in packed bed contactors treating dilute acidic water. Ph.D. Dissertation, Department of Civil Engineering, Syracuse University, 1986.

4. Sjöberg, E.L., and Richard, D. The influence of experimental design on the rate of calcite dissolution. Geochemica et Cosmochemica Acta. 47: 2281-2285, 1983.

5. Lund, K., Fogler, H.S., McCune, C.C., and Ault, J.W. Acidization - II. The dissolution of calcite in hydrochloric acid. Chem. Eng. Sci. 30: 825-835, 1975.

6. Plummer, L.N., and Busenberg, E. The kinetics of dissolution of dolomite in $CO_2$-$H_2O$ systems at 1.5 to 65°C and 0 to 1 ATM $P_{CO2}$. Amer. Jour. of Sci. 282: 45-78, 1982.

7. Plummer, L.N., and Wigley, T.M. The dissolution of calcite in $CO_2$ saturated solutions at 25°C and 1.0 atm. total pressure. Geochemica et Cosmochemica Acta. 40: 191-202, 1976.

8. Berner, R.A., and Morse, J.W. Dissolution kinetics of calcium carbonate in sea water: IV. Theory of calcite dissolution. Am. J. Sci. 274: 108-134, 1974.

9. Chan, P.K., and Rochelle, G.T. Limestone dissolution: Effects of pH, $CO_2$, and buffers modeled by mass transfer. ACS Symposium Series. 188: 75-97, 1982.

10. Bjerle, I., and Rochelle, G. Limestone dissolution in acid lakes. Vatten. 38: 156-163, 1982.

11. Plummer, L.N., Wigley, T.M., and Parkhurst, D.L. The kinetics of calcite dissolution in $CO_2$ water systems at 5°C to 60°C and 0.0 to 1.0 Atm. $CO_2$. Amer. J. Sci. 278: 179-216, 1978.

12. Wallin M., and Bjerle, I. A mass transfer model for limestone dissolution from a rotating cylinder. Chem. Eng.

Sci. 44: 61-67, 1989a.

13. Wallin M., and Bjerle, I. Rate models for limestone dissolution: A comparison. Geochemica et Cosmochemica Acta. 53: 1171-1176, 1989b.

14. Schott, J., Brantley, S., Crerar, D., Guy, C., Borscik, M., and Williame, C. Dissolution kinetics of strained calcite. Geochemica et Cosmochemica Acta. 53: 373-382, 1989.

15. Boynton, R.S. Chemistry and Technology of Lime and Limestone. Second Edition. John Wiley and Sons, 1980.

16. Murray, J.A., et al. J. Am. Ceram. Soc. 37:323-328, 1954.

17. North, F.J. Limestones: Their Origin, Distribution, and Uses. Thomas Murby & Co., London, 1930.

18. Sjöberg, E.L. A fundamental equation for calcite dissolution kinetics. Geochemica et Cosmochemica Acta. 40: 441-447, 1976.

19. Plummer, L.N., Wigley, T.M., Parkhurst, D.L. Critical review of the kinetics of calcite dissolution and precipitation. Amer. Chem. Soc. Symp. Ser. 93: 537-573, 1979.

20. Bjerle, I., and Rochelle, G. Limestone dissolution from a plane surface. Chem. Eng. Sci. 39: 183-185, 1984.

21. King, C.V., and Liu, C.L. The rate of solution of marble in dilute acids. J. Amer. Chem. Soc. 55: 1928-1940, 1933.

22. Tominaga, H., Azumi, H., and Isobe, T. The viscosity effect on the rate of solution of calcium carbonate in hydrochloric acid. Chem. Soc. of Japan. 14: 248-252, 1939.

23. Kaye, C.A. The effect of solvent motion on limestone solution. J. Geol. 65: 34-36, 1957.

24. Weyl, P.K. The solution kinetics of calcite. J. Geol. 66: 163-176, 1958.

25. Nierode, D.E., and Williams, B.B. Characteristics of acid reaction in limestone formation. Soc. Petrol. Jour. Trans. 251: 406-418, 1971.

26. Sjöberg, E.L., and Rickard, D. Temperature dependence of calcite dissolution kinetics between 1 and 62°C at pH 2.7 to 8.4 in aqueous solutions. Geochemica et Cosmochemica Acta. 48: 485-493, 1984a.

27. Sjöberg, E.L., and Rickard, D. Calcite dissolution kinetics: Surface speciation and the origin of variable pH dependence. Chem. Geol. 42: 119-136, 1984b.

28. Sjöberg, E.L., and Richard, D. The effect of added dissolved calcium on calcite dissolution kinetics in aqueous solutions at 25°C. Chem. Geol. 49: 405-413, 1985.

29. Compton, R.G., and Daly, P.J. The Dissolution kinetics of Iceland spar single crystals. J. Colloid Interface Sci. 101: 159-166, 1984.

30. Holdren, G.R., Jr., and Berner, R.A. Mechanism of feldspar weathering: I. Experimental studies. Geochemica et Cosmochemica Acta. 43: 1161-1171, 1979.

31. Schott, J., Berner, R.A., and Sjöberg, E.L. Mechanism of pyroxene and amphibole weathering: I. Experimental studies of iron-free minerals. Geochemica et Cosmochemica Acta. 45: 2123-2135, 1981.

32. Berner, R.A., and Schott, J. Mechanism of pyroxene and amphibole weathering: II. Observations of soil grains. Amer. J. Sci. 282: 1214-1231, 1982.

33. Schnoor, J.L. Kinetics of chemical weathering: A comparison of laboratory and field weathering rates. In: Aquatic Chemical Kinetics: Reaction Rates of Processes in Natural Waters. John Wiley and Sons, New York. 1989. pp. 475-503.

34. Chou, L., and Wollast, R. Study of the weathering of albite at room temperature and pressure with a fluidized bed reactor. Geochemica et Cosmochemica Acta 48: 2205-2217, 1984.

35. Sverdrup, H.U. The Kinetics of Base Cation Release due to Chemical Weathering. Lund University Press, Lund, Sweden. 1990.

36. Burton, W.K., Cabrera, N., and Frank, F.C. The growth of crystals and the equilibrium structure of their surfaces. Royal Soc. London Philos. Trans. A-265: 299-358, 1951.

37. Compton, R.G., and Daly, P.J. The dissolution of Iceland spar crystals: The effect of surface morphology. J. Colloid Interface Sci. 113: 12-20, 1986.

38. Holdren, G.R., Jr., and Speyer P.M. Reaction rate-surface area relationships during the early stages of weathering: I. Initial observations. Geochemica et Cosmochemica Acta. 49: 675-681, 1985.

39. Holdren, G.R., Jr., and Speyer, P.M. Reaction rate-surface area relationships during the early stages of weathering: II. Data on eight additional feldspars. Geochemica et Cosmochemica Acta. 51: 2311-2318, 1987.

40. Rauch, H.W., and White, W.B. Dissolution kinetics of carbonate rocks. 1. Effects of lithology on dissolution rate. Water Resour. Res. 13: 381-394, 1977.

41. Palmer, A.N. Origin and morphology of limestone caves. Geol. Soc. of Amer. Bull. 103: 1-25, 1991.

42. Herman, J.S., and White, W.B. Dissolution kinetics of dolomite: Effects of lithology and fluid flow velocity. Geochemica et Cosmochemica Acta. 49: 2017-2026, 1985.

43. Rickard, D., and Sjöberg, E.L. Mixed kinetic control of calcite dissolution rates. Amer. J. Sci. 283: 815-830, 1983.

44. Terjesen, S.G., Erga, O., Thorsen, G., and Ve, A. Phase boundary processes as rate determining steps in reactions between solids and liquids. Chem. Eng. Sci. 14: 248-252, 1961.

45. Warfvinge, P,. and Sverdrup, H. Modeling limestone dissolution in soils. Soil Sci. Am. J. 53: 44-51, 1989.

46. Chu, I., Kaill, J., and Wetteroth, W.A. Mass transfer in fluidized beds. Chem. Eng. Prog. 49: 141-149, 1953.

47. Riddiford, A.C. The rotating disk system. In: P. Delahay (ed.), Advances in Electrochemistry and Electrochemical Engineering, Electrochemistry. Vol. 4., 1966. pp. 47-116.

48. Lund, K., Fogler, H.S., and McCune, C.C. Chem. Engr. Sci. 28: 691, 1976.

49. Barton, P., and Vatanatham, T. Kinetics of limestone neutralization of acid waters. Envirn. Sci. and Tech. 10: 262-266, 1976.

50. Snoeyink, N., and Jenkins, D. Water Chemistry. John Wiley and Sons, New York, 1980.

# Appendix A

## MECHANISM OF HETEROGENOUS REACTIONS

Heterogenous reactions, which include mineral dissolution in aqueous systems, involve several steps (Stumm and Morgan, 1981),

1. mass transport of dissolved reactants from the bulk solution to the mineral surface,
2. adsorption of solutes,
3. interlattice transfer of reacting species,
4. chemical reactions,
5. detachment of reactants from the surface, and
6. mass transport into the bulk solution.

The net rate of the heterogenous reaction process is determined by the combined effects of its separate stages. The rate of the entire process is governed by the slowest step if one step is significantly slower than the others. In cases where the slow step involves the introduction or removal of reactants, the reaction is said to be diffusion controlled and is governed by the laws of diffusion kinetics. If, on the other hand, the chemical or physical transformation constitutes the slow step, the rate of the reaction is determined by the kinetics of these processes.

The overall rate of reaction can be characterized as being either transport controlled, surface chemical reaction controlled or a combination of effects, i.e., mixed-kinetics controlled.

### Transport Control/Diffusion Kinetics

The transport of a solute in a moving liquid is governed by two quite different mechanisms,

1. molecular diffusion as a result of concentration differences, and,
2. transport of entrained solute particles by the moving liquid.

The combination of these mechanisms is called convective

diffusion of solute in a liquid. A simple example of convective diffusion is mass transfer in a system where a heterogenous reaction occurs at the surface of an infinite rotating disk.

When the surface chemical reaction rate is larger than the rate of introduction or removal of ions from the reaction surface, the reaction is said to be transport-controlled. All species approaching the surface react instantaneously. The overall rate of the heterogenous reaction is determined by the slower rate of mass transfer. The rate of the transport-controlled reaction is a function of the bulk solution flow velocity.

Nernst (1904) assumed that all heterogenous reactions were transport controlled and their rates could be described by,

$$dC/dt|_T = D(A/V)(C_s-C)/\delta_N \qquad (1A)$$

where D is the molecular diffusion coefficient, $C_s$ and C the concentration at the surface and in the bulk respectively, V the volume of solution, A is the surface area exposed to the solution, $\delta_N$ the thickness of the fluid layer attached to the surface through which molecular diffusion is the major mass transport process. This is also called the diffusion boundary layer (DBL). For the rotating disk $\delta_N$ is given by (Pleskov and Filinovski, 1976).

$$\delta_N = 1.6D^{1/3}\nu^{1/6}\omega^{-1/2} \qquad (2A)$$

where $\nu$ is the kinematic viscosity and $\omega$ the rotational velocity of the disk. The transport rate constant $k_L$ is given by

$$k_L = D/\delta_N = D/(1.6D^{1/3}\nu^{1/6}\omega^{-1/2}) \qquad (3A)$$

The transport rate is

$$dC/dt|_T = k_L A(C_s-C)/V \qquad (4A)$$

Surface Chemical Reaction Control

When chemical transformations constitute the slow step, the rate of the reaction is controlled by the kinetics of these processes. Since the rate of mass transfer is large, the concentration of the entire solution is constant.

For dissolution reactions the rate of the first order surface chemical reaction is proportional to the chemical potential difference between the concentration of the dissolving solute at the solid-liquid interface, $C_s$, and the concentration of the solute in equilibrium with the solid, $C_{eq}$,

$$dC/dt|_C = k_c A(C_{eq}-C_s)/V \qquad (5A)$$

where $k_c$ is the rate constant for chemical reaction.

Mixed Kinetic Control

When the rates of transfer of the reactants and of the chemical reaction are comparable, the reaction is said to controlled by mixed kinetics.

For steady-state, the diffusion rate must balance the chemical reaction rate,

$$dC/dt|_T = dC/dt|_C \qquad (6A)$$

Solving Equation 6A for $C_s$ and substituting it into either Equation 4A or Equation 5A yields the general rate equation,

$$dC/dt = k_o(A/V)(C_{eq}-C) \qquad (7A)$$

which reduces to Equation 4A for $k_L<<k_c$ and to Equation 5A for $k_c<<k_L$. In Equation 7A, $k_o$ is the overall rate constant given by,

$$k_o = k_L k_c/(k_L + k_c) \qquad (8A)$$

## Appendix B

## CHEMICAL EQUILIBRIUM CALCULATIONS

In all the equations described below the concentrations of the species in the carbonate system, including carbon dioxide, bicarbonate and carbonate, are given in terms of the total inorganic carbon concentration, $C_T$, and ionization fractions, i.e.,

$$[H_2CO_3] = C_T \alpha_o \quad (1B)$$

$$[HCO_3^-] = C_T \alpha_1 \quad (2B)$$

$$[CO_3=] = C_T \alpha_2 \quad (3B)$$

where,

$$\alpha_o = 1/\{1+(K_1/[H^+])+(K_1K_2/[H^+]^2)\} \quad (4B)$$

$$\alpha_1 = 1/\{1+([H^+]/K_1)+(K_2/[H^+])\} \quad (5B)$$

$$\alpha_2 = 1/\{1+([H^+]/K_2)+([H^+]^2/K_1K_2\} \quad (6B)$$

$K_1$ and $K_2$ are the temperature and activity corrected values of the first and second ionization constants for carbonic acid. Values of equilibrium constants at 25°C were taken from Snoeyink and Jenkins (1980) (see Table 1B). The Davies equation was used to calculate activity coefficients for correcting the equilibrium constants for ionic strength (Table 2B).

Equilibrium pH and Equilibrium Calcium Concentration

When calcium carbonate dissolves under a closed-to-atmospheric-carbon dioxide condition, the acidity and the difference between the alkalinity and the calcium concentration

TABLE 1B VALUES OF EQUILIBRIUM CONSTANTS AT 25°C AND I=0

| | |
|---|---|
| First ionization constant for carbonic acid, $K_1$ | $10^{-6.35}$ |
| Second ionization constant for carbonic acid, $K_2$ | $10^{-10.33}$ |
| Ion Product of water, $K_W$ | $10^{-14}$ |
| Henry's Law constant, $K_H$ | $10^{-1.47}$ |

TABLE 2B EQUATIONS USED TO CORRECT EQUILIBRIUM CONSTANTS FOR ACTIVITY

Activity coefficients were calculated using the Davis equation, i.e.,

$$\log(f_i) = -0.5z^2\{[I^{1/2}/(1+I^{1/2})]-0.2I\}$$

where,

z - charge of the ion

I - ionic strength in moles/L

$f_1$ - activity coefficient for charge of +/- one

$f_2$ - activity coefficient for charge of +/- two

The activity corrected equilibrium constants given by:

$$K_1 = K_1/(f_1)^2$$

$$K_2 = K_2/(f_2)$$

$$K_{sp} = K_{sp}/(f_2)^2$$

$$K_w = K_w/(f_1)^2$$

remain constant. The equilibrium pH and calcium ion concentration can be determined with the following equations,

$$\text{acidity} = C_T(\alpha_1+2\alpha_o)+[H^+]-K_w/[H^+] \quad (7B)$$

$$(\text{alkalinity} - \text{Ca}) = C_T(\alpha_1+2\alpha_2)+K_w/[H^+]-[H^+]-2[\text{Ca}] \quad (8B)$$

$$[\text{Ca}] = K_{sp}/(\alpha_2 C_T) \quad (9B)$$

where $C_T$ is in moles per liter and $K_w$ is the ion product of

water. $K_{sp}$ is the solubility product for $CaCO_3$.

For known amounts of initial acidity, initial alkalinity and initial calcium ion concentrations, Equations 7B, 8B and 9B are solved simultaneously to calculate the equilibrium pH. Equation 9B gives the equilibrium calcium concentration.

Intermediate Calcium Ion Concentration

For dilute acidic water with dissolving $CaCO_3$ the charge balance relationship is,

$$(2S + alk_o) = (C_{To}+S)(\alpha_1+2\alpha_2)+K_w/[H^+]-[H^+] \qquad (10B)$$

where S is the molar concentration of calcium carbonate dissolved, $C_{To}$ is the initial concentration of the dissolved inorganic carbon (DIC). Equation 10B is based on the assumption that the dissolution of 1 eq/L of calcium carbonate increases the alkalinity by 1 eq/L and increases the dissolved inorganic carbon concentration by 1 mole/L.

Equation 10B is solved for S for a given pH by substituting known values of initial alkalinity and DIC.

Open-to-Atmosphere Equilibrium pH and Calcium Concentration

The following equations are used to calculate the equilibrium pH and equilibrium calcium concentration when calcium carbonate dissolves in a solution that is in equilibrium with atmospheric carbon dioxide.

$$2[Ca] + C_C + [H^+] = K_H P_{CO2}(\alpha_1+2\alpha_2)/\alpha_0 + K_w/[H^+] + C_a \qquad (11B)$$

$$[Ca] = K_{sp}\alpha_0/(\alpha_2 K_H P_{CO_2}) \qquad (12B)$$

$C_C$ and $C_a$ are the influent concentrations in equivalents per liter of cations excluding hydrogen, and anions excluding inorganic carbon species and hydroxide, respectively. $K_H$ is the Henry's Law constant in mols/L atm and $P_{CO_2}$ is the partial

pressure of carbon dioxide in atmospheres. Equation 11B and Equation 12B are solved numerically for the equilibrium calcium ion concentration and the pH using known values of $K_{sp}$.

# Appendix C
## METHYL RED EXPERIMENTS

A series of experiments was performed using methyl red dye to check if the solution in the reaction vessel was well-mixed and if the response time of the pH electrode had an adverse affect on the recorded results. The dye was prepared by dissolving 1 g of the sodium salt of methyl red in 1 L of DI water. A 1 mL quantity of this solution was added to 600 mL of experimental solution in the reaction vessel. Methyl red is red at low pH (pH<4) and becomes yellow as the pH is increased above approximately 7.

A Brinkman dipping probe colorimeter (Model PC800) equipped with a red (545 nanometer wavelength) filter was used to measure the absorbance of the solution in the reactor. The colorimeter probe tip was positioned in the vessel in the same position as the bulb of the pH electrode but on the opposite side of the rotating disk. During each run the absorbance readings were recorded on a high speed, strip chart recorder while the pH readings were logged on a personal computer.

A calibration curve of normalized absorbance versus pH was first prepared by stepwise titrating the experimental solution (initial pH=4 and ionic strength of 0.079M) with 0.01N KOH. The experimental solution was stirred using a magnetic stirrer. Approximately 0.2 mL of base was added each step. The pH and absorbance were recorded after each increment of base had been added and the readings had stabilized.

A second calibration curve was prepared using the above procedure. However, the solution was stirred by the rotating disk operating at 400 rpm. The disk was covered with plastic wrap so that the limestone was not in contact with the solution. A 1 mL volume of dye was rapidly injected into the stirred solution. The absorbance reading stabilized almost instantaneously (< 1 s) indicating that the solution was well mixed. The solution was then titrated with 0.01 N KOH, as described above, and the pH and absorbance recorded.

Two free drift experiments, using initial pH values of 4 and 5, were conducted with disks of WM stone dissolving in the solution and with methyl red dye present. The pH values recorded with time were used with the pH versus absorbance calibration curve (described above) to prepare a plot of absorbance versus time. This was compared with the absorbance versus time curve measured during the experiment. The curves obtained with slow stepwise titration with strong base and the curves obtained with dissolving stone are in good agreement (see Figure 1C). This indicates that the response time of the pH electrode is not a significant factor in the free drift experiments.

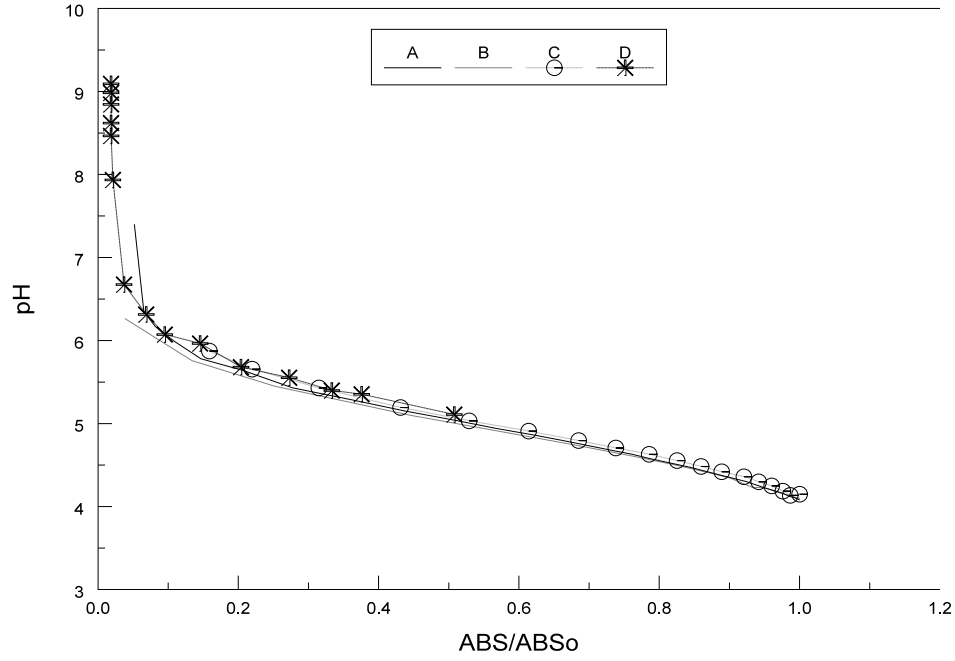


Figure 1C pH versus normalized absorbance for methyl red titration in the rotating disk apparatus used to test the rate of response of the pH measuring system. Curve A and B are for base addition by reagent dispenser with mixing by magnetic stirrer and inert rotating disk. Curve C and D are for calcium carbonate dissolution from the WM stone with an initial acidity of 0.1 meq/L and 0.01 meq/L respectively.

# Appendix D

## EQUILIBRIUM MODEL CALIBRATION

The pH values measured during a rotating disk experiment were substituted in the charge balance equation (Equation 10B, Appendix B) to calculate corresponding values of the theoretical amount of calcium dissolved. In Figure 1D, pH is plotted as a function of calcium ion concentration calculated for different amounts of initial dissolved inorganic carbon concentration (DIC) and calcium ion concentration measured by the AAS. For experiments with 0.01 meq/L of initial acidity, good agreement was obtained by solving the charge balance equation with some amount of initial DIC. In all such experiments the solution seems to be in equilibrium with atmospheric $CO_2$. The experimental solution was boiled to remove $CO_2$ but the solution could have dissolved $CO_2$ when it was being transferred to the reactor. The bubbling of the solution by nitrogen before beginning the experiment could have also dissolved some carbon dioxide. Once the experiment was started no further exchange of $CO_2$ took place. This is evident from the good agreement obtained between the measured calcium and calcium concentrations calculated by solving the charge balance equation. The charge balance equation is written for a closed system with no exchange of atmospheric $CO_2$. For the experiments with 0.1 meq/L of initial acidity, the mineral acidity is much greater than the carbon dioxide acidity, therefore, DIC is still present but it has a minimal effect on the calculated calcium ion concentrations.

The calcium measurements by the AAS were verified by measuring the alkalinity in some experiments. Figure 2D, in which the alkalinity calculated from calcium measurements is plotted against the measured alkalinity, shows that the calcium dissolved contributed to all the acid neutralizing capacity measured in the experimental solution.

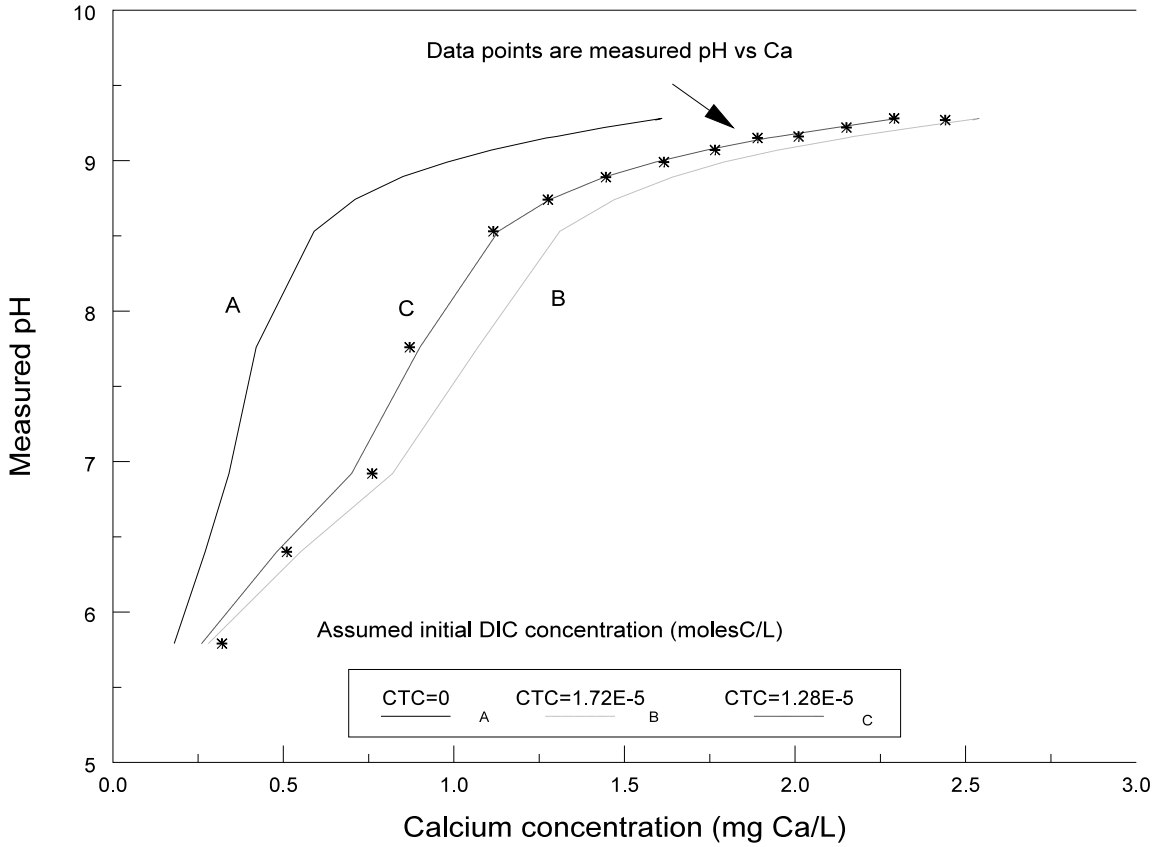


Figure 1D Measured pH versus measured calcium concentrations for the SL stone, w = 600 rpm and initial acidity = 0.01 meq/L. The three theoretical curves were determined using the measured pH, the equilibrium model discussed in Appendix B and several assumed values of the initial dissolved inorganic carbon concentrations (CTC) in the rotating disk reactor solution.

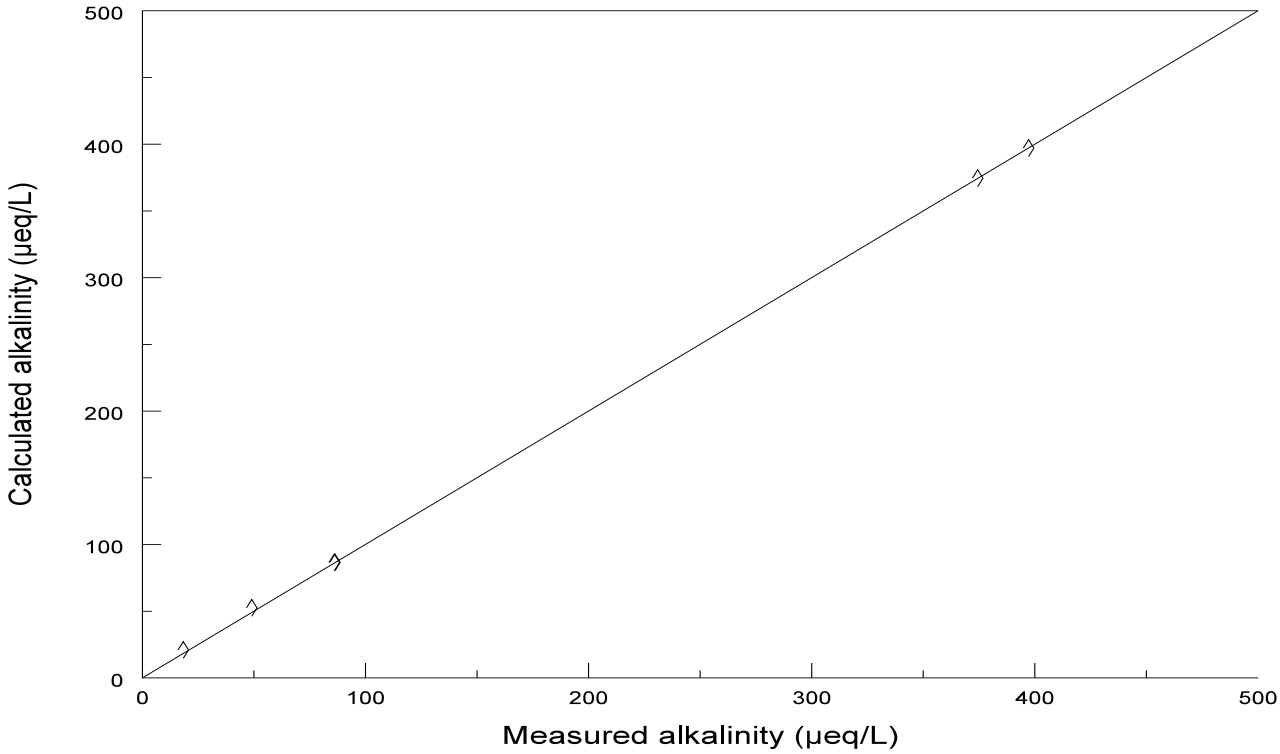


Figure 2D Alkalinity calculated from the measured calcium concentrations plotted against the measured alkalinity. All experimental points are close to 1:1 line indicating that essentially all the calcium is derived from the dissolution of calcium carbonate.

# Appendix E

## SOLUBILITY PRODUCT DETERMINATION

The solubility product of the calcium carbonate in the WM, SL, A, C, F and I stone samples was determined by equilibrating samples of the stone with quantities of acidified solution in open beakers. Samples of stone were broken into coarse granules (approximately 0.5 cm in diameter) using a mortar and pestle. The granules were rinsed with DI water and air dried. The surface area of the granules was approximately 14 $cm^2$.

Four solutions were used in the experiment. Two solutions had mineral acidities of 0.01 and two had acidities of 0.10 meq/L. The background electrolyte was 0.079 M KCl. The solutions were stirred with a magnetic stirrer under an open-to-the-atmosphere condition. The temperature was 25 ± 1°C.

The calcium concentration and pH were measured with time as shown in Figures 1E to 4E. The temperature was recorded each time samples were collected for pH and calcium measurement. The volume of the samples used to determine the calcium concentration was 1.5 mL. Each sample was centrifuged for 15 minutes at 15,000xg and then 1 mL of centrifugate was withdrawn with an automatic pipette. The calcium ion concentration was determined by AAS.

At about 600 hours of stirring the pH had been essentially constant for approximately 50 hours. At this point several samples were taken for measuring the alkalinity. The alkalinity was determined using 75 mL of solution made by diluting 2 mL of centrifugate to 100 mL with distilled water.

The measured pH and alkalinity were used to calculate the carbonate ion concentration with the expression,

$$[CO_3^{=}]=\{0.833[alk+[H^+]-K_w/[H^+]\}/\{1+(2K_2/[H^+])\} \qquad (1E)$$

where alk is the alkalinity in equivalents per liter and $K_2$ is the second ionization constant of carbonic acid. The molar

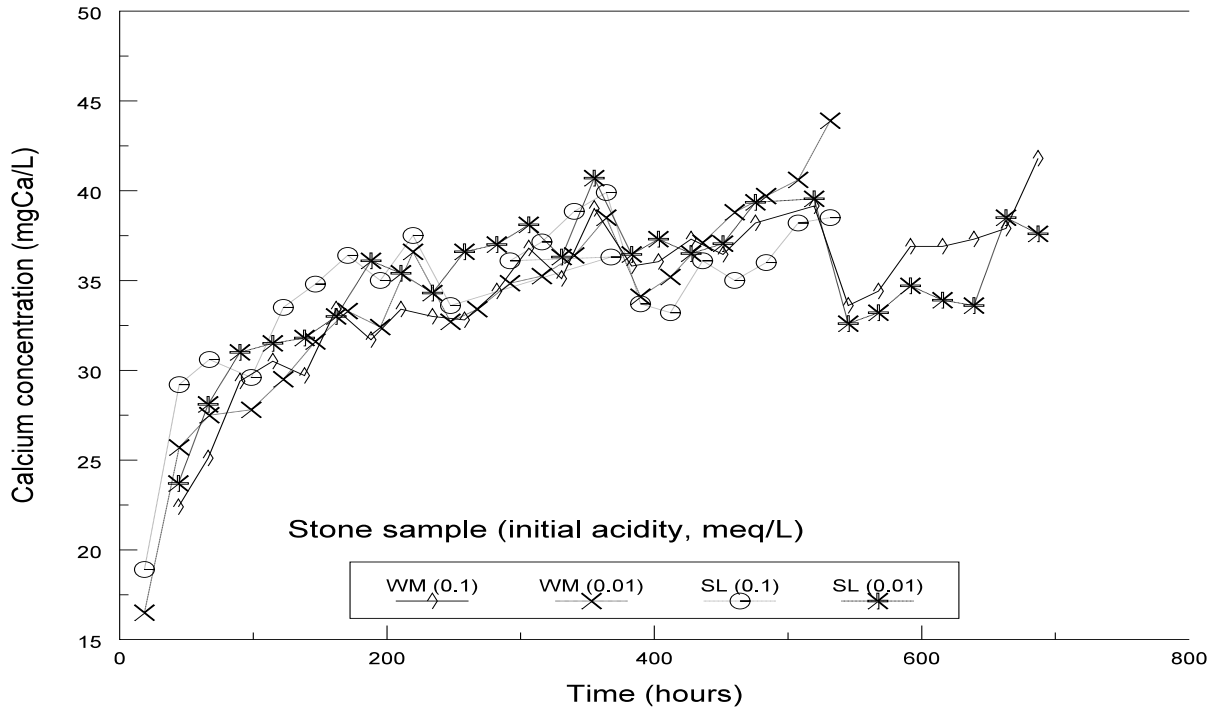


Figure 1E Variation of calcium concentration with time in open batch reactor. Used to determine the apparent solubility product of calcium carbonate in the SL and WM stone samples.

concentrations of calcium and carbonate ion were then used in the following equation to determine the solubility product,

$$K_{sp} = \gamma_{++}\gamma_{=}[Ca^{++}][CO_3^{=}] \qquad (2E)$$

where $\gamma_{++}$ and $\gamma_{=}$, the activity coefficients for the calcium and carbonate ions, were calculated using the Debye-Hückel equation and I = 0.079. Representative results ($pK_{sp}$ versus time) are plotted in Figure 5E. The last 10 or so $pK_{sp}$ values were averaged for the samples analyzed and the results are listed in Table 5.2.1.

The charge balance equation for a system open-to-atmospheric carbon dioxide was used with the solubility product equation to

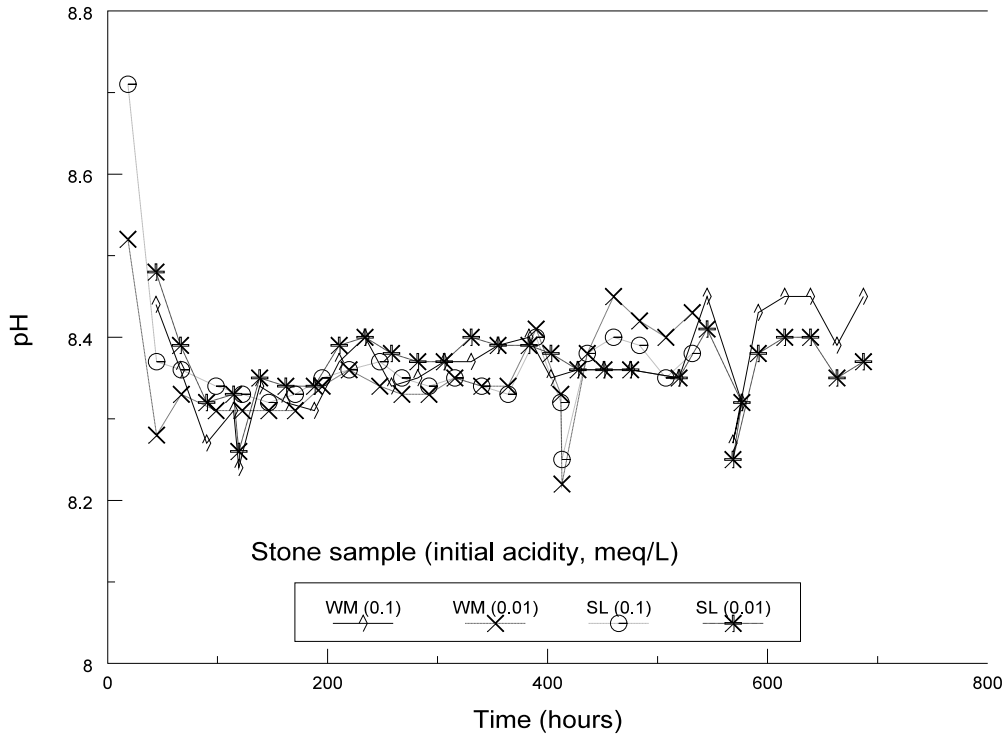


Figure 2E pH versus time results for the experiments of Figure 1E.

check the values of $K_{sp}$ determined using Equation 2E. The expressions used are,

$$2[Ca^{+}] + [H^{+}] = (K_H P_{CO2}/a_0)(a_1+2a_2) + K_w/[H^{+}] + [Cl^{-}] \quad (3E)$$

and

$$[Ca^{+}] = K_{sp}\{a_0/(a_2\ K_H P_{CO_2})\} \quad (4E)$$

where $K_H$ is Henry's law constant and $P_{CO_2}$ is the atmospheric partial pressure of carbon dioxide, $a_0$, $a_1$, and $a_2$ are the ionization fractions for the carbonate system (see Appendix C) and $[Cl^{-}]$ is the strong acid anion concentration. The ion product ($K_w$) of water and the ionization constants for carbonic acid used

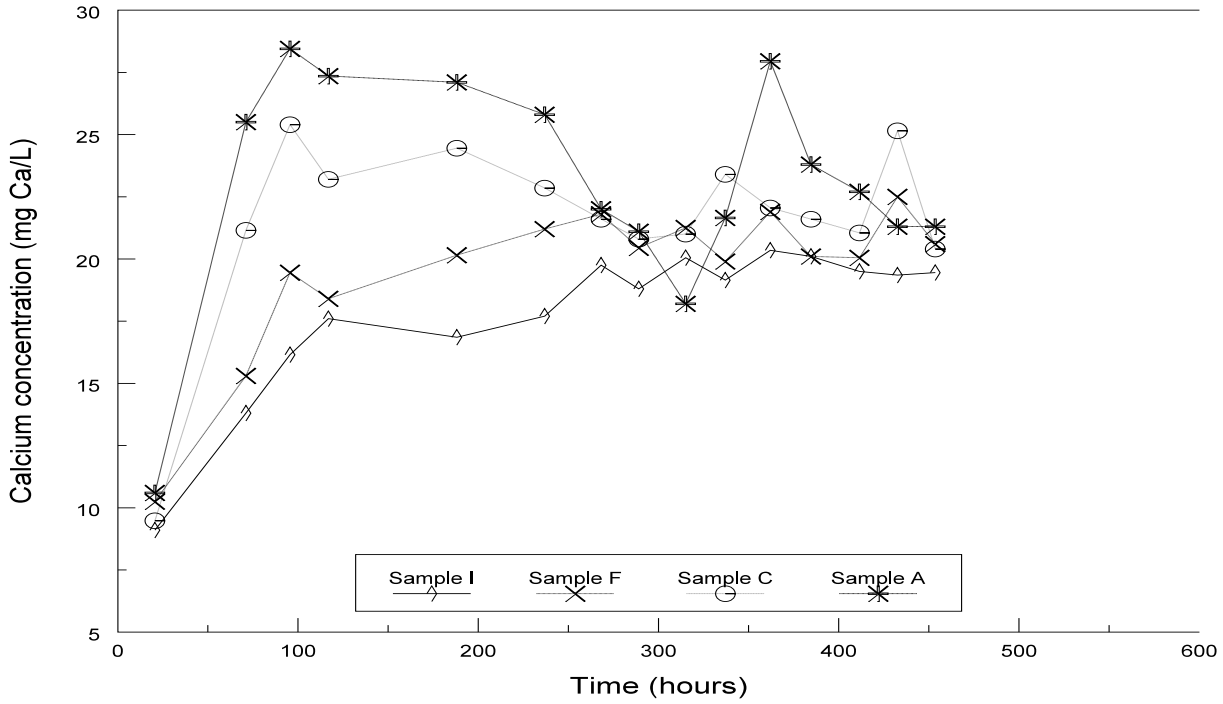


Figure 3E Variation of calcium concentration with time in the experiments used to determine the solubility product of calcium carbonate in stone samples A, C, F and I.

in calculating $a_0$, $a_1$, and $a_2$ were corrected for ionic strength. It was assumed that $K_H P_{CO2} = 10^{-4.7}$.

Equations 3E and 4E were solved numerically for the equilibrium calcium ion concentration and the pH using assumed values of $K_{sp}$. The best agreement between the measured and calculated values of pH and calcium concentration was obtained using values of $pK_{sp}$ (8.14 for the WM sample and 8.29 for the SL sample) that are in reasonable agreement with the values obtained using the measured pH, calcium ion concentration and alkalinity and Equations 1E and 2E.

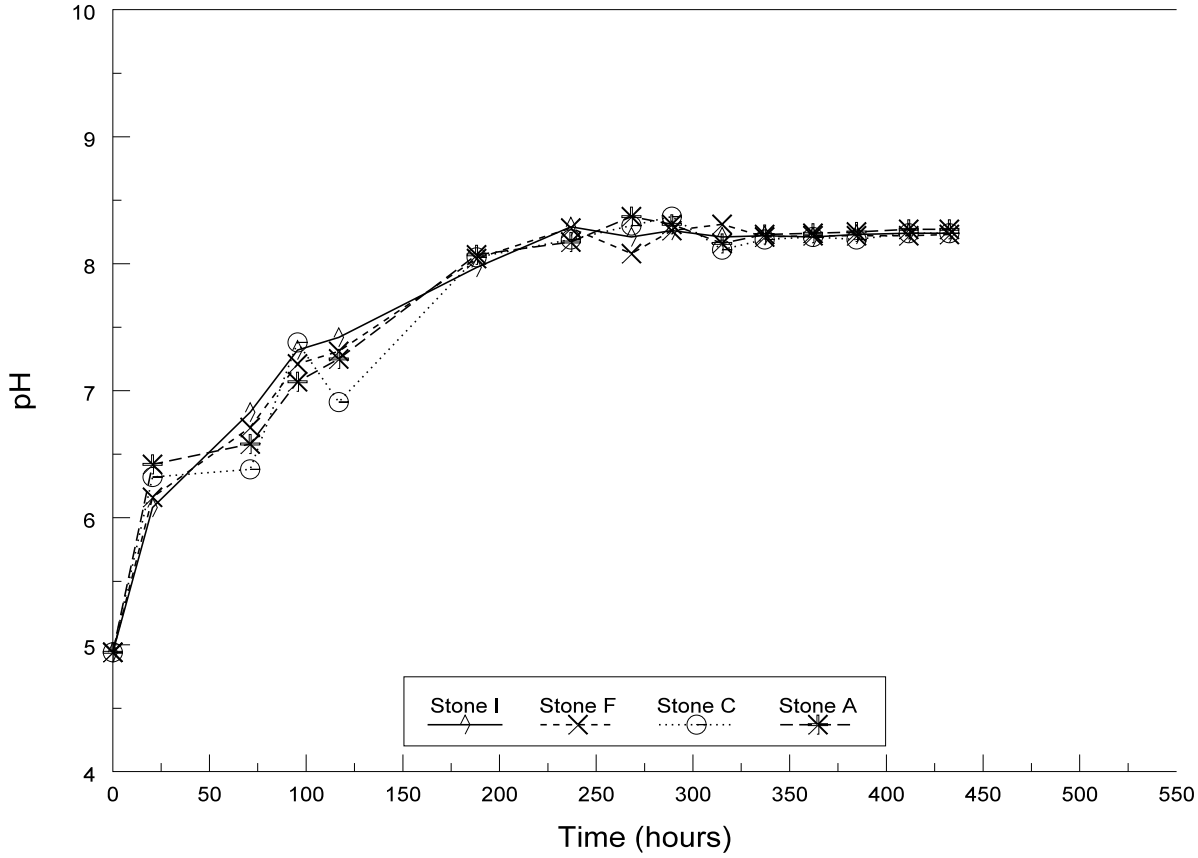


Figure 4E pH measurements from the experiments used to determine Ksp for stone samples A, C, F and I.

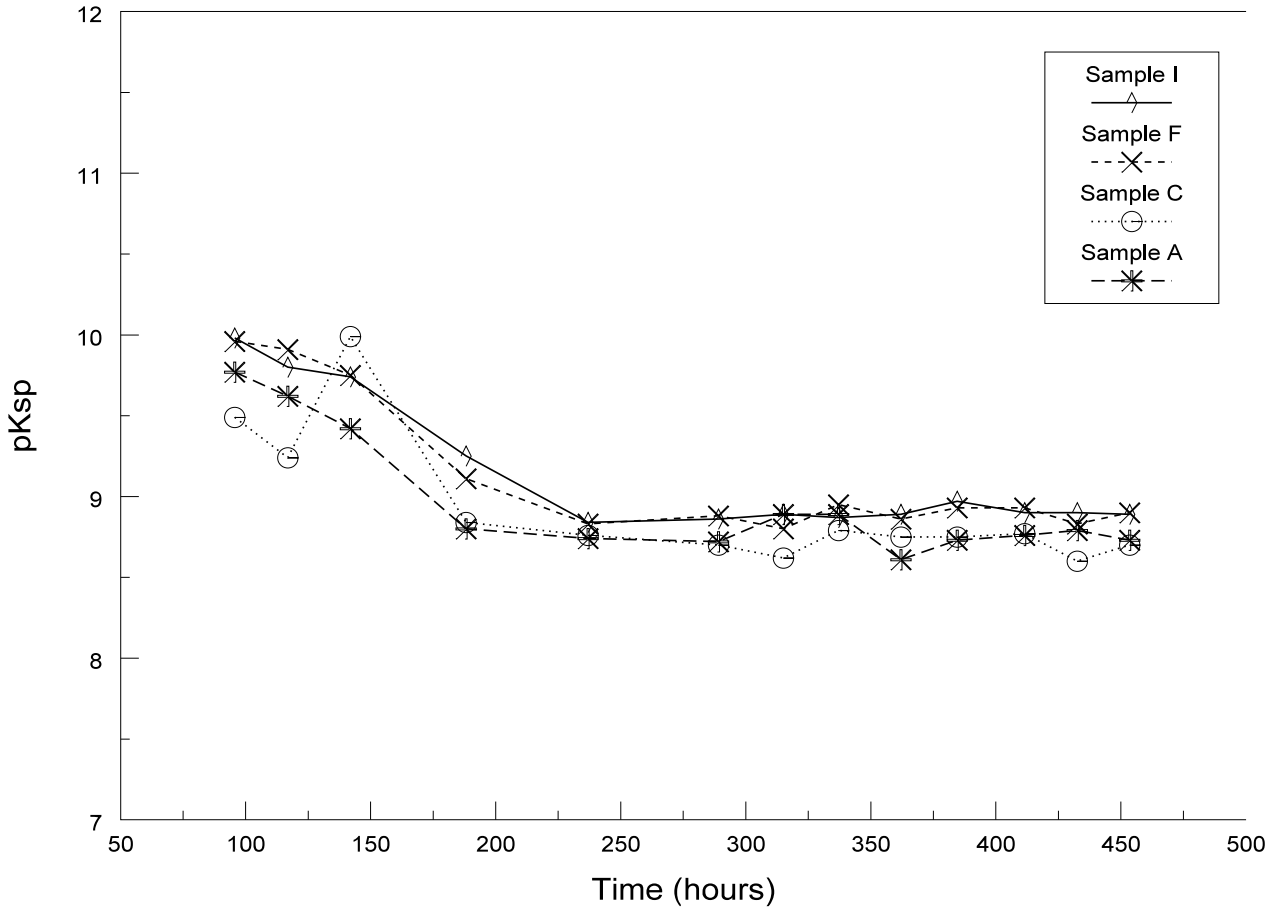


Figure 5E Values of pKsp calculated using the calcium concentration and pH values in Figures 3E and 4E.

# Appendix F
# CALCIUM ION DIFFUSIVITY

A set of rotating disk experiments was used to determine the calcium ion diffusivity at 25°C. Rearranging Equation 8A in Appendix A and substituting Equation 3A for $k_L$ yields,

$$1/k_o = 1.61\nu^{1/6}D^{-2/3}\omega^{-1/2} + 1/k_c. \quad (1F)$$

According to Equation 1F, if $1/k_o$ is plotted as a function of $\omega^{-1/2}$ the slope, S, of the straight line fitted to these points is equal to $1.61\nu^{1/6}D^{-2/3}$ and the intercept, I, is equal to $1/k_c$. The magnitude of D and $k_c$ can, therefore, be determined using,

$$D = 2.04\ \nu^{1/4}\ S^{-3/2} \quad (2F)$$

and

$$k_c = I^{-1} \quad (3F)$$

Experiments were performed at 25°C using the WM stone and initial acidities of 0.1 and 0.01 meq/L. The rotational speed was varied from 400 to 1200 rpm. A systematic increase in $k_o$ with increasing rotational speed is shown in Figures 1F and 2F for constant experimental conditions.

Values of $1/k_o$ from Figures 1F and 2F are plotted as a function of $\omega^{-1/2}$ in Figures 3F and 4F, respectively. The values of D and $k_c$ obtained from the slopes and intercepts in Figures 3F and 4F are listed in Table 1F. The magnitude of D is $0.93 \times 10^{-5}$ $cm^2/s$ for an initial acidity of 0.1 meq/L and $0.50 \times 10^{-5}$ $cm^2/s$ for an initial acidity of 0.01 meq/L. While these values differ by a factor of approximately 2, this difference is not statistically significant at a 95% confidence level.

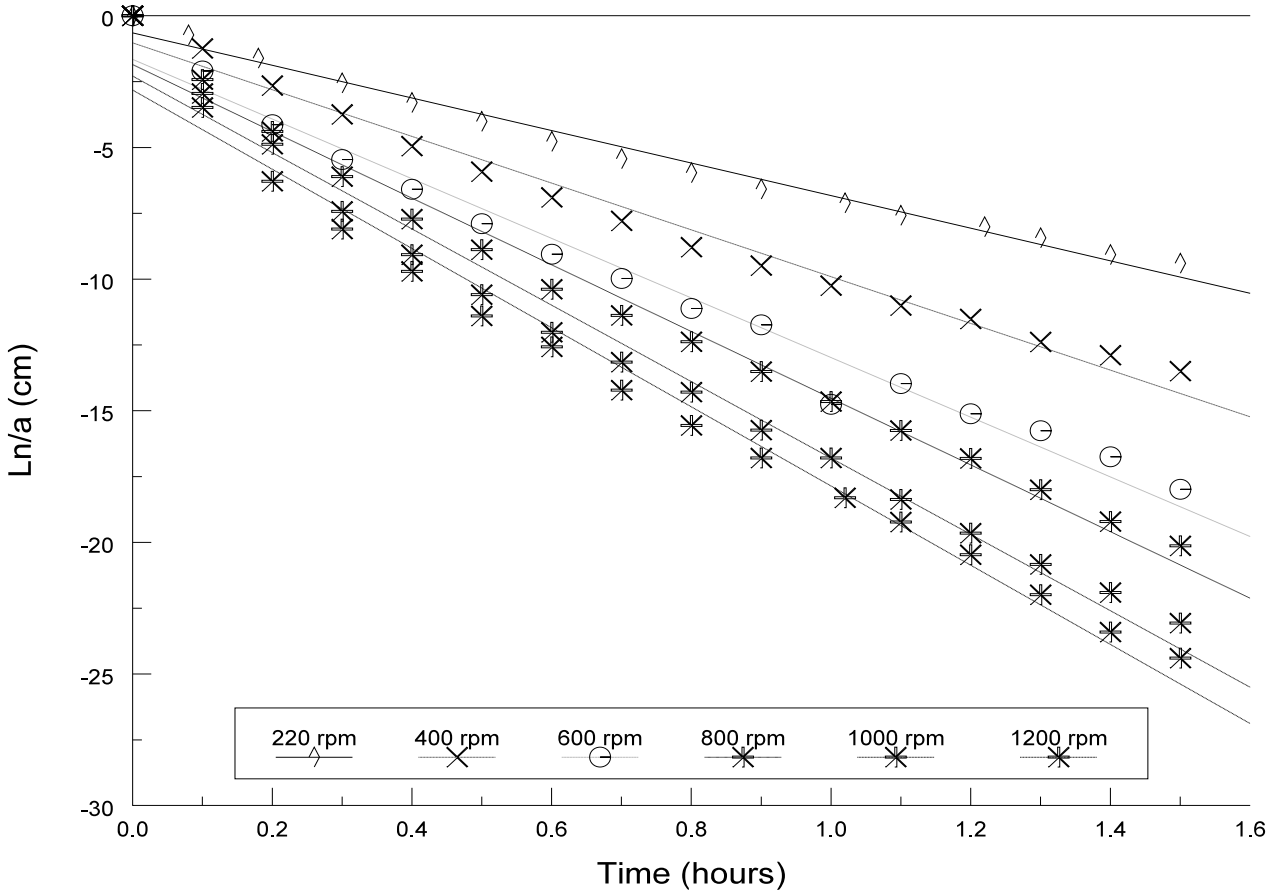


Figure 1F Effect of disk rotational speed on plots of ln{(Ceq -C)/Ceq}V/A versus time; WM stone sample and initial acidity of 0.1 meq/L.

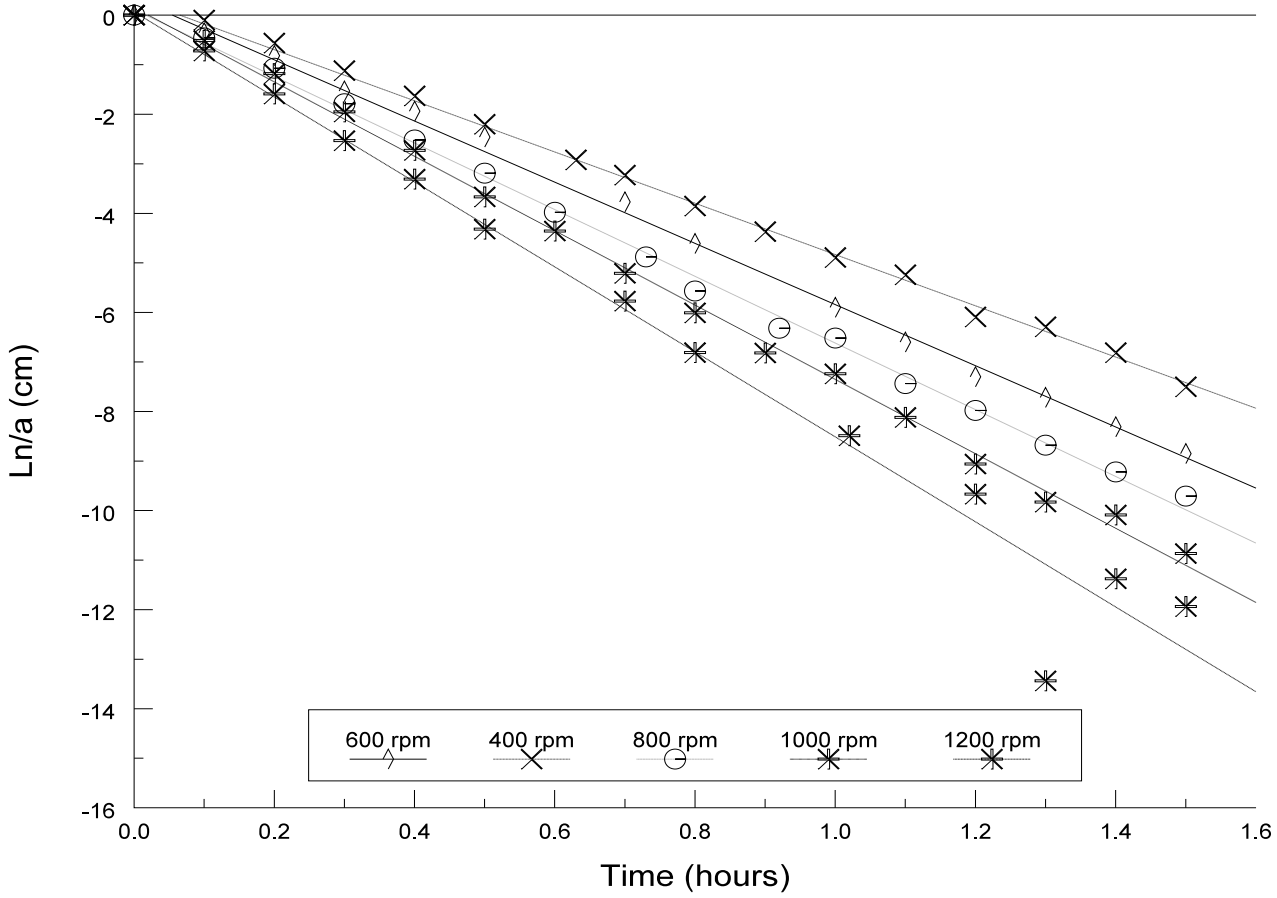


Figure 2F Effect of disk rotational speed on plots of ln{(Ceq-C)/Ceq}V/A versus time; WM stone sample and initial acidity of 0.01 meq/L.

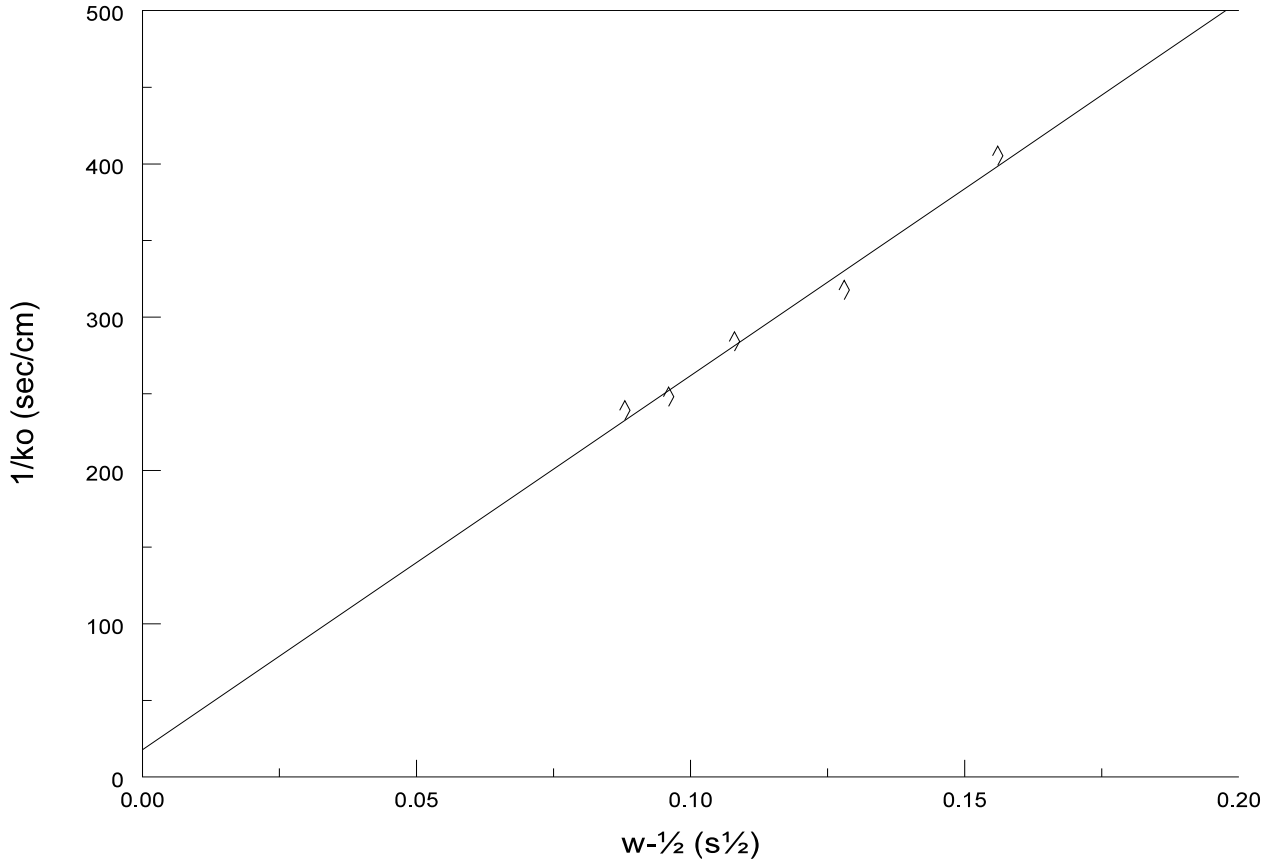


Figure 3F Inverse of the overall dissolution rate constant versus $\omega^{-1/2}$; WM stone and initial acidity = 0.1 meq/L.

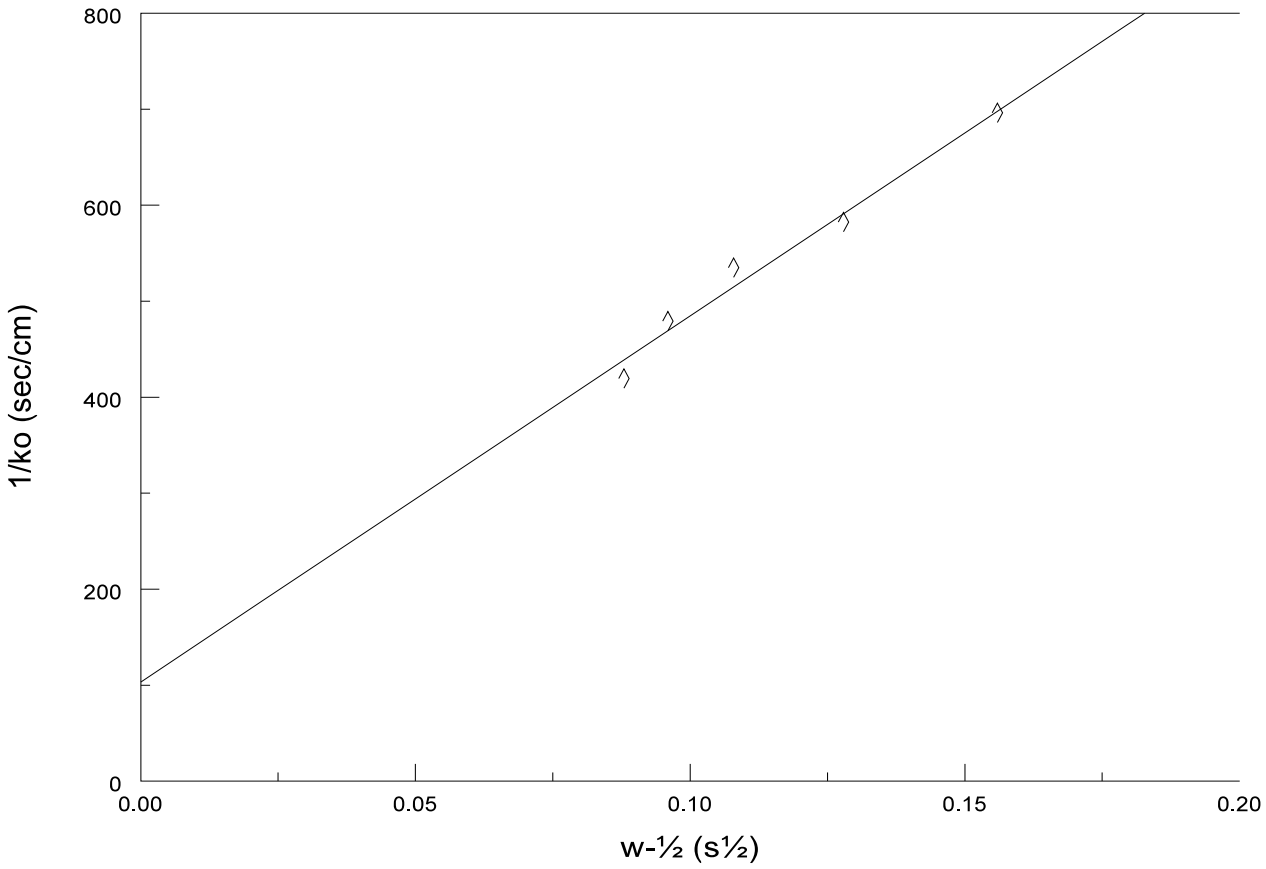


Figure 4F Inverse of the overall dissolution rate constant versus $\omega^{-1/2}$; WM stone and initial acidity = 0.01 meq/L.

TABLE 1F CALCIUM ION DIFFUSIVITY, D, AND $k_c$ FOR THE WM SAMPLE AND 25°C.

| Initial Acidity (meq/L) | D x $10^5$ ($cm^2$/sec) | $k_c$ x $10^3$ (cm/sec) |
|---|---|---|
| 0.10 | 0.93 | 1.38 |
| 0.01 | 0.50 | 0.02 |

The values of D from this study are in general agreement with those from the literature (see Table 2F). The values of D listed in Table 2F were averaged and this quantity (D = 0.8 x $10^{-5}$ $cm^2$/s at 25°C) was used in the analysis of results.

TABLE 2F. CALCIUM ION DIFFUSIVITY AT 25°C

| Reference | Ionic Strength | Calcium ion diffusivity x $10^5$ at 25°C ($cm^2$/s) |
|---|---|---|
| This study | 0.079 | 0.50<br>0.93 |
| Sjöberg and Richard (1984a) | 0.7<br>0.7<br>0.7<br>0.1 | 0.84<br>0.85<br>0.74<br>0.79 |
| Wallin and Bjerle (1989) | 0.1 | 0.79 |
| Hodes (1972) | 0.05<br>0.5 | 0.85<br>0.75 |